

Clay mineral formation and
fluid-rock interaction in fractured
crystalline rocks of the
Rhine rift system:

Case studies from
the Soultz-sous-Forêts granite (France)
and the Schauenburg Fault (Germany)

INAUGURAL-DISSERTATION
zur
Erlangung der Doktorwürde
der
Naturwissenschaftlich-Mathematischen Gesamtfakultät
der Ruprecht-Karls-Universität
Heidelberg

Vorgelegt von

Diplom-Geologin Anja Schleicher

Heidelberg, April 2005

Gutachter: Dr. Laurence Warr
Dr. Norbert Clauer

Promotionsprüfung: 25. Mai 2005

Ich erkläre hiermit,

- a) dass ich die vorgelegte Dissertation selbst verfasst und mich dabei keiner anderen als der von mir ausdrücklich bezeichneten Quellen und Hilfen bedient habe und
- b) dass ich an keiner anderen Stelle ein Prüfungsverfahren beantragt bzw. die Dissertation in dieser oder anderer Form bereits anderweitig als Prüfungsarbeit verwendet oder einer anderen Fakultät als Dissertation vorgelegt habe

Heidelberg, den 12. April 2005

Anja Schleicher

Was du mir sagst, das vergesse ich
Was du mir zeigst, daran erinnere ich mich
Was du mich tun lässt, das verstehe ich
Konfuzius 500 v.Chr.

Acknowledgements

I would like to say „thank you“ to all friends and colleagues who were with me and supported me during my time in Heidelberg. My special gratitude and respect go to my supervisor Laurence Warr, who was always there when I needed him, despite the distance between Heidelberg and Strasbourg at the end of the thesis. Additionally, I would like to thank Norbert Clauer for very helpful discussions about illite and K-Ar isotopes as well as agreeing to examine the thesis.

Also special thanks to my greatest friends for constantly helping through numerous good and bad times: Julia Berger and Jana Just.

and to:

The Heidelberg Sultz-group for their helpful and constructive discussions: Agnes Kontny, Bernd Kober, Emmanuel Laverret, Sven Traxel, Jana Just and Laurence Warr.

Ben van der Pluijm, Don Peacor and John Solum from the University of Michigan for their friendly reception and support in Ann Arbor. Being there was a great experience for me.

The Landesgraduiertenförderung and the DFG (GRK 273: Fluid-rock interaction) for the financial support.

Birgit Dietrich, Gesine Lorenz, Jens Grimmer and Roswitha Marioth for effectively helping with the english language, reading the thesis and finding lots of mistakes.... and for always being there.

Axel Emmerich, Carsten Vahle, Carstens Laukamp, Edilma Andrade, Fabio Lapponi, Francis Cueto, my ex-roommate Heiko Hofmann, Johanna Kontny, Kirsten Maciejczyk, Luca Nano, Marta Gasparrini, Margot Isenbeck-Schröter, Michael Bühler, Michael Seeling, Oliver Rügner, Rike Bauer, Thomas Angerer, Tanja van der Beek, Thierry Marbach, Yutta Frank and Zbynek Veselovsky for the unforgettable time in Heidelberg.

All the Strasbourg people who made me feel comfortable and welcome.

The badminton group (Christian, Dörte, Uwe, Doro) for the sportive motivation.

The few non-geologists for discussions not about geology: Anja Beul, Sandra Hamann and Christoph Hummel.

My parents and my brother Frank, to whom I always can rely on.

TABLE OF CONTENTS

Summary and “Zusammenfassung“

List of symbols and abbreviations

	page
1 INTRODUCTION	
1.1 Faulting and fluid-rock interaction	1
1.2 Clay formation and fluids in hydrothermal environments of the Rhine rift setting	2
1.3 Motivation and selection of localities	4
2 GEOLOGY	
2.1 Introduction	5
2.2 Post-granite history and thermal activity in the Rhine rift area	6
2.3 Tertiary rifting	6
2.4 The Rhine rift system and the selected localities of the study	7
2.4.1 The Soultz-sous-Forêts granite	8
2.4.2 The Heidelberg granite and Permian rhyolite	8
2.4.2.1 The Schauenburg Fault	9
3 ANALYTICAL METHODS	
3.1 X-ray diffraction	10
3.1.1 Identification of clay mineral phases	11
3.1.2 Peak behavior of clay minerals after glycolization and heating	12
3.1.3 Calculation and modelling of crystallite thickness distribution	12
3.1.4 Illite polytype determination	13
3.1.5 X-ray textural goniometry	14
3.2 Electron microscopy	15
3.2.1 Scanning electron microscopy and energy dispersive X-ray detection	15
3.2.2 Transmission electron microscopy	15
3.2.2.1 Selected area electron diffraction	16
3.2.2.2 Analytical electron microscopy	17
3.3 K-Ar isotope geochemistry	17
4 ALTERATION HISTORY OF THE SOULTZ-SOUS-FORÊTS GRANITE, BURIED RHINE RIFT BASEMENT	
Abstract	
4.1 Introduction	19
4.1.1 Sample material and analytical procedure	20
4.2 Results and Interpretation	24
4.2.1 Illite microscopic characteristics	24
4.2.2 Illite compositional characteristics	25
4.2.3 X-ray diffraction characteristics of the grain-size separates	27
4.2.4 K-Ar values of the different grain size fractions	29
4.2.5 Analysis of illite mixtures based on K-Ar values, polytypes and crystallite thickness distributions	31

4.3.	Discussion	32
4.3.1	The timing and mechanism of episodic illite crystallization	32
4.4	Conclusions	34
5	ALTERATION HISTORY OF THE SCHAUENBURG FAULT, UPLIFTED RHINE RIFT MARGIN	
	Abstract	
5.1	Introduction	35
5.1.1	Sample material and field relationships of the Schauenburg Fault	36
5.1.2	Analytical procedure	37
5.2	Results	38
5.2.1	Sample characteristics and mineral assemblages	38
5.2.2	X-ray diffraction analysis	38
5.2.3	Rock texture	41
5.2.4	Microstructure and chemical analysis	42
	5.2.4.1 Scanning electron microscopy	42
	5.2.4.2 High resolution electron microscopy	43
5.2.5	Compositions of illitic minerals	46
5.3	Discussion	48
5.3.1	Hydrothermal illitization of feldspars	48
5.3.2	Exhumation and flushing of the fault	50
5.4	Conclusion	51
6	SYNTHESIS AND DISCUSSION	
	Abstract	
6.1	Introduction	52
6.2	Mineral reactions and clay formation	53
6.3	Mechanisms of illite crystallization	58
	6.3.1 Development of platy hexagonal illite	60
	6.3.2 Development of lath and fibrous illite	60
6.4	Fabric development	61
6.5	History of alteration and fluid-rock interaction	64
	6.5.1 Permian mineralization	65
	6.5.2 Mesozoic mineralization	67
6.5.3	Cenozoic mineralization	69
6.6	Concluding remarks	71
	LITERATURE LIST	73
	APPENDIX	88

List of symbols and abbreviations

α	Mean of the natural logarithms of the crystallite sizes
Å	Ångstrom ($10\text{Å} = 1\text{nm}$)
Ab	Albite
AEM	Analytical Electron Microscopy
β^2	Variance of the natural logarithms of the crystallite
Bt	Biotite
B-W-A	Bertaut-Warren-Averbach-method (calculation of crystallite thickness)
Cps	Counts Per Second (intensity)
CTD	Crystallite thickness distribution
cv	Cis-vacant
E	East
FWHM	Full Width at Half Maximum
Gly	Ethylene-glycol
G^2	Specific structural factor
Hem	Hematite
(HR)TEM	(High resolution) transmission electron microscope
ICP-MS	Inductively Coupled Plasma – Mass Spectrometry
I	Illite
I/S	Illite-smectite mixed layering
Kfs	Potassium feldspar
Kln	Kaolinite
km	Kilometer
Lp	Lorentz-polarisation
m	Meter
m.r.d.	Multiples of random distribution
N	North
nm	Nanometer
Pl	Plagioclase
PVP	Polyvinylpyrrolidone
Qz	Quartz
SAED	Selected Area Electron Diffraction
SEM	Secondary Electron Microscopy
SEM-EDX	SEM-Energy Dispersive-X-ray-spectroscopy
Sm	Smectite
S	South
tv	Trans-vacant
W	West
wt%	Weight percent
XRD	X-ray Diffractometer
XTG	X-ray texture goniometry
μm	Micrometer

SUMMARY

The following study deals with the fluid-alteration history of fractured and faulted crystalline granitic basement in the Rhine rift system, based on the analytical investigation of clay mineral assemblages. This region is particularly suitable for such a study because of the well preserved Tertiary rift structure and the diverse geological development of the drilled and exposed basement rocks. The granitic rocks belong to a series of Late Variscan intrusions of Carboniferous age (ca. 330-335 Ma). These rocks were then exhumed to the surface during Late Carboniferous/Early Permian times and locally influenced by Permian (ca. 290 Ma) volcanic activity and hydrothermal activity. A series of rift events are documented to occur during both Mesozoic and Cenozoic times associated with the North Atlantic extensional activity. On a broader European scale, many of these phases were associated with enhanced geothermal conditions and hydrothermally related mineralization. The most prominent rift phase evident today is the Cenozoic intracontinental Rhine system. However, despite the young age of this structure and the large amount of studies conducted on sedimentary basin, the nature of cogenetic mineralization in the underlying basement rocks is not well defined.

This thesis evaluates the argillite mineralizations along faults and fracture zones at key tectonic positions in relation to the upper Rhine graben rift structure. It assesses the timing and episodic nature of clay mineral formation that occurred within both the buried basement rocks and similar exhumed units exposed in the uplifted rift shoulders. The rock alteration history is established largely on the basis of combined X-ray diffraction, X-ray textural goniometry, electron microscopy and isotopic (K-Ar) techniques. Special emphasis is also given to detailed examination of the fault rock material by transmission electron microscopy, allowing insight into the clay mineral microstructure and composition at the nanometer-scale.

Following an introduction to the study, the geological setting and the analytical techniques used, the results are presented in three main chapters (4-6). The fourth chapter presents results from the granitic basement rocks of the 2230m deep EPS-1 drilling site at Soultz-sous-Forêts, situated in the western part of the Upper Rhine graben basin (France). Pure illite without any sign of mixed-layerings could be distinguished in the different hydrothermal altered and fractured granite and argillite veins. The morphology of these illites varies clearly in the different rock types, with pseudo-hexagonal, platy $2M_1$ illite polytypes dominating the veins and thin and fibrous to lath shaped $1M$ trans-vacant illite polytypes common in pores of the granite matrix. The separated grain size fractions ($> 63\mu\text{m}$, $10-63\mu\text{m}$, $4-10\mu\text{m}$, $2-4\mu\text{m}$, $1-2\mu\text{m}$, $0.4-1\mu\text{m}$, $0.2-0.4\mu\text{m}$, $< 0.2\mu\text{m}$) indicate mixtures of both illite shapes and polytypes to characterize all samples, which based on K-Ar isotope results, occurred during three main crystallization episodes spanning over 200 Ma in time. The oldest illite crystallization recognized is of Permian age, which is most evident in the argillite veins (2176m) and samples of hydrothermally altered granite (e.g. 1570m). In contrast, a mixture of Jurassic and Cretaceous (or younger) illite was recorded in fractured rocks at 2167m, but Tertiary K-Ar values were not encountered in the limited amount of sample studied here. Younger Tertiary ages have, however, been reported in other studies. The multiple episodes

of local illite crystallizations are suggested to reflect the range of fluid events documented from quartz fluid inclusions. The Permian vein mineralization probably relates to the high temperature CO₂-rich fluids and the Mesozoic and Cenozoic illite to the younger, lower temperature saline brines. On the basis of the mineral characteristics presented, it is also suggested that the 2M to 1M transition was favored by lowering of the rock permeability and the related increase in the state of fluid saturation, which occurred during successive episodic crystallization and progressive sealing of the granite.

The fifth main chapter presents the results from the uplifted shoulder locality of the Schauenburg Fault, near Heidelberg. These fault rocks occur along a E-W trending dextral oblique-slip fault (displacement ca. 100m), which separates the Variscan Heidelberg granite from younger Permian volcanics. In comparison to the Soultz-granite, the alteration assemblages of the Schauenburg indicate a retrograde sequence of fluid-controlled, low-temperature clay mineral reactions, ranging from Jurassic times to more recent activity during uplift of the rift shoulder. The progressive decrease in fluid temperatures caused a back-reaction of 2M₁ illite to 1M_d (R3) illite-smectite, as well as smectite and kaolinite. The enhanced rock permeability and fluid movement along the cataclastic fault zone is evident from the illite texture and rock fabric.

The last chapter synthesizes and discusses the different alteration histories of both studied localities of the Rhine Graben rift structure and evaluates the nature of clay mineral reactions and the timing and mechanisms of crystal growth in relation to the history of fluid-rock interaction. Despite the petrological similarities of both Variscan granites, there are notable differences in mineral alteration history. The hydrothermal alteration of the buried Soultz-sous-Forêts granite shows a number of episodic pure illite crystallization events with repeated transition from 2M to 1M polytypes occurring during Permian, Jurassic and Cretaceous (to younger) time. In contrast, the exhumed Schauenburg Fault rocks document a similar hydrothermal illite crystallization event during the Jurassic, but was subsequently flushed by more dilute meteoric waters attributed to rift shoulder uplift.

ZUSAMMENFASSUNG

Die vorliegende Studie befasst sich mit der Fluid-Alterationsgeschichte des granitischen Grundgebirges im Rheingraben Riftsystem und basiert vor allem auf der Analyse der darin vorkommenden Mineralparagenesen. Wegen seiner granitischen Aufschlüsse und Bohrungen in das kristalline Grundgebirge ist diese markante tertiäre Riftstruktur für detaillierte Untersuchungen der Alterationsprodukte von besonderem Interesse. Die Gesteine des kristallinen Grundgebirges gehören zu einer Abfolge spätvariszischer Intrusionen (ca. 330 Ma), die während dem späten Karbon und dem frühen Perm zum Teil an die Oberfläche gelangten und lokal durch permische vulkanische Aktivität (ca. 290 Ma), sowie hydrothermale Alterationen beeinflusst wurden. Mesozoische und känozoische Mineralisationen im gesamten europäischen Raum werden mit der nordatlantischen Dehnungsaktivität in Verbindung gebracht, wobei viele dieser Phasen ebenfalls mit lokal erhöhten geothermischen Gradienten und hydrothermalen Alterationen assoziiert sind. Trotz zahlreicher Untersuchungen der Sedimente und des granitischen Grundgebirges dieses bekannten intrakontinentalen Riftsystems ist die Entwicklung kogenetischer Mineralisationen noch relativ wenig erforscht.

In dieser Dissertation wurden tonige Alterationsprodukte entlang relevanter tektonischer Störungen und Bruchzonen des Oberen Rheingrabens untersucht. Dabei wurde die zeitliche Abfolge episodisch wachsender Tonminerale sowohl in den tiefen Stockwerken des Grundgebirges als auch den gehobenen Riftflanken bearbeitet. Durch kombinierte Analyseverfahren wie Röntgendiffraktometrie, Texturgoniometrie, Elektronenmikroskopie und Isotopie konnte die lokale Alterationsgeschichte anhand zweier Fallstudien rekonstruiert werden. Von besonderer Bedeutung waren dabei detaillierte Untersuchungen am Transmissions-Elektronenmikroskop, welche Einblicke in die Mikrostruktur und chemische Zusammensetzung der Tonminerale im Nanometerbereich erlaubt.

Der Einleitung der Arbeit folgt der geologische Rahmen, sowie die Beschreibung der analytischen Methoden. Die Ergebnisse werden in drei Kapiteln dargestellt (Kapitel 4-6), wobei das 4. Kapitel die Alterationsgeschichte der granitischen Grundgebirgsgesteine der 2230m tiefen EPS-1 Bohrung bei Soultz-sous-Forêts im westlichen Riftbecken (Frankreich) präsentiert. Reine Illite ohne Anzeichen einer Wechsellagerung wurden dabei aus unterschiedlich hydrothermal alterierten und frakturierten Gesteinen und den darin vorkommenden Adern separiert und untersucht. Die Morphologie dieser Illite unterscheidet sich deutlich in den jeweiligen Gesteinsproben. In den Adern dominieren pseudo-hexagonale, plattige $2M_1$ Illit-Polytypen, in der Matrix treten hingegen bevorzugt dünne, fibrös bis stängelige 1M trans-vakante Illit-Polytypen auf. Alle untersuchten Proben weisen jedoch Mischungen aus beiden Illitformen und -Polytypen auf. Mit Hilfe der K-Ar Datierung von Illiten an unterschiedlichen Korngrößenfraktionen ($> 63\mu\text{m}$, $10-63\mu\text{m}$, $4-10\mu\text{m}$, $2-4\mu\text{m}$, $1-2\mu\text{m}$, $0.4-1\mu\text{m}$, $0.2-0.4\mu\text{m}$, $< 0.2\mu\text{m}$) konnten drei Kristallisations-Episoden über eine Zeitspanne von 200 Ma dokumentiert werden. Die ältesten Illitsignaturen sind permischen Alters, erkennbar sowohl in Adern (2176m) als auch dem hydrothermal alterierten Nebengestein (1570m). Eine Ausnahme bildet die Matrix im frakturierten Bereich (2167m) mit jurassischen

bis kretazischen (oder jüngeren) Illitaltern. Tertiäre K-Ar Alter wurden in dieser Arbeit nicht dokumentiert, treten jedoch in anderen granitischen Gesteinen der EPS-1 Bohrung auf. Diese Ergebnisse weisen auf multiple Episoden lokaler Illit-Kristallisationen durch unterschiedliche Fluidereignisse hin. Frühere Untersuchungen an Quarz-Fluideinschlüssen geben ebenfalls Hinweise auf multiple Fluidepisoden mit verschiedenen Temperaturen und Salinitäten, die wahrscheinlich mit der vermehrten Kristallisation von Illiten in Verbindung stehen können.

Das fünfte Kapitel beinhaltet die Untersuchung der Alteration der kristallinen Gesteine in der Schauenburg Störung nördlich von Heidelberg. Die kataklastischen Gesteine entstammen der E-W streichenden, schrägen Abschiebung (Versatz ca. 100m) mit einem nahezu senkrechten Einfallen in Richtung SSE. Diese Störung versetzt den Heidelberg-Granit gegen den stratigraphisch darüberliegenden Rhyolit. Im Gegensatz zum Soultz-Granit zeigt sich in der Schauenburg Störung eine retrograde, fluid-kontrollierte und niedrig temperierte Sequenz von Tonmineralreaktionen, welche die Alterationsgeschichte vom Mesozoikum bis zur Heraushebung der östlichen Riftflanke beschreibt. Dies dokumentiert eine fortschreitende Abnahme der Fluidtemperatur mit einer Rückreaktion von $2M_1$ Illit zu $1M_d$ (R3) Illit-Smektit zu Smektit und Kaolinit. Die untersuchten Illit-Texturen und -Gefüge belegen erhöhte Gesteinspermeabilitäten mit assoziierten Fluidbewegungen.

Das letzte Kapitel der Arbeit vergleicht und diskutiert die unterschiedlichen Alterationsgeschichten der beiden untersuchten Lokalitäten und evaluiert die Eigenschaften von Tonmineralreaktionen sowie den relativen zeitlichen Ablauf und den Mechanismus von Kristallwachstum in Bezug zur Fluid-Gesteins-Wechselwirkung. Trotz der äußerlich petrologischen Ähnlichkeiten der beiden variszischen Granite des Oberrheingrabens zeigt sich eine komplexe und unterschiedliche Alterationsgeschichte der jeweiligen Gesteine. Die hydrothermale Alteration des im Meso- und Känozoikum versenkten Soultz-sous-Forêts Granits zeigt eine Anzahl von episodischen Illit-Kristallisations-Episoden mit wiederholter Kristallisation von $2M$ und $1M$ Polytypen im Perm, Jura und Kreide (oder später). Die exhumierten Gesteine der Schauenburg Störung dokumentieren eine ähnliche hydrothermale Illit-Kristallisation im Jura, wurde jedoch anschließend durch die Hebung der Riftflanken bis heute stark durch meteorische Wässer beeinflusst.

1 INTRODUCTION

Studying clay formation, fluid-flow and faulting is an important aspect of understanding upper crustal processes. Clay minerals are common constituents of soils, sediments, compacted sedimentary rocks and alteration zones associated with igneous and metamorphic rocks. They are very fine-grained, (particulate) hydrous minerals which form within water-rich environments ranging from the surface to depths of < 10km, characterized by diagenetic, very low-grade metamorphic or hydrothermal conditions. In the crustal regime, clays are typical of low temperature, hydrous fluid-dominated and permeable environments, as found within fault and fracture zones of brittle deformed rocks (Evans 1990, Fisher & Byrne 1990, Knipe 1993, Warr & Cox 2001). The main focus of this thesis was to investigate the nature of fault rock mineral assemblages from the micron- to nano-scale by high-resolution microscopy and X-ray diffraction techniques. In combination with K-Ar isotope techniques, results were used to establish alteration processes and the history of fluid-rock interaction for the studied fault and fracture zones of the Rhine Graben rift system.

1.1 Faulting and fluid-rock interaction

Faults and fracture systems present ideal sites to investigate mineral alteration and to assess the interplay between faulting, fluid migration and clay formation. When tectonic stresses in the upper crust are released during faulting, motion along the fault plane commonly results in brittle deformation and cataclastic breakdown into very fine-grained fault rocks. The principle planes of displacements within fault zones are therefore frequently characterized by layers of cataclasite or more incoherent fault gouge. Traditionally, such fine-grained gouge material (often referred to as clay gouge) was viewed largely as a result of mechanical breakdown of particles during brittle deformation (e.g. Sibson 1977, Chester & Logan 1986, Rutter et al. 1986). More recent studies, however, have shown that mineral reactions associated with fluid flow are also important in the formation of fine-grained fault rock (Vrolijk & van der Pluijm 1999, Sibson 1994, McCaffrey et al. 1999). Wintsch et al. (1995), for example, showed how different minerals precipitated as veins and hydrothermal alteration of the fault rocks can lead to varying mechanical behavior of brittle faulting in granite. Rock alteration and mineral growth processes clearly influence the porosity and permeability of rocks (Sausse et al. 1998, Surma & Geraud 2003) and thus are of central importance in determining fault rock strength. The formation of micas due to feldspar hydrolysis and a resultant lowering of the shear strength were also observed in exhumed granitic fault zones of the San Andreas Fault (Wu et al. 1975, Janecke & Evans 1988). Such alterations can lead to improved rock fabrics within clay shears and locally influence the anisotropy permeability, porosity and therefore fault strength (Morrow et al 1984, Wintsch et al. 1995, Wibberley 1999, Warr & Cox 2001). A number of models have been developed based on fluid-induced reaction weakening, and this mechanisms has been put forward to explain the creep behavior along some segments of the San Andreas Fault (e.g. Hickman & Evans 1992, Chester et al. 1993).

The formation of clays in fault rock may occur pre-, syn- or post-fault activity. In some cases

faults may form along pre-existing, clay-rich horizons: a principle well known from landslides (Wen & Aydin 2003, Egashira et al. 2000). Clay formation can also occur in response to the earthquake cycle. This is particularly characteristic of large slip events, when dilation along the fault plane leads to the rapid influx of fluids. These fluids then drive mineral reactions during the longer interseismic periods (Chester & Logan 1986, Chester et al. 1993, Warr & Cox 2001). The third origin of fault rock clays are those formed once the fault is no longer active. This occurs when the structure is not well sealed, and continues to be a site of fluid migration. In this case, the fine-grained nature of the fault rock material is particularly susceptible to alteration in the presence of hydrous fluids.

Although clay minerals can form in all faults of the Earth's crust characterized by the presence of hydrous fluids, a particularly interesting setting to study clay-bearing fault rocks are the thermally active extensional rift zones. Continental rift zones are formed in response to horizontal extensional stresses within the lithosphere, and are commonly over 1000km in length. Numerous rift zones are known around the globe, some of the well studied examples are the North Sea graben, the East-African rift system and the Rhine Graben rift of Western Europe. In such rifts, the enhanced temperatures and fluid circulation, in association with brittle fracturing, are ideal conditions for driving fault-related hydrothermal mineral reactions and clay formation.

1.2 Clay formation and fluids in hydrothermal environments of the Rhine rift setting

It is well known that some areas of the Rhine rift have high thermal gradients up to 100°C/km, which are typically associated with intense hydrothermal alterations. The best known example is the Soultz-sous-Forêts site, in the Alsace region of France, which is one of the case studies presented in this thesis. A general east-west directed fluid-flow through the rift has been postulated, which alters the sediments and underlying granite basement (Gérard et al. 1984, Clauser & Villinger 1990, Flores-Marquez & Royer 1993). These fluids are considered to originate from circulating meteoric waters, driven primarily by topographic flow from the higher rift flanks to depths, leading to the formation of higher temperature brines and extensive fracture related rock alteration and mineralization (Lampe et al. 2001, Aquilina et al. 1997, Pribnow & Clauser 2000, Stober & Bucher 2004; Fig. 1.1).

Such hydrothermal environments are well known and have been studied in a large range of surface and upper crustal locations. Notable examples are the volcanic rocks of the Broadlands-Ohaaki hydrothermal system, New Zealand (Yan et al. 2001, Peacor et al. 2002), the shales of the Salton Sea geothermal system, California (Kim & Peacor 2002), the volcanoclastic sediments of the active Kakkonda hydrothermal system, Japan (Inoue & Kitagawa 1994, Inoue et al. 2004) and the rhyolitic hyaloclastite of Ponza Island, Italy (Ylagan et al. 1996). Based on analyses of clay minerals, variations in formation mechanisms and controlling parameters with depth can be related to the alteration of rocks by hydrothermal solutions.

A large amount of data is available on the chemistry of water samples from various boreholes and thermal waters in the Rhine Graben rift complex and adjacent areas (Carlé 1958, Aquilina et

al. 1997, Stober & Bucher 2000, Durst & Vuataz 2000). The hot waters ($> 137^{\circ}\text{C}$) collected from the Soultz-sous-Forêts or the Cronenbourg borehole sites in basement granite of the rift basin yielded weakly acidic (pH 4.7–5.2) saline brines containing significant concentrations of NaCl, as well as Li and Sr (Pauwels et al. 1993, Aquilina et al. 1997). Similarly weak acidic NaCl brines are reported from the Black Forest crystalline rocks outside of the rift basin to the east (Stober & Bucher 2000). In the Urach 3 borehole, reliable water brines with temperatures of 150°C were recovered from depths of 3.3–3.4km (Stober & Bucher 2004, Durst & Vuataz 2000) with a pH between 4.2 and 5.9.

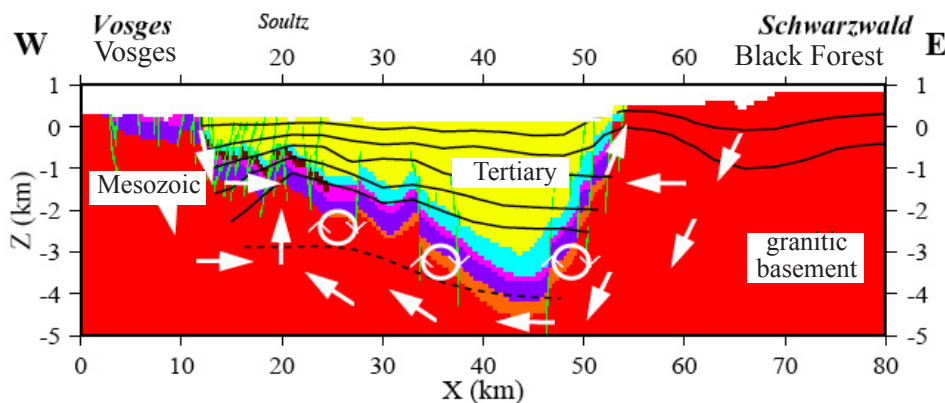


Fig. 1.1: Schematic diagram of the fluid flow along the cross section through the Upper Rhine Graben (Pribnow & Clauser 2000). Subvertical structures are fault zones. The arrows indicate the flow direction

Saline, thermal waters are also found along the flanks of the Rhine Graben shoulder (see Fig. 2.2a, page 7). NaCl thermal waters and radium-bearing Ca-brines occur at Baden-Baden, and also at the Heidelberg thermal borehole drilled in 1939 (Carlé 1975). The Heidelberg borehole was located 1km west of the graben boundary fault, lying just 8km south of the Schauenburg Fault locality, which reflects the second case study investigated. The exceptionally saline nature of the Heidelberg water recovered from 998m depth was attributed to the interaction with Miocene salts (Carlé 1975). The high carbonate content and neutral to slightly alkaline character of these solutions is not typical of the crystalline brines described elsewhere in the region. At shallower levels in the borehole (411m and 570m), the saline waters are diluted by meteoric solutions and show clear signs of organic matter reactions (sulphur-bearing). More diluted and mixed waters, transitional between saline brines and meteoric solutions, are documented along the Rhine flank in this region by Bender (1995), with radiogenic isotope contents of these waters indicating residence times of up to 35 000 years at 3000m depth.

1.3 Motivation and selection of localities

The motivation of this study was to investigate in detail clay mineral formation processes in faulted crystalline (granitic) basement rocks of the Rhine rift system and to relate the alteration history to the geological history of the fault zones studied. For this purpose, two localities were selected as case studies, both offering excellent opportunities to investigate alteration processes in different parts of the graben structure. The first case study presented was conducted at the Soultz-sous-Forêts thermal energy site; a deep drilling project into a horst structure of the granitic basement beneath the rift sedimentary succession. Samples were selected from depths between 1431m and 2176m (see appendix). The second case study was conducted in the uplifted shoulder of the rift system just north of Heidelberg. Here, the E-W striking Schauenburg Fault zone forms a vertical contact between the Variscan Heidelberg granite and the overlying Permian rhyolite. Samples from the granite, the cataclasite and the rhyolite were taken across a distance of 500m (see appendix), obtained during the archaeological trenching of the Schauenburg castle site. Unfortunately due to refilling of the trench, the fault is no longer exposed today.

Based on X-ray techniques (XRD, XTG), electron microscopy (SEM, HRTEM) and K-Ar isotopic investigations of the clay minerals, the two case studies were conducted with the following objectives:

- 1) To characterize the alteration products that result from fluid-rock interaction along faults and fractures within the crystalline basement rocks of felsic composition
- 2) To assess the relation between clay growth, fluid-rock history and fabric development over time within the different parts of the Upper Rhine Graben system
- 3) To reconstruct the mineral reactions and microstructural changes, which occur at the crystal lattice scale in fault-related mineralizations. Particular emphasis is given to the formation mechanisms of the clays (e.g. layer-by-layer replacements versus dissolution and neocrystallization)
- 4) To evaluate the timing of clay mineral reactions in relation to the geological history of the Rhine rift fault rocks

2 GEOLOGY

2.1 Introduction

Granitoids and their metamorphic equivalents, which make up around 75% of the Earth's crust (Dietl 2000), are the most abundant basement rocks of the continental crust and form the major part of crystalline rocks exposed at the surface. In the Rhine rift area, a number of granitic outcrops and deep drillings have been well documented, in particular in relation to their origin, evolution and thermal fluid-rock history (Illies 1963, Altherr et al. 1999, Stein 2001, Greiling & Verma 2001, Echtler & Altherr 1993, Genter & Traineau 1991, Prier 1969, Lippolt et al. 1990, Maurin & Niviere 2000, Schumacher 2002).

The two granite bodies investigated in this thesis are both situated in the Rhine rift area (the Soultz-sous-Forêts granite and the Heidelberg granite) and formed as Late Paleozoic, Variscan subduction related I-type intrusions (Flöttmann & Oncken 1992) generated beneath the Mid-German Crystalline High of the Saxothuringian Zone (Henes-Klaiber 1992; Fig. 2.1).

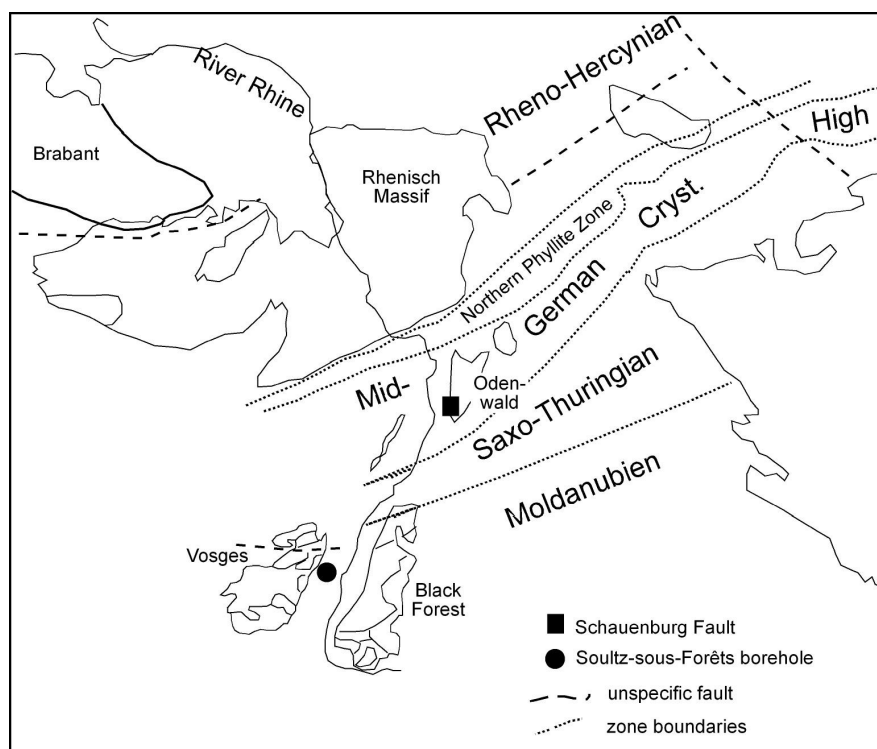


Fig. 2.1: General geological map of the European Variscan orogenic belt (modified after Dallmeyer et al. 1995) and the position of the Upper Rhine Graben with the both localities investigated

These intrusions belong to a group of granite plutons that intruded into the western part of the central European Variscan orogenic belt during Mid-Carboniferous times. This period of intrusion occurred during an NW-SE directed orogenic compression in Carboniferous times and was followed by a transition to E-W directed lithospheric extension in the Permo-Triassic. The latter development was accompanied by large-scale wrenching and block rotations (Blès et al. 1989, Ziegler 1993, Oncken 1998, Edel et al. 2003, Illies 1962).

2.2 Post-granite history and thermal activity in the Rhine rift area

The Variscan granites of the Rhine rift area were affected by a complex tectono-thermal alteration history, that was accompanied by intense hydrothermal mineralizations caused by the circulation of hot, highly saline fluids (Bartels et al. 2000, Lampe et al. 2001, Pauwels et al. 1992). During Late Carboniferous and Early Permian, western Europe was characterized by a period of widespread basin formation, accompanying magmatic activity and elevated geothermal gradients. Extensive Late Palaeozoic volcanism, in combination with the widespread development of faults and dykes in the northern Variscan foreland, favored increasing heat transport and enhanced fluid circulations (Benek et al. 1996).

Widespread mineralizations of Jurassic age led to abundant ore and mineral deposits across central Europe and along the Palaeo-Atlantic margins, suggesting mobilization and migration of fluids over a large scale (Mitchell & Halliday 1976). The Rhine rift area was also affected by this mineralization event, and a number of Jurassic K-Ar age data on hydrothermal illite growth are available from a range of different rock types (Marbach 2002, Brockamp et al. 2003), including vein deposits of the Black Forest (Meyer et al. 2000, Brockamp et al. 1994). This points to a range of fluid migration episodes causing extensive alteration along entire fault systems about 150 Ma ago.

2.3 Tertiary rifting

In the Rhine region, Tertiary rifting began its development ca. 45-60 Ma ago. In earlier studies, Illies (1965) suggested that this tectonic structure was formed by the up-doming of the crust-mantle boundary due to magmatic intrusions at a depth between 80 and 100km. This formation was thought to be accompanied by extensive erosion of the uplifted basement and sedimentation into the graben trough. However, Turcotte & Oxburgh (1973) asserted that tensional stresses in the continental lithosphere caused the failure of the rift, allowing hot mantle rocks to penetrate the lithosphere, accompanied by crustal doming and volcanic activity occurring as a later, secondary process.

The uplifted shoulders of rift systems may be explained by two basic mechanisms: thermal and/or flexural uplift. Whereas stretching of the subcrustal lithosphere in an upward tapering region can lead to a wider zone of diffuse mantle stretching and additional heating causing thermal uplift (Allen & Allen 1990), flexural uplift occurs in response to the sediment load (Kooi & Cloetingh 1992, McKenzie 1978). Once initiated, subsidence in the Rhine rift was accommodated by reactivation of old Variscan fault zones in the Early Pliocene 40-35 Ma ago (Illies 1968). By the middle Oligocene, fault activity had shifted northward, with increased thermal and flexural uplift of the graben shoulders leading to exhumation of the Variscan granite within the rift flanks (Laubscher 2001). Today, the Rhine rift is characterized by a high surface heat flow (ca. 80mW/m², Schulz & Schellschmidt 1991), whose origin is explained by fluid convection in the upper crust and rapid redistribution of the heat not thought to be related to crustal thickness (Werner & Doebl 1974, Elsass et al. 1995, Pribnow & Schellschmidt 2000).

2.4 The Rhine rift system and the selected localities of the study

The Rhine rift forms the central segment of the European Cenozoic rift system that extends over a distance of more than 1000km from the North Sea to the Alpine mountain chain (Illies & Fuchs 1974, Prodehl et al. 1995). Limited by the Rhenish Massif (Frankfurt, Germany) in the north and the Jura Mountains (Basel, Switzerland) in the south, the NNE trending Upper Rhine Graben has a more restricted length of about 300km and a width of ~ 30-40km (Schumacher 2002; Fig. 2.2a). This part of the graben is filled with a thick sequence (3000-3400m) of post-Cretaceous sediments (Illies 1968), and the vertical offset between the elevated graben shoulders and the basement within the graben reaches a maximum of 4500m.

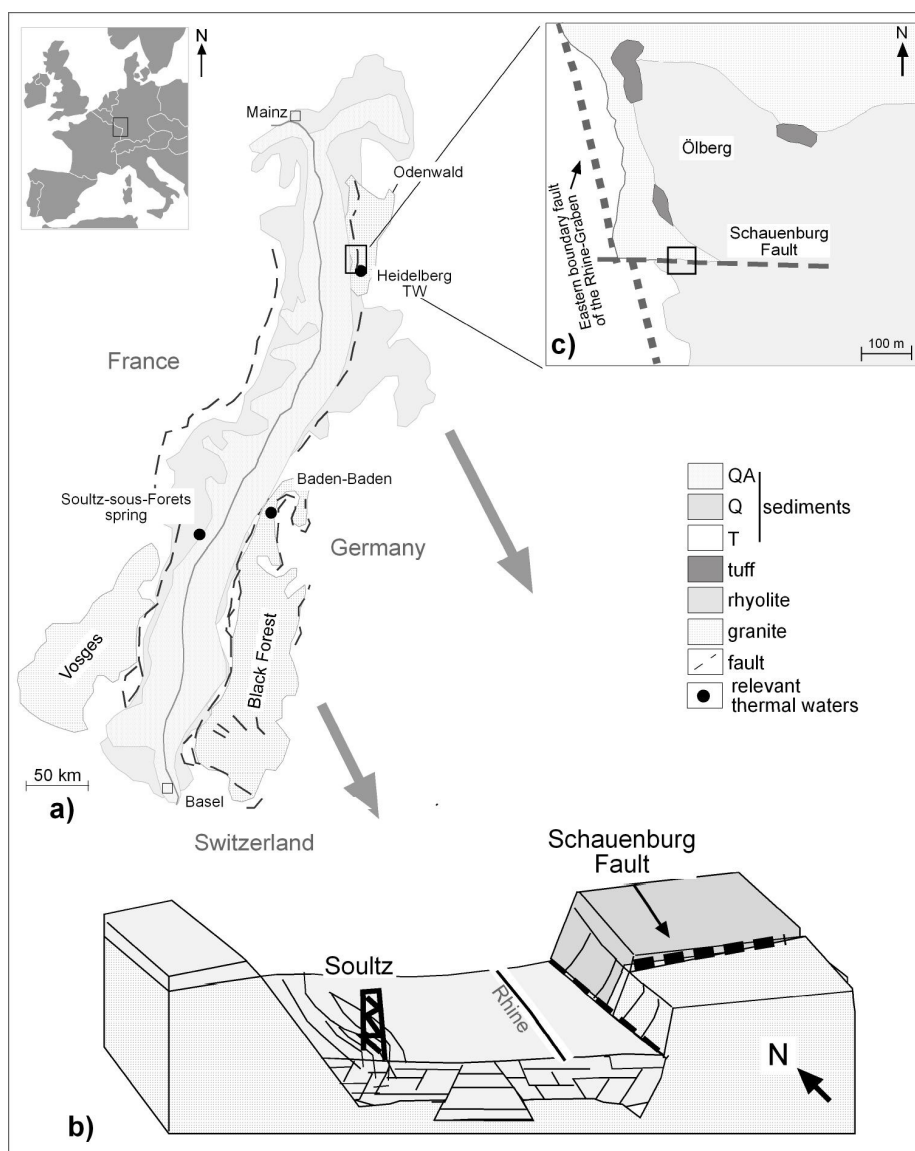


Fig. 2.2: a) Location map showing the Upper Rhine Graben rift and the position of the Soutz-sous-Forêts hydrothermal borehole and the Schauenburg Fault. (QA: Quaternary Alluvium, Q: Quaternary, T: Tertiary), b) the schematic geological cross-section presents an E-W profile across the Rhine rift, with both localities investigated. The vertical scale is exaggerated, c) the map is modified after Andrae & Osann (1907) and shows the Schauenburg working area, which is situated at the eastern Rhine rift shoulder in the Odenwald forest, north of Heidelberg

2.4.1 The Soultz-sous-Forêts granite

The Soultz-sous-Forêts granite is located in the northwestern region of Alsace (France) and forms part of the crystalline basement buried beneath the western part of the Tertiary Upper Rhine rift system (Fig. 2.2b). Due to the high geothermal heat flow (up to 100°C), it has been selected as a test site for thermal energy and is currently being investigated within the framework of the European „Hot Dry Rock“ project (Genter et al. 2000). In the 2230m deep EPS-1 borehole, located in a N-S striking horst structure, the contact between sedimentary cover rocks and the granite was encountered at a depth of 1420m.

The investigated granite belongs to a series of late to post-tectonic Variscan granitoids that occur in the Vosges mountains, and have been dated by various isotopic methods (Bonhomme et al. 1975, Montigny & Faure 1969). The Soultz-sous-Forêts granite is a porphyritic variety with K-feldspar megacrysts, quartz, plagioclase, biotite, hornblende and accessory apatite, titanite and magnetite (Genter & Traineau 1991). Its age of crystallization has been dated by Alexandrov et al. (2001) to be 331 ± 9 Ma based on U-Pb dating of zircons. It is well established that the entire pluton was affected by an early hydrothermal pervasive (propylitic) alteration, followed by more localized fluid percolations inducing siliceous and argillitic vein assemblages, as well as fracture related younger mineralizations (Sausse et al. 1998). The secondary vein minerals are predominantly quartz, barite, pure white mica (illite), mixed-layered illite-smectite (I-S), carbonates and iron oxides, as well as some localized mixed-layered tosudite (Genter & Traineau 1991, Pauwels et al. 1993, Lédésert et al. 1999). Based on fluid-inclusion studies, the earliest stage of pervasive alteration was largely characterized by fluids of moderate salinity (2-7 wt% eq. NaCl) trapped under temperatures of 180-340°C (Dubois et al. 1996). However, vein quartz was also formed from lower temperature brines (ca. 150°C) of varying salinity (Smith et al. 1998).

Although a significant number of studies have been undertaken to characterize the nature of hydrothermal alteration in the Soultz-sous-Forêts granite, little attention has been given to the characterization of the illite and isotopic dating of these mineral phases. Despite the general lack of age constraints, many of the fractures and associated argillitic mineralizations are often assumed to be relatively young and are attributed to Oligocene (or younger) rifting episodes in the Rhine Graben (Dubois et al. 1996, Genter & Traineau 1996, Elsass et al 1995).

2.4.2 The Heidelberg granite and Permian rhyolite

The Heidelberg granite is situated in the Odenwald, at the eastern flank of the Rhine Graben and belongs to the “Bergsträßer Odenwald” crystalline massif, the largest continuous outcrop of the Mid-German Crystalline Rise (Kossmat 1927, Fig. 2.1). This intrusive complex consists of gabbros and diorites, that were successively intruded by granodiorites and granites (Okrusch et al. 2000), whereas the intrusion depth for the quartz-diorite and the granite was estimated to be about 15km (Altherr et al. 1999). U-Pb dating on single zircons provided concordant intrusional ages for the Heidelberg granite of 342 and 332 Ma (Hess & Lippolt 1996) and recorded well defined $^{40}\text{Ar}/^{39}\text{Ar}$ ages of 332 ± 3 and 328 ± 1 Ma obtained on hornblendes and sericite-free plagioclase,

confirming earlier K-Ar and Ar-Ar dates around 335 Ma (Lippolt et al. 1990).

The Permian rhyolite was derived from a single volcanic source at the “Wachenberg” in Weinheim (Odenwald), which formed the eruptive centre. The southern rhyolitic lava flow of Schriesheim-Dossenheim was supplied by this volcanic center, forming widely distributed tuff layers (Okrusch et al. 2000, Flick 1986, Prier 1969). Geodynamically this stage of volcanism was not related to syn-orogenic granites, but such volcanism is related to late to post-orogenic granite intrusions elsewhere in the Variscan orogenic belt. $^{40}\text{Ar}/^{39}\text{Ar}$ age measurements on sanidine, biotite and muscovite in the overlying Permo-Carboniferous rhyolite give an age of 291 ± 6 Ma. Compared to the ages obtained from plutonic rocks of the Odenwald, an age difference of about 45 to 55 Ma exists between plutonism and rhyolitic volcanism (Hess & Lippolt 1996).

2.4.2.1 The Schauenburg Fault

The E-W trending Schauenburg Fault is situated along the eastern Rhine Graben shoulder, close to Heidelberg (Fig. 2.2) and is positioned ca. 280m above the level of the graben flat, forming a vertical contact between the outcropping Permian rhyolite and the Carboniferous (Variscan) granite (Fig. 2.2c, Fig. 5.1 page 36). Geological mapping of this clay-rich fault zone reveals an oblique dextral strike-slip displacement of ca. 100m, with a down-throw to the south (Schleicher 2001). This fault intersects and appears to off-set the N-S trending Rhine Graben bounding fault just 100m to the west (Fig. 2.2c). Due to faulting, the granite-rhyolite structural contact has been altered to a weak, clay-rich cataclastic material, where locally the original igneous textures are no longer evident (Fig. 5.1 page 36).

The geochemistry and isotopic signature of the Schauenburg Fault has been recently reported by Marbach (2002) and Marbach et al. (in press). Rare earth elements are notably concentrated along the fault zone, indicating a shift in chemical environment from reducing to oxidizing conditions. A whole rock Rb-Sr isochron of the altered granite yielded a late Jurassic age, interpreted to represent hydrothermal alteration. Based on U-Th redistribution in the cataclasite, a younger event of between 100,000 years and 1 Ma was recognized (Marbach 2002), whereby the youngest signatures (Quaternary) were attained from the margins of the altered fault zones, rather than from its centre.

3 ANALYTICAL METHODS

The analytical tools used in this study are presented in this section and the basic principles are briefly outlined. More specific details concerning sample preparation, analytical procedure and a summary of the equipment are given in the individual case study chapters (4 and 5) and in the appendix.

3.1 X-ray diffraction

X-ray diffraction (XRD) is one of the most important methods used to identify and characterize clay minerals. It allows description of the unit cell and gives crystal-chemical information concerning individual mineral phases, as well as quantification of mixed-layered structures. The basics of X-ray diffraction analyses, methodology and applications are given in Brindley & Brown (1980), Jasmund & Lagaly (1993) and Moore & Reynolds (1997).

The diffraction of X-rays occurs at specific lattice layers containing a continuous spatial configuration of atoms in a crystalline substance. The X-rays are generated when high-energy electrons are released from a heated filament in a X-ray tube and accelerated to a Cu anode. The resulting radiation emerges from a thin beryllium window, and is focused to produce a sub-parallel beam which is directed onto the sample. The coherence between the wavelength of the incident beam, the angle of incidence and the lattice spacing in the crystal structure can be described according to Bragg's Law:

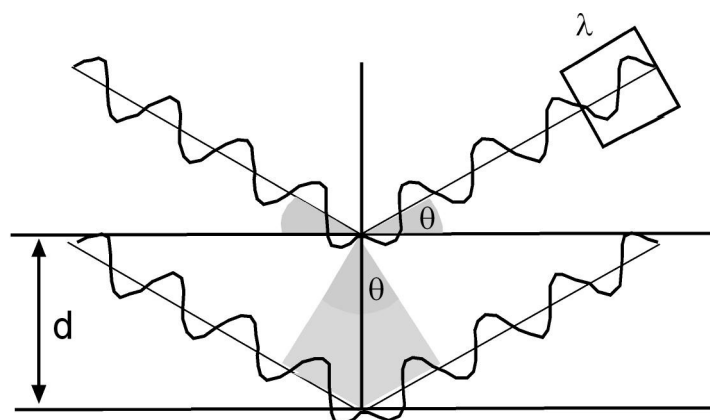


Fig. 3.1: Bragg's law and the diffraction of waves by crystal lattices

$$n \lambda = 2d \sin \theta$$

with n = integral number of wavelengths; λ = wavelength of the X-rays; d = lattice spacing (\AA); θ = angle of diffraction. The diffracted beam passes through a crystal-monochromator, which filters unwanted radiation and enters the detector. In the resulting X-ray diffraction pattern, the horizontal scale is conventionally presented as the 2θ angle and the vertical scale as the intensity of diffracted radiation (Fig. 3.2).

3.1.1 Identification of clay mineral phases

Clay minerals can be routinely identified from X-ray diffraction patterns measured on oriented aggregates that enhance the intensities of the characteristic basal (001) reflections (Fig. 3.2). The hkl reflections measured on unoriented powder preparations are also important for identifying dioctahedral and trioctahedral varieties as well as polytype structure. (Moore & Reynolds 1997). Clay mineral diffraction peaks can be defined by their peak position (d-value), intensity, shape and also width (Fig. 3.2). Whereas the d-value of the peak can be easily determined by Bragg's law, the relative (001) peak intensity is controlled by a range of factors, namely chemical composition, the positions of atoms in the unit cell and some instrumental effects. The peak width (expressed as the full-width-at-half-maximum) can provide information about the mean crystallite size (for example using the Scherrer equation) and also the presence of mixed-layered minerals. For XRD peaks reflecting pure mineral phases, the shape of the reflections can be used to calculate the thickness distribution of X-ray scattering domains (crystallites) as well as lattice distortion (microstrain) effects (Eberl et al. 1996). In addition to mineral identification, quantification of illite and quartz components in selected samples was undertaken using the mineral standard mixtures and calibration curve of Rügner (2000).

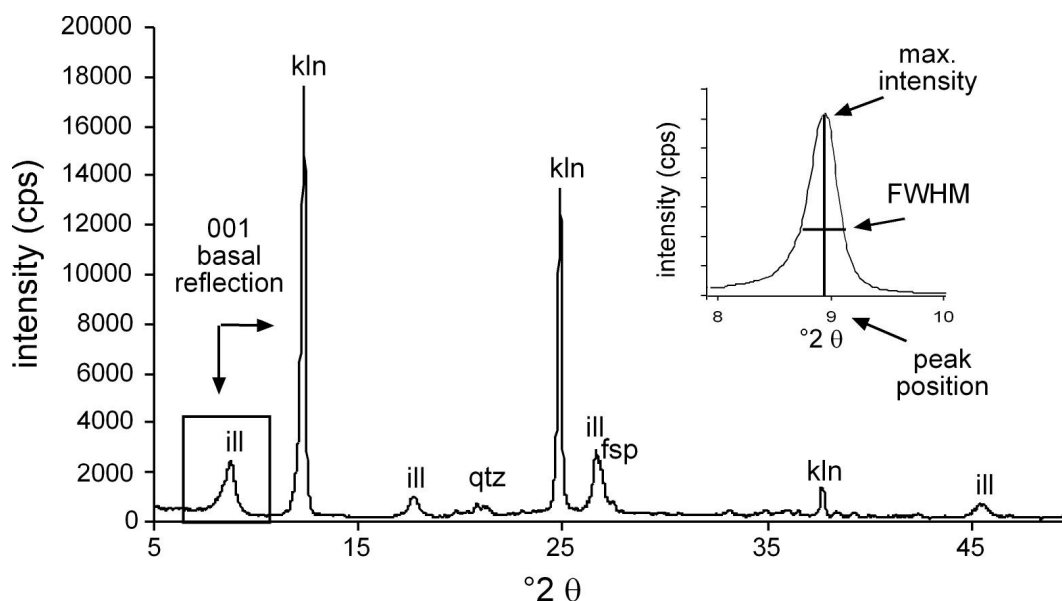


Fig. 3.2: X-ray diffraction diagram showing a texture sample of an altered granite with typical reflections of illite (ill) and kaolinite (kln).

Clay mineral identification was also aided by comparison with simulated XRD patterns using the computer program NEWMOD (Reynolds & Reynolds 1996). This tool was used primarily to investigate the nature of mixed-layered structures, such as the abundance of illitic and smectitic components and the degree of ordering (Reichweite). A more detailed description of this program is outlined in Moore & Reynolds (1997) and Reynolds & Reynolds (1996).

3.1.2 Peak behavior of clay minerals after glycolization and heating

An important aspect of successful clay mineral identification is to use the sensitive behavior of these minerals to changes in physical-chemical conditions in the laboratory. For example, expandable (swelling) clay minerals show structural changes in the c-direction by absorption of water-layers into intracrystalline sites. The amount of water-layers incorporated depends strongly on the interlayer cations and the relative air humidity. The sorption of organic compounds can also be used to identify smectitic materials. Here, ethylene-glycol ($C_2H_6O_2$), glycerine ($C_3H_8O_3$) or polyvinylpyrrolidone (PVP) can be used to cause large expansion of the lattice layers to characteristic d-values suitable for identification of the swelling clays (Bradley 1945). These treatments are particularly useful in aiding the identification and quantification of mixed-layered minerals, such as illite-smectite.

Another important aspect in identification of clay minerals is to use changes caused by thermal treatment. Heating causes dehydration and dehydroxylation of the phyllosilicate structures, with a breakdown of the lattice distances at characteristic temperatures. These temperatures commonly lie between 350°C and 550°C and can be used to aid mineral recognition. For example, kaolinite dehydroxylates at 450-500°C, whereas illite and chlorite are stable to ca. 550°C. The different types of Fe- and Mg-chlorite also show contrasting thermal behavior.

3.1.3 Calculation and modelling of crystallite thickness distribution

MudMaster (Eberl et al. 1996) is a computer program that calculates the crystallite thickness distribution (CTD) for minerals from X-ray diffraction data and is based on the fact that XRD peaks are broadened as a function of decreasing crystallite size (Eberl & Velde 1989). MudMaster uses X-ray diffraction peak shapes of single phased minerals to calculate the mean crystallite size distribution according to the Bertaut-Warren-Averbach method. This method extracts the information from the interference function by first calculating and removing the broadening effects of the Lorentz-polarisation (L_p) and sample specific structural factors G^2 . The theoretical background of these effects (L_p , G^2) is outlined in Moore & Reynolds (1997).

Using the (001) illite peak measured by XRD, crystallite sizes can be calculated and plotted by comparison against theoretical lognormal curves (Fig. 3.3). In order to obtain the excellent particle orientation, a special ultra-thin clay film was prepared using a silicon single-crystal glass slide (Schliephake 1970). This substrate produces less background interference in comparison to conventional glass or synthetic slides. The MudMaster results give averaged crystallite thickness, the crystallite size distribution and calculates shape parameter α and β^2 (α = mean of the natural logarithms of the crystallite sizes is calculated from the distribution, β^2 = the variance of the natural logarithms of the crystallite size is calculated from the distribution). For crystallite thickness distributions that are considered to represent mixtures of more than one size population, the program “Unmixer” was used to decompose individual components assuming each to be lognormal in shape. This program was kindly provided by D. Eberl of the USGS.

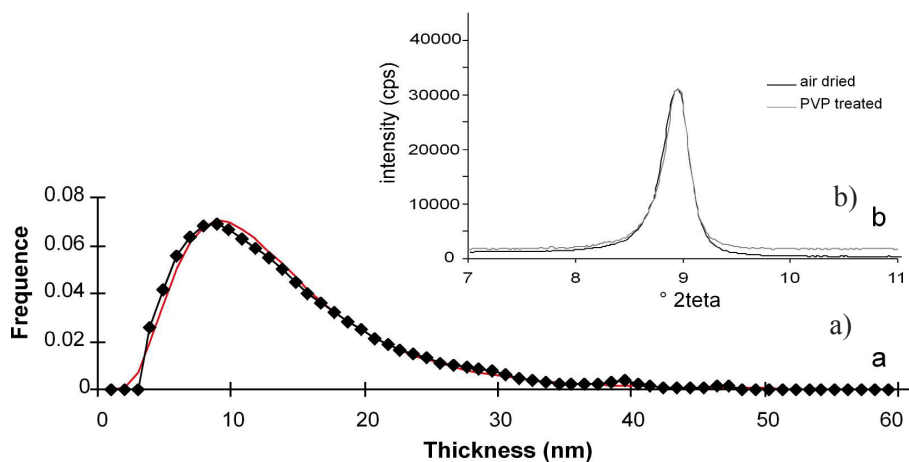


Fig. 3.3: a) Crystallite thickness distribution (CTD) of a sample from Sultz-sous-Forêts, calculated with the MudMaster program (Eberl et al. 1996). The log-normal shape is considered to present the dominance of a single illite phase, b) the X-ray diffraction pattern showing no difference between PVP-treated and air dried samples, confirming the lack of smectite interlayers

3.1.4 Illite polytype determination

Polytypism is a form of structural disorder generated by the systematic displacement of lattice layers within a stacking sequence along the crystallographic *c*-direction (Brindley & Brown 1980, Moore & Reynolds 1997). A layer rotation in a mica causes a shift in the X-Y plane of the unit-cell center: a shift normal to the (001) plane results in a 1M cis-vacant polytype (Drits et al. 1993, Reynolds & Thomson 1993); a series of successive 120° rotations makes up a 1M trans-vacant polytype (previous referred to as 3T) and a $\pm 120^\circ$ rotation produces a 2M₁ polytype (Fig. 3.4).

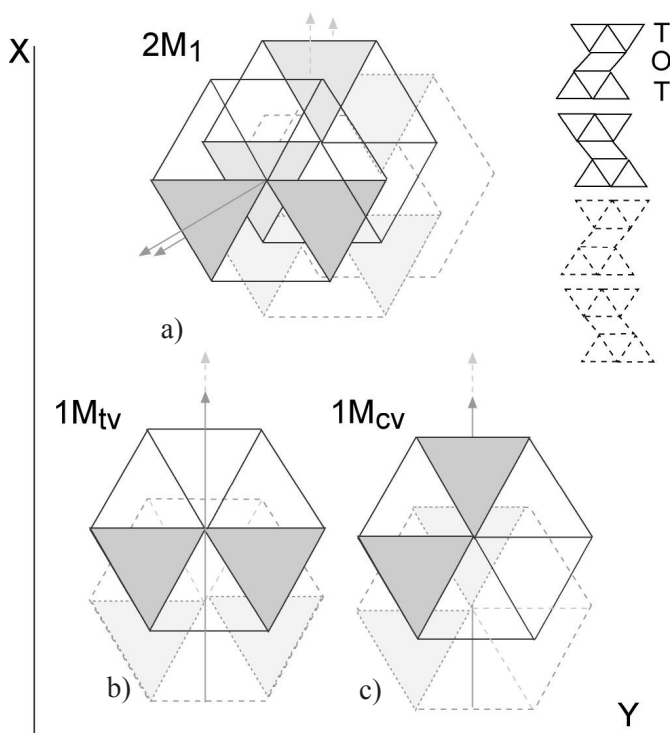


Fig. 3.4: The different illite polytypes modified after Moore & Reynolds (1997) and Meunier & Velde (2004). Layer rotation cause a translation of the unit cell in the X-Y plane, a) rotation plus minus 120° forming the 2M₁ polytype, b)+c) view normal to the (001) plane showing the 1M polytype. The atomic planes are not oriented in the same directions according to the position of the vacant site. These position difference (trans-vacant and cis-vacant) can be identified by X-ray diffraction based on intensity of the 112-112 and 111-113 peaks.

The illite polytype analyses in this study was conducted following the procedure of Laverret (2002) using XRD patterns obtained from randomly-oriented powders, which were measured by slow step scanning between 19 and $34^\circ 2\theta$ ($= 4.67$ - 2.64 \AA). Identification of peaks was based on comparisons with the reference data given by Bailey (1980) and Brindley & Brown (1980) for $1M$ and $2M_1$ polytypes, and Drits et al. (1993) for $1M_{TV}$ ($1M$ polytype with trans-vacant octahedral cation occupancy) and $1M_{CV}$ ($1M$ polytype with cis-vacant octahedral cation occupancy) polytypes. The relative intensities of the hkl reflections strongly differ between the $1M_{CV}$ and $1M_{TV}$ illite polytypes (Drits et al. 1993). The percentage of $1M$ and $2M_1$ polytypes was estimated from the ratio of the (112) and (114) reflections; a value which varies linearly according to the relative abundance of the two polytypes present.

3.1.5 X-ray textural goniometry

The crystallographic-preferred orientation of illite was measured using a X-ray texture goniometer (XTG). The X-ray pole figure device for the Enraf-Nonius CAD4 automated single-crystal diffractometer, housed at the Geology department of the University of Michigan, USA, is equipped with a Mo source, allowing measurement of the crystallographic preferred orientation of minerals in transmission mode (van der Pluijm et al. 1994; Fig. 3.5). It determines the average crystallographic orientation from thin sections (ca. $200\mu\text{m}$) over a sample area of tens of mm^2 (e.g. Oertel 1985, Schmid & Casey 1986). The diffractometer counter is preset to the correct diffraction angle for a given crystal plane (hkl), in the case of illite at a d -value of 10\AA . The drive motors cause the sample to rotate over an angular sampling grid with intensity (I_{hkl}) being measured at each grid point. After some corrections, the results are presented in the form of a contoured pole figure (van der Pluijm et al. 1994).

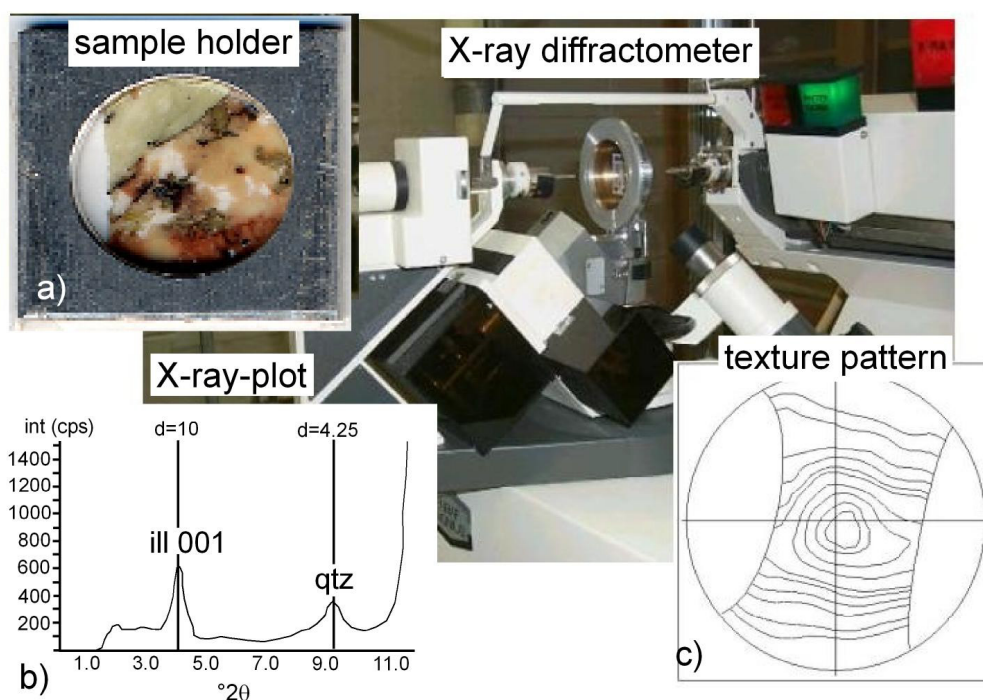


Fig. 3.5: X-ray texture goniometer (XTG), a) $200\mu\text{m}$ thick, thin-section fixed on an aluminium-holder, b) X-ray diffraction plot of a 001 illite peak, c) texture pattern showing normalized intensity values plotted on a contoured pole figure

3.2 Electron microscopy

3.2.1 Scanning electron microscopy and energy dispersive X-ray detection

The scanning electron microscope (SEM) uses a series of magnetic lenses to focus an electron beam that is accelerated by a high potential on the specimen. It images the surface topography by detecting the intensity of secondary electrons emitted by different regions of the sample. Whereas the topography of rough textured surfaces can be described by secondary electron images, back scattered electron (BSE) imaging is based on differences in atomic density and applied on even surfaces. In this study the SEM was used to recognize the different clay minerals based on appearance (textures, shapes and sizes) as well as composition. Detailed information on methods and technical description is given in Welton (1984). Mineral identification using back-scattered electrons was confirmed by the energy dispersive X-ray system (EDX), which measures the relative concentration of the elements that can be compared to the composition of known minerals.

3.2.2 Transmission electron microscopy

Whereas the TEM can also be applied for surface imaging, it is here primarily used to image and analyze internal crystal lattices by high resolution study of ultra-thinned rock sections. The TEM electron beam passes through the sample and is detected below on a phosphorescent screen. Different structural densities within the sample absorb electrons to different degrees, creating sufficient contrast to resolve crystallographic microstructures.

A high-resolution transmission electron microscope (HRTEM) enables minerals to be studied down to the atomic scale. It can be used for studying specific mineral relations at the nanometer-scale, their textures, intergrowths and layer replacements, including analysis of crystallography by electron diffraction, mineral defects, reaction textures and mechanisms, as well as their microstructural complexities. The TEM can be operated in an imaging mode (e.g. to view lattice fringes), in the diffraction mode for selected area diffraction (SAED), and for microchemical analysis using analytical electron microscope (AEM) techniques (Fig. 3.6). A detailed description concerning operation of the TEM as applied to the study of clay minerals is outlined by Peacor (1992). All studies were conducted using a Philips CM 12 instrument housed at the “EMAL laboratory” of the University of Michigan, USA (see appendix for details concerning instrumental setting).

The incident electron beam is scattered by the specimen and focused by an objective lens to form the primary image, which is further magnified by additional lenses (Buseck 1993). In the process of forming this primary image, the objective lens produces a diffraction pattern at its back focal plane. The relation between lattice fringe contrast, clay mineral structure and composition is described by Guthrie & Veblen (1989), who provided a quantitative basis for interpretation of lattice fringe images. The distinct advantage of a scanning TEM is, that the focused beam may provide images and chemical analysis for areas of diameter approaching 100Å, depending on the type of filament.

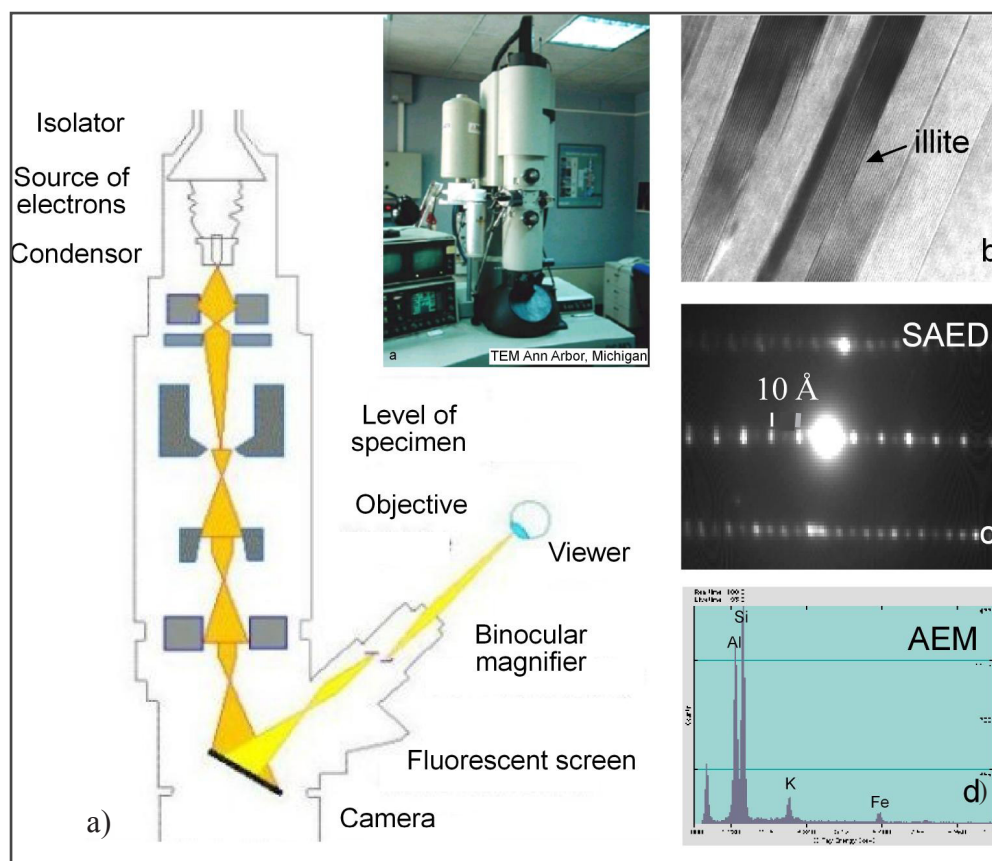


Fig. 3.6: a) Schematic construction of a transmission electron microscope (upper middle: the Philips CM 12 used in this study), b) lattice fringe image of well ordered illite crystallites, c) SAED pattern of a $2M_1$ illite polytype, d) EDX pattern of K-rich illite

3.2.2.1 Selected area electron diffraction

The crystallographic structure of clay minerals can be studied by imaging the hkl reflections in selected area electron diffraction (SAED) patterns (Fig. 3.6c, 3.7). In order to obtain diffraction patterns and lattice fringe images, it is necessary to orientate grains with the c-direction normal to the electron beam, i.e., with (001) layers positioned approximately normal to the specimen surface and parallel to the beam (Peacor, 1992). The specimen areas to be analyzed are chosen using a “selected area” aperture inserted in the image plane of the objective lens, or in the image plane of the diffraction lens. This aperture alters the beam path so that the electron diffraction pattern of the area chosen is projected onto the viewing screen. A detailed description of SAED study is discussed in Merriman & Peacor (1999) and Steeds & Morniroli (1992).

High quality SAED patterns can provide important information about polytypism ($1M_D$, $1M$ and $2M_1$ polytypes for illite). SAED results have the advantage over those of X-ray diffraction methods that they can be obtained from single crystallites, rather than representing an average of the bulk rock material. The most useful information concerning polytype structures is obtained along the reciprocal lattice rows that are normal to the scattering plane. Diffuse scattering parallel to the c-direction of the (001) reflections (non-001 reflections), for example, may reflect mixed-layering or disorder in the polytypic $1M_D$ layer sequence, whereas well defined non-001 reflections correspond to ordered $1M$ or $2M_1$ polytypes (Fig. 3.7)

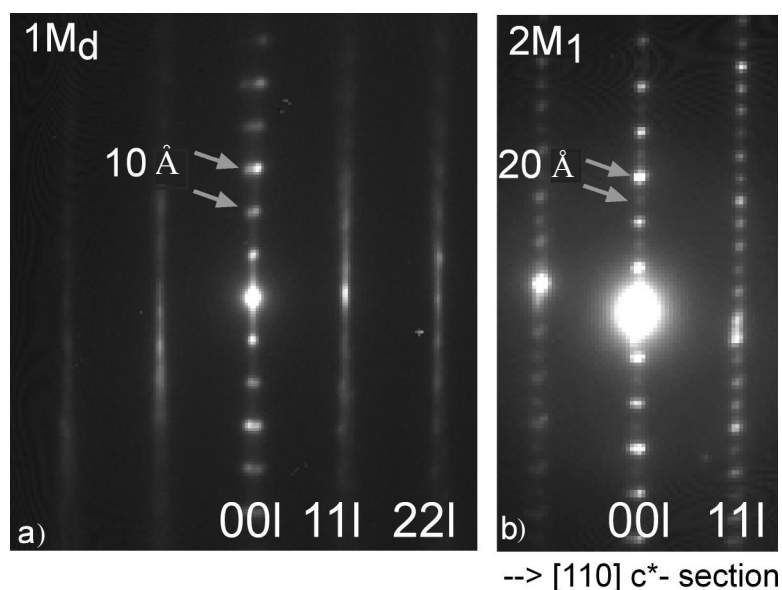


Fig. 3.7: Selected area diffraction patterns (SAED) of a) typical 1M_d illite polytype with a strong disordering of (11 l) reflections, b) well defined set of (00 l) and (hkl) reflections of the 2M₁ illite polytype

3.2.2.2 Analytical electron microscopy

Transmitted, inelastically scattered electrons emitted by the area of the sample also produce X-rays, which can be detected by an energy dispersive spectrometer (EDX) system. These transmitted energies are characteristic for the different elements in the specimen and provide chemical information referred to as “analytical electron microscopy” (AEM, Fig. 3.6d). This chemical analysis can approach the accuracy of electron microprobe results, but have a higher spatial resolution of up to a few hundred Å. The obtained concentration (k) ratios can be converted to a structural formula by normalizing to the numbers of oxygen atoms in the unit formula for the different minerals. In this study, the microchemical data for illite was exclusively normalized to O₁₀(OH)₂. A detailed description of normalization procedures can be found in Peacor (1992).

Sample damage can be a problem in obtaining accurate AEM results for clay minerals and the effects of direct atom displacement, ionisation and heating give rise to a variety of errors (Peacor 1992). For example changes in count ratio caused by diffusion may occur and can be detected by time dependent changes or by moving the beam to an area adjacent to the area beam-specimen interaction. Diffusive loss is most severe for K, intermediate for Na and smallest for Al.

3.3 K-Ar isotope geochemistry

The ⁴⁰K/⁴⁰Ar-method is based on the radioactive decay of ⁴⁰K isotope to ⁴⁰Ca_{rad} and ⁴⁰Ar_{rad} (Clauer & Chaudhuri 1995) accompanied by β emission (β⁺, β⁻), electronic capture and the production of X-rays. This method is generally applied to rocks with a high content of potassium-rich minerals, such as feldspar and mica and is suitable for studying the low temperature nucleation and growth of crystals (Lippolt & Kirsch 1994). The relatively short half-life of ⁴⁰K

(1.3×10^9 years) allows geological age determination from Precambrian to Quaternary times.

The K-Ar isotopic analyses of this study followed a procedure close to that developed by Bonhomme et al (1975), measured at the CNRS in Strasbourg/France. Potassium was measured by atomic absorption with a global accuracy of $\pm 1.5\%$. For Ar analysis, the samples were pre-heated under high vacuum at 100°C for at least 12 hours to reduce the amount of atmospheric Ar adsorbed on the mineral surfaces during sample preparation and handling. Ar isotopic results were controlled by repetitive analysis of the international GL-O standard that averaged $24.38 \pm 0.12 \times 10^{-6} \text{ cm}^3/\text{g STP}$ (2s) of radiogenic Ar for 3 determinations. The blank of the extraction lines and the mass spectrometer was also periodically determined, the amount of residual ^{40}Ar being systematically below $1 \times 10^{-7} \text{ cm}^3/\text{g STP}$. The usual decay constants were adopted for age calculations (Steiger & Jäger 1977) and the global error of the K-Ar age determination was evaluated to be better than 2%. For all isotopic methods of dating, a closed-system condition of the material is essential. This is especially critical for the K-Ar method, because Ar as a noble gas is not strongly bonded to other atoms or ions in a mineral phase and a discharge of radiogenic ^{40}Ar out of the crystal lattice is possible under certain circumstances. This can lead to younger ages, that are much lower in comparison to the real cooling or formation ages. One cause of early ^{40}Ar escape is diffusion-loss due to thermal or mechanical strains of the crystals (Clauer & Chaudhuri 1995). In comparison to the longer half-life of $^{238}\text{U}/^{206}\text{Pb}$ and $^{87}\text{Rb}/^{87}\text{Sr}$ isotopes the decay of ^{40}K leads to faster enrichment of ^{40}Ar and therefore provides better age resolution (Simon 1968).

4 ALTERATION HISTORY OF THE SOULTZ-SOUS-FORÊTS GRANITE, BURIED RHINE RIFT BASEMENT

ABSTRACT

Episodic and localized illite mineralization is documented in the hydrothermal altered Soultz-sous-Forêts granite (Upper Rhine Graben, France). Separated grain size fractions of argillite veins and altered granite samples contain mixtures of both 2M₁ and 1M trans-vacant illite varieties. The platy pseudohexagonal 2M₁ illite crystals dominate the vein fillings, whereas the 1M illite occurs largely as a fibrous pore-filling variety, which is particularly abundant in the granite matrix. Multiple phases of fluid injections into the granite body have resulted in different illite assemblages, each sample containing a mixture of two crystal generations, but formed during different crystallization events. On the basis of mineralogical and K-Ar isotopic constraints, the age of these mineralization events can be evaluated by plotting the K-Ar values of the various grain size fractions against polytype abundance or fitted crystallite thickness distributions. All of the argillite veins studied were formed during Permian hydrothermal activity, with secondary episodes of illite crystallization occurring in both veins and granite during Mesozoic (and younger) times.

4.1 INTRODUCTION

Illite is recognized as the most important clay mineral phase subscribed for reconstructing the geological history of fluid-rock interaction in diagenetic, hydrothermal and very-low grade metamorphic settings (e.g. Clauer & Chaudhuri 1995, Inoue et al. 2004, Merriman & Frey 1999). Its usefulness relates to its widespread occurrence in the broad range of low temperature geological environments (< 300°C), its diverse crystal-chemical structure, and its relatively high K-content, which allows it to be dated using well established K-Ar or Ar-Ar isotopic techniques (Bailey et al. 1962, Hunziker et al. 1986, Clauer et al. 1995, 2003, Imaoka et al. 2001, Altaner et al. 2003). Although there are a number of analytical complications associated with the reliable study of illite due to its small particle size and common mixed-layered structure (Bailey et al. 1962, Clauer et al. 1995), one particular challenge is to resolve and date the crystallization history of complex illite assemblages typical of many natural geological samples (Clauer & Chaudhuri 1995).

In addition to direct observations by electron microscopy, a principle technique applied to study complex illite mixtures is to separate and analyze the different grain sizes that make up the rock. This approach is common practice when studying clastic sedimentary rocks (Hower et al. 1963, Clauer et al. 1995, Rousset & Clauer 2003, Liewig & Clauer 2000, Reuter 1985), fault gouges (van der Pluijm 1999, van der Pluijm et al. 2001) and altered volcanic and igneous rocks (Glasmacher et al. 2001, Honty et al. 2004). In such studies the rocks are split into several grain sizes and the mineralogical and isotopic data are interpreted from the way the crystal-chemistry varies in the different fractions. In most natural illite assemblages, the finest size fraction (e.g. < 0.2µm) is typically dominated by younger illite and the coarse fraction by older K-mica phases.

In the case of isotopic dating, when a mixture of two such components are present in all grain size fractions, the youngest and oldest end-member values should approach the true ages of the illite components present (Hunziker et al. 1986).

The key features important in resolving the history of illite crystallization from complex argillite assemblages are the direct observation of crystal shape and size (Srodon et al. 2002), analysis of illite compositions (Yates & Rosenberg 1998, Srodon 1984), the identification of polytype structures (Grathoff et al. 2001, Grathoff & Moore 2002), and more recently, measurement of crystallite thickness distributions (Eberl et al. 1987, Kim & Peacor 2002). Until now, the most used approach to identify and separate different generations of illite is to determine and quantify the illite polytypes (1M and 2M varieties) in the grain size fractions by powder XRD methods (Drits et al. 1997, Grathoff & Moore 2002). Such constraints can be plotted against K-Ar age values in order to extrapolate modelled illite ages from the graphical intercepts representing pure end member phases (Hunziker et al. 1986, Clauer & Chaudhuri 2001, Ylagan et al. 2002, Laverret 2002.).

In this chapter, the nature of illite in the hydrothermally altered granite from the Soultz-sous-Forêts borehole was investigated, which is located in the Upper Rhine rift valley, France (see Fig. 2.2 page 7). The mineral assemblages of this granite body are particularly suitable for unravelling the crystallization history because: i) the alteration products of the granite resulted from direct precipitation during hydrothermal fluid migration, with no magmatic micas present in the fine-grain sizes, ii) the samples are generally K-rich (3-11 wt.%) enabling accurate determination of the K-Ar systematics, iii) the separated fractions studied consist mostly of illite with many of the finer fractions actually approaching monominerallic composition, and iv) a variety of characteristic crystal shapes and polytypes occur in varying concentrations within each sample studied. Based on XRD, SEM, HRTEM and K-Ar dating of this relatively pure material, it is shown how combining these methods allows recognition of the timing and episodic nature of illite crystallization in the hydrothermally altered Soultz-sous-Forêts granite.

4.1.1 Sample material and analytical procedure

The material selected for this study comes from the EPS-1 borehole, which has been continuously cored to a depth of 2230m. Two representative whole-rock granites and three argillite veins were selected from different depths of the borehole profile (Fig. 4.1, appendix page 87). The shallowest sample studied (vein-1) is located just beneath the unconformity at 1431m depth and consists of a cataclased porphyric granite containing an argillite (illite-rich) vein. About 140m deeper into the core section, at 1570m, a typical pervasively altered granite was sampled, which lacks visible fracturing (granite-1). The remaining three samples were all selected from the lower section of the core between 2160-2176m, and lie within a fracture zone characterized by active fluid flow (Genter & Traineau 1996). These samples (granite-2 and vein-2, 3) comprise of hydrothermally altered host rock granite and two argillite veins (2 and 3) of precipitated illite and quartz.

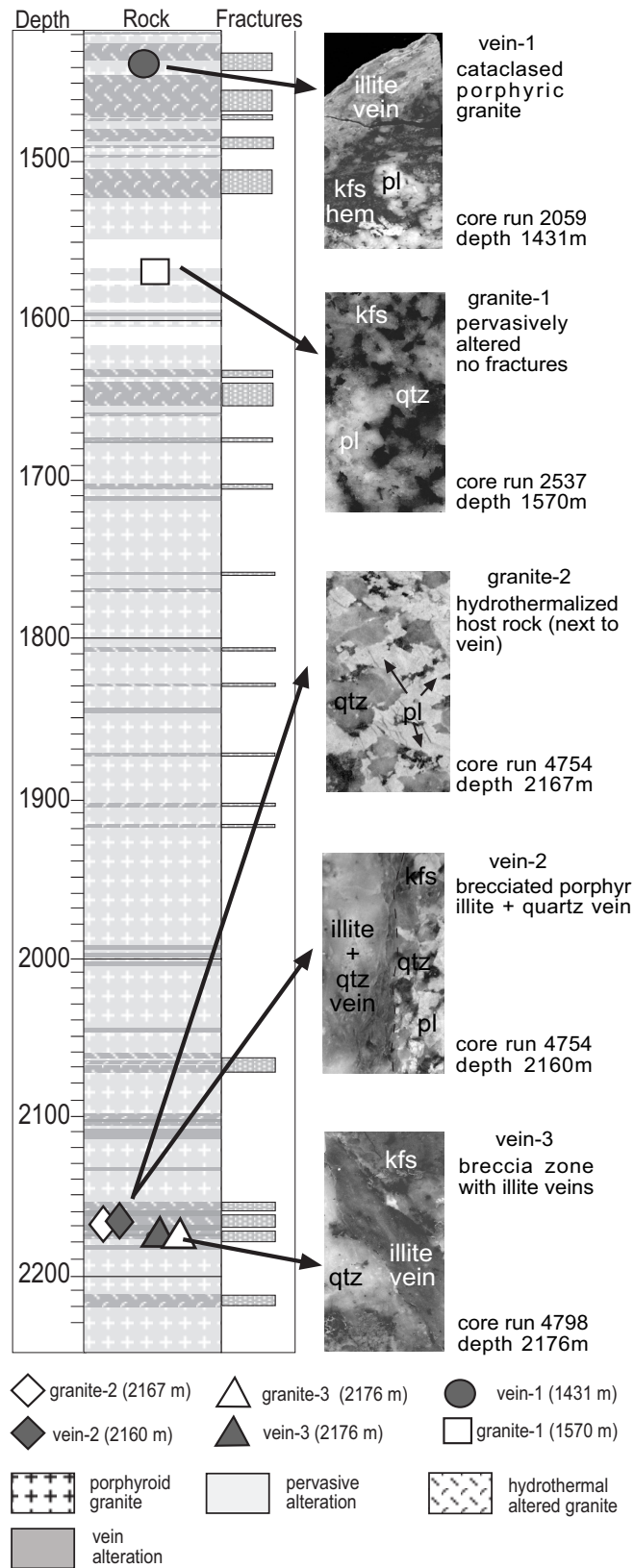


Fig. 4.1: Lithologic section of the EPS-1 drill core between the 1414m to 2230m depth interval (modified after Genter & Traineau 1996). The investigated five samples were selected from different depths, consisting of two whole rock granites and three argillaceous veins. The sample numbers are according to the nomenclature of the core index

Tab. 4.1: XRD results for the different grain size fractions of two granite rocks three veins and three veins

sample (depth/m)	grain size (μm)	Gew. %	intensity 001 peak (cps)	FWHM 001 peak ($^{\circ}$ 2 θ)	best mean T	Thickness α	Variance β^2	K-Ar age (Ma)	CTD A	CTD B	%2M1 (3.2Å)	%1Mt (3.07Å)
vein-1 (1431m)	< 2	--	9542	0.36	--	--	--	232.4 (2.8)	--	--	--	--
	< 0.2	--	2461	0.28	--	--	--	182.0 (3.2)	--	--	--	--
	> 63	92.2	22355	0.17	--	--	--	--	--	--	--	--
granite-1 (1570 m)	10 - 63	4.86	35751	0.21	33.80	3.22	0.23	--	--	--	--	--
	4 - 10	1.02	13665	0.22	23.90	2.84	0.45	255.5 (6.5)	--	--	--	--
	2 - 4	0.71	9531	0.29	17.60	2.50	0.64	236.4 (6.0)	--	--	--	--
	1 - 2	0.70	4485	0.50	10.40	2.17	0.55	213.4 (5.2)	--	--	--	--
	0.4 - 1	0.40	3754	0.63	7.40	2.05	0.59	201.4 (4.9)	--	--	--	--
	0.2 - 0.4	0.19	2639	0.76	5.40	1.73	0.39	190.9 (4.6)	--	--	--	--
--	< 0.2	0.04	2190	0.84	5.50	1.71	0.42	193.6 (5.7)	--	--	--	--
	> 63	78.90	--	--	--	--	--	--	--	--	--	--
granite-2 (2167 m)	10 - 63	9.66	3118	0.40	8.30	2.07	0.51	--	--	--	--	--
	4 - 10	2.34	6754	0.40	9.30	2.17	0.43	156.1 (2.8)	59	41	98	2
	2 - 4	2.54	13696	0.38	10.23	2.23	0.36	153.8 (2.5)	74	26	93	7
	1 - 2	1.67	17905	0.40	11.86	2.32	0.31	135.6 (1.8)	88	12	74	26
	0.4 - 1	0.66	40203	0.44	13.95	2.47	0.28	133.3 (1.7)	96	4	54	46
	0.2 - 0.4	2.19	38739	0.62	10.92	2.27	0.22	110.4 (1.6)	100	0	12	88
--	< 0.2	0.82	--	--	8.15	2.05	0.18	93.9 (1.4)	100	0	1	99
	> 63	79.20	--	--	--	--	--	--	--	--	--	--
vein-2 (2160 m)	10 - 63	8.31	4759	0.35	7.80	1.98	0.62	--	--	--	--	--
	4 - 10	2.53	7719	0.46	11.34	2.37	0.42	256.4 (4.6)	61	39	81	19
	2 - 4	2.23	27298	0.33	13.63	2.51	0.36	238.7 (3.5)	33	67	73	27
	1 - 2	1.56	36342	0.32	16.6	2.65	0.30	248.0 (3.3)	14	86	57	43
	0.4 - 1	3.66	48949	0.39	17.48	2.71	0.28	238.3 (2.9)	8	92	34	66
	0.2 - 0.4	0.89	46313	0.45	15.53	2.62	0.26	230.5 (2.6)	3	97	24	76
--	< 0.2	1.31	42924	0.46	13.4	2.52	0.27	211.0 (2.7)	2	98	13	87
	> 63	84.60	--	--	--	--	--	--	--	--	--	--
vein-3 (2176 m)	10 - 63	6.54	2472	0.31	13.00	2.49	0.47	--	--	--	--	--
	4 - 10	1.76	4393	0.31	18.55	2.78	0.27	279.8 (3.4)	100	0	67	33
	2 - 4	1.41	5702	0.31	19.47	2.82	0.26	274.0 (3.1)	100	0	70	30
	1 - 2	1.51	8271	0.31	22.2	2.95	0.24	274.3 (3.0)	100	0	48	52
	0.4 - 1	2.67	16439	0.32	21.34	2.92	0.24	279.3 (3.2)	100	0	41	59
	0.2 - 0.4	0.73	12676	0.40	18.17	2.77	0.25	252.3 (3.0)	25	75	20	80
--	< 0.2	0.61	9550	0.43	14.03	2.50	0.28	247.9 (3.4)	20	80	3	97

For XRD and K-Ar analyses, parts of these rock samples were initially hand-crushed into small mm-sized fragments and the white to pale green argillaceous-rich rock portions selected by hand. A total of eight grain size fractions ($> 63\mu\text{m}$, $10\text{-}63\mu\text{m}$, $4\text{-}10\mu\text{m}$, $2\text{-}4\mu\text{m}$, $1\text{-}2\mu\text{m}$, $0.4\text{-}1\mu\text{m}$, $0.2\text{-}0.4\mu\text{m}$ and $< 0.2\mu\text{m}$) were separated using a combination of sedimentation and centrifugation settling times calculated using Stokes' law (Clifton et al. 1999, see appendix). The weight-% of each grain size fraction was also determined as a proportion of the whole-rock fraction (Tab. 4.1, appendix page 89).

XRD analyses of the material, both as random powder and texture preparations (appendix page 93), followed the analytical methods described by Moore & Reynolds (1997). For calculation of the crystallite thickness distribution (CTD), thin films were prepared following the method of Eberl et al. (1998). 2.5mg of clay and 2.5ml of distilled water were dispersed ultrasonically and pipetted onto a silicon wafer to reduce background effects. As tests with polyvinylpyrrolidone and ethylene-glycol had no effects on the illite XRD profiles, these reagents were not routinely used. Polytype identification followed the procedure of Drits et al. (1993), with identification based on the relative intensities of the 112 and 114 peaks for $1M_{\text{TV}}$ and $2M_1$ polytypes, respectively.

For SEM investigation, small rock fragments were used for secondary electron imaging, and polished thin sections for backscattered electron images. Qualitative analyses of mineral composition were obtained by EDS. Key samples were then selected and investigated using high resolution TEM and AEM techniques following the analytical procedures outlined by Peacor (1992) and Warr & Nieto (1998). Thin-sections of ca. $100\mu\text{m}$ thickness were prepared and small Cu-washers (1mm diameter) adhered to the illite-rich portions of the sections. The samples were then ion-milled to an appropriate thickness and investigated using a Philips CM 12 scanning-transmission electron microscope with a Kevex Quantum solid-state detector (see Fig. 3.6, page 16). All high-resolution lattice-fringe images were undertaken at a 100,000 x magnification. Quantitative EDS chemical analyses were obtained in scanning TEM mode using a beam diameter of 5nm and a scanning area of $30 \times 30\text{nm}$. The TEM study combines lattice-fringe imaging and selected area electron diffraction for the illite polytypes, whereby compositional data were calibrated using the k-values of available laboratory standards (Peacor 1992).

The grain size fractions of the selected samples were analyzed by the conventional K-Ar technique (Bonhomme et al. 1975). However, the $> 63\mu\text{m}$ fraction was not included to avoid contamination of biotite and K-feldspar present in some of the samples. The details of the K-Ar methodology used are given in the Analytical methods chapter (page 17).

4.2 RESULTS AND INTERPRETATION

4.2.1 Illite microscopic characteristics

SEM images reveal a variety of illite crystal sizes and shapes in the hydrothermally altered granite and vein samples studied. Relatively large illite of a platy shape, commonly around 5 to 10 μm in basal length, is most abundant in the argillite veins (Fig. 4.2a, b). The crystals are generally pseudo-hexagonal in shape, commonly arranged in stacks and display some sutured crystal edges suggestive of particle dissolution. A number of microstructures can be observed in the vein samples with local and poorly developed microfolds and associated hinge porosity (Fig. 4.2a), as well as anastomosing fabrics (Fig. 4.2b).

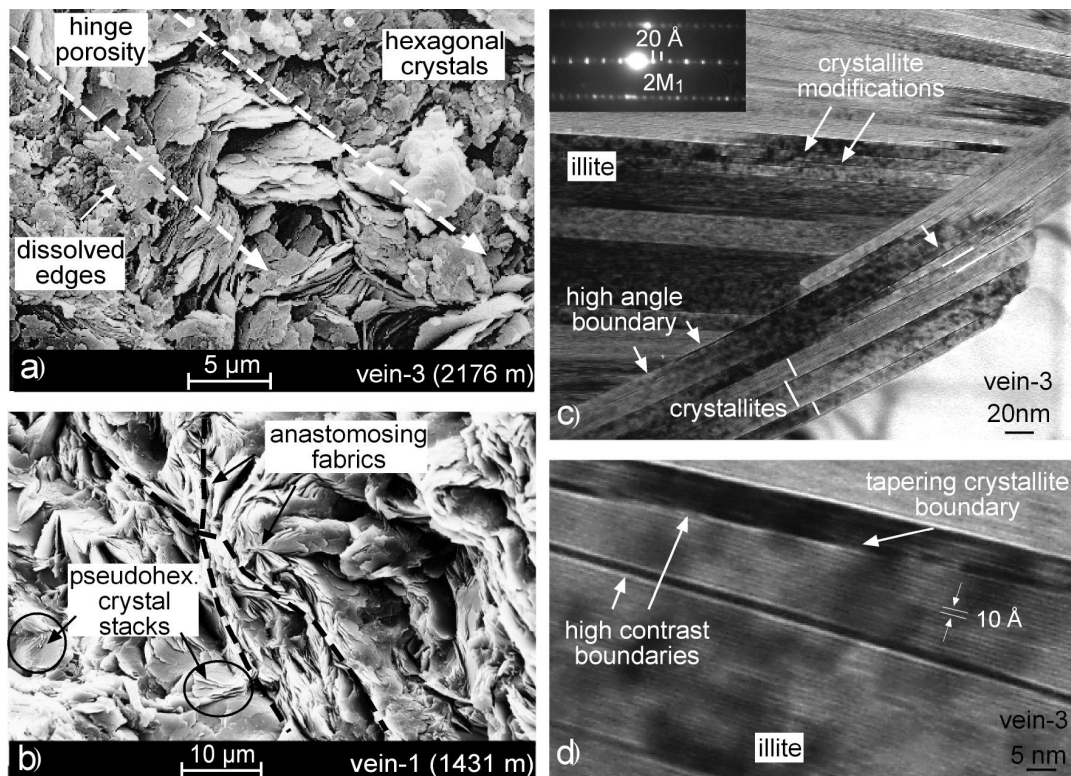


Fig. 4.2: Electron microscopy images of typical vein illite, a) SEM image of relatively large platy illite showing pseudo-hexagonal crystal shapes and some irregular, sutured crystal edges (2176m). Note the occurrence of the local and poorly developed microfolds and associated hinge porosity, b) SEM image of vein illite showing the local development of an anastomosing fabric with pseudo-hexagonal crystal stacks (1431m), c+d) TEM lattice fringe images of illite stacks showing subparallel thick packets containing numerous thinner crystallites (ca. 10-15nm thickness) attributed to intracrystalline deformation. The SAED image (top left) shows the $2M_1$ nature of the illite polytype (2176m)

TEM lattice fringe images of the platy vein illite reveal the internal structure of the stacks. Thick packets of the $2M_1$ illite polytype can be recognized showing similar contrast and hence orientation (Fig. 4.2c). Their thickness ranges up to 80nm, with high angle grain boundaries developed between adjacent stacks. Closer examination of the packets reveal the presence of numerous high-contrast fringes and low-angle domain boundaries, producing crystallite thicknesses commonly around 10nm. The crystallites show remarkable lateral variations in thickness (Fig. 4.2d), and are sometimes associated with zones of intracrystalline deformation. These features

imply that the crystallites represent low-angle subgrain boundaries formed by the migration of crystal defects during intracrystalline deformation (Warr & Peacor 2002).

An additional 1M illite polytype is recognized in the vein samples and adjacent granite based on crystal size and shape. Here, a network of thin and fibrous illite occurs in pore spaces (Fig. 4.3a). The crystals may reach over 10 μ m in length but are notably thin and commonly < 1 μ m broad. Crystal shapes range from fibrous needles to flat blades (Fig. 4.3b) and form a network of illite crystals without any observable preferred orientation but sometimes they do occur as grain coatings. TEM lattice fringe images of this illite reveal an array of thin crystallites with notable contrast differences between individual packets. The crystallites are laterally continuous, contain numerous layer terminations and are separated by distinct low-angle crystallite boundaries. In contrast to the platy vein illite, these crystallite boundaries probably represent crystal growth surfaces rather than sub-grain boundaries.

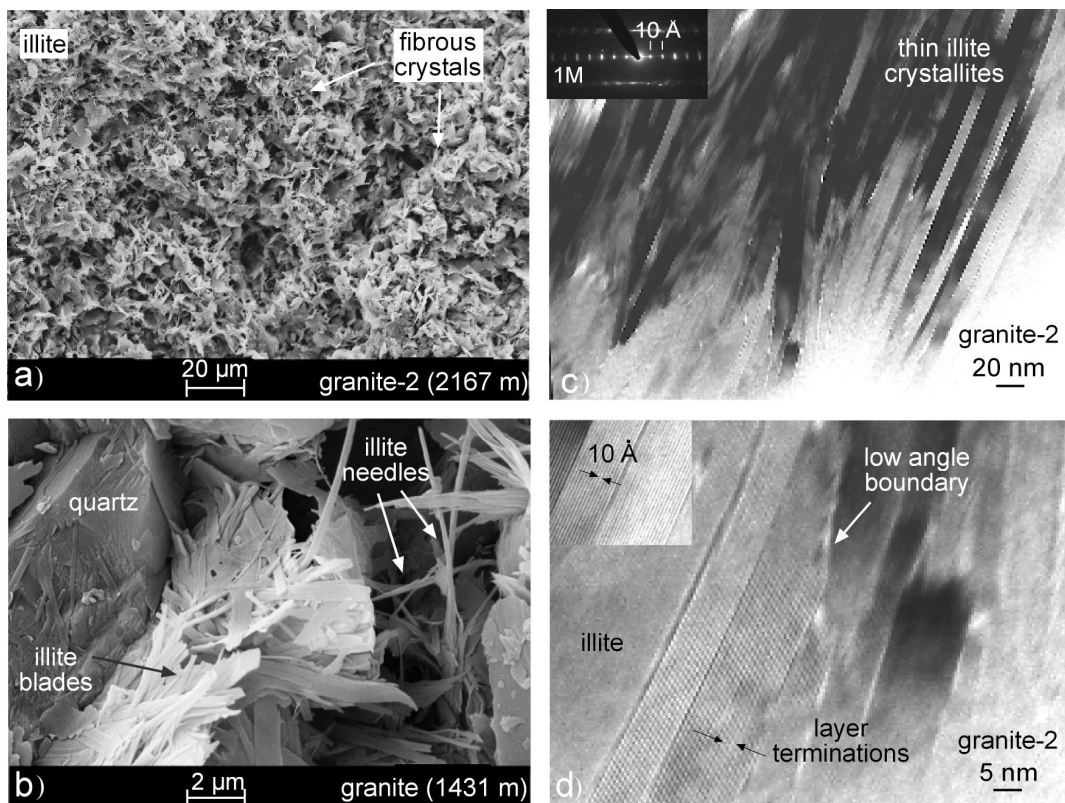


Fig. 4.3: Electron microscopy images of typical granite-host rock illite (2167m and 1431m), a) network of thin and fibrous illite crystals have grown in the pore spaces, b) crystal shapes range from fibrous needles to flat blades with no visual preferred orientation, but sometimes they do occur as grain coatings, c+d) TEM lattice fringe images show high contrast and tapering crystallite boundaries. The crystallites are more laterally continuous, contain numerous layer terminations and are separated by distinct low-angle crystallite boundaries. SAED patterns (top left in Fig. 4c) show typical 1M polytypes (2167m)

4.2.2 Illite compositional characteristics

The structural formulae of illite (normalized to O₁₀(OH)₂) based on AEM analyses show a broad range of compositions, but no recognizable core depth variations. The most K-enriched illite, with an average composition of K_{0.92}(Al_{1.5}Fe_{0.17}Mg_{0.08})[Si_{3.34}Al_{0.66}]O₁₀(OH)₂, was recorded

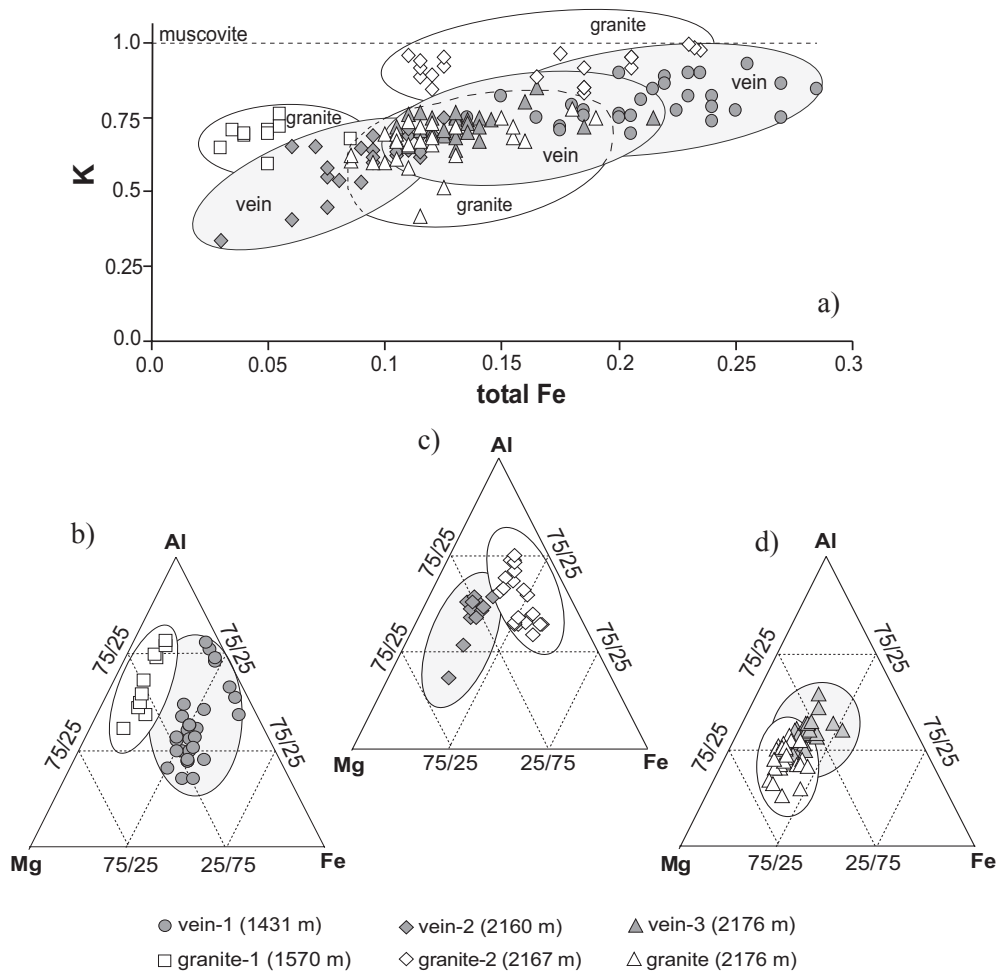


Fig. 4.4: Composition of illite in the altered host granite samples and the argillaceous mineral veins a) plot of interlayer K versus total Fe showing the wide range of K and Fe contents b) triangular Al-Mg-Fe plots showing compositional variations related to octahedral occupancy

from the altered host-rock granite-2 in the lower section of the borehole (2167m depth; Fig. 4.4a). However, the most K-enriched vein illite was measured in the uppermost argillite vein-1 (1431m depth), with a typical composition of around $K_{0.8}(Al_{1.65}Fe_{0.21}Mg_{0.13})[Si_{3.27}Al_{0.73}]O_{10}(OH)_2$. The most K-depleted illite was recorded in vein-2 at 2160m, just 7 meters above from the sample containing the most K-rich illite within the granite. Significant variations are observed when plotting interlayer K against octahedral Fe for the vein illite, with a general trend ranging from low K and Fe to high K and Fe varieties (Fig. 4.4a). These compositional variations indicate that a Fe substitution in octahedral sites causes variation in interlayer charge and thus K content. The octahedral cation content (Al-Mg-Fe) of illite also shows notable differences in the veins and host-rock granite (Fig. 4.4b). The variation in Fe content of the vein illite appears to be related to Al or Mg exchange. The most variable compositions are observed in the host-rock illite with Al-Mg-Fe varieties (Fig. 4.4b) characterizing the pervasively altered host rock (1570m), Al-Fe-Mg varieties (Fig. 4.4c) within the fractured granite (2167m) and Mg-Al-Fe varieties (Fig. 4.4d) recorded in the deepest sampled granite breccia (2176m). In contrast, the composition of the vein illite shows less variation, where two main composition fields can be distinguished. In the upper section, the vein

illite show a Al-Fe-Mg octahedral content (Fig. 4.4b), whereas the lower, brecciated veins have a Mg-Fe-Al content (Fig. 4.4c).

4.2.3 X-ray diffraction characteristics of the grain size separates

The eight separated grain size fractions of the granite and vein samples (Tab. 4.1) are all enriched in illite with only minor amounts of accessory minerals, particularly quartz in the coarse fractions ($> 1\mu\text{m}$) and dolomite in the finest ($< 0.4\mu\text{m}$) grain sizes (Fig. 4.5). The weight % of the separates reveal 5-35% of these samples to be made up of particles $< 10\mu\text{m}$ in size (Tab. 4.1). Additionally, based on the peak intensities of the (001)-reflection and the XRD mineralogy,

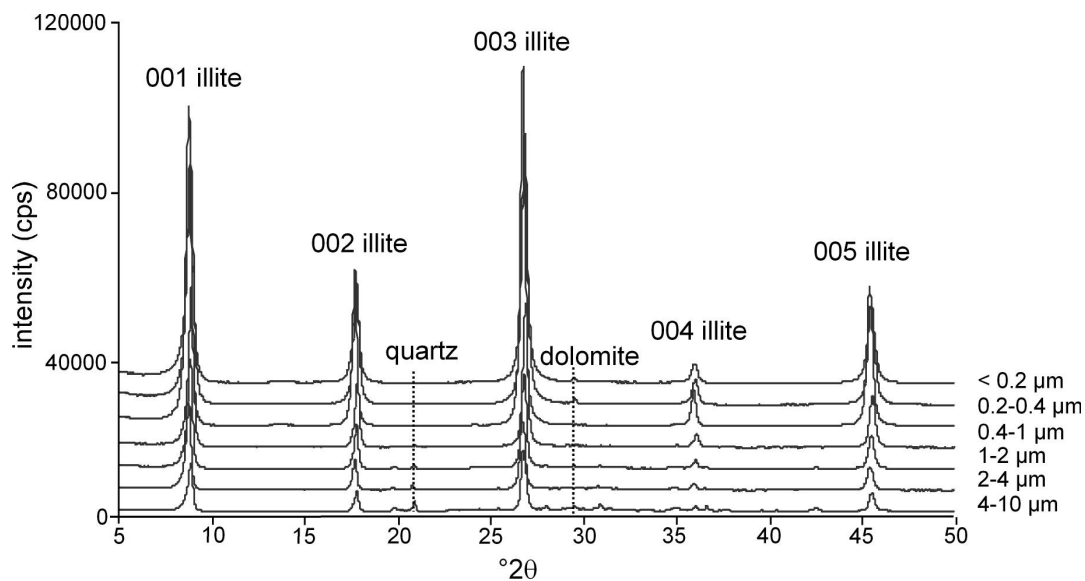


Fig. 4.5: Typical orientated X-ray diffraction patterns of the eight different grain sizes in the vein at 2176m depth

the highest abundance of illite is seen to occur in the 0.4-1 μm fraction. This is not so obvious in the host granite (1570m), due to the presence of biotite in the coarser fractions. The (001) basal reflections show large variations between the different size fractions, but they are generally broader towards the smaller sized separates (FWHM: $\sim 0.17\text{-}0.84^\circ 2\theta$). Ethylene-glycol and PVP treatment of selected samples show no difference between natural air-dried patterns, indicating no measurable mixed-layered smectite in these samples.

The crystallite thickness distributions (CTDs) calculated using the MudMaster program (Eberl et al. 1996) reveal varying best mean thickness and shape (α , β^2) parameters (Tab. 4.1). Only the host granite (1570m) shows the typical behavior of decreasing mean thicknesses corresponding to decreasing grain size, as described in other studies (Bove et al. 2002, Dudek et al. 2002). However, the three other samples (one granite and two veins) show different trends, with the largest mean thickness occurring in the fine 0.4-1 μm fraction. The CTDs of the grain size fractions show two common shapes (Fig. 4.6): near log-normal and asymmetrical non-lognormal distributions.

The complex asymmetrical distributions characterize the coarse fractions of the veins (e.g. the 4-10 μm fraction of vein-2 at 2160m in Fig. 4.6) and the altered host granite, with a notable concentration of crystallites toward smaller thicknesses. These fractions are taken to reflect mixtures of different types of illite, as observed by electron microscopy, show the highest degree of thickness variance (β^2 values in Tab. 4.1). These mixtures were fitted using the program UNMIXER (provided by D. Eberl) in an attempt to group them into two populations of CTDs (component A and component B), assuming each population is characterized by a log-normal shape. The areas of the fitted CTDs were then used to estimate the abundance of illite phases present (Tab. 4.1). Simpler types of distributions could only be fitted by a single log-normal shape, which is considered to represent the dominance of a single illite phase. These distributions, however, are suspected to contain mixtures of illite, but the minor component present could not be effectively separated by the UNMIXER program.

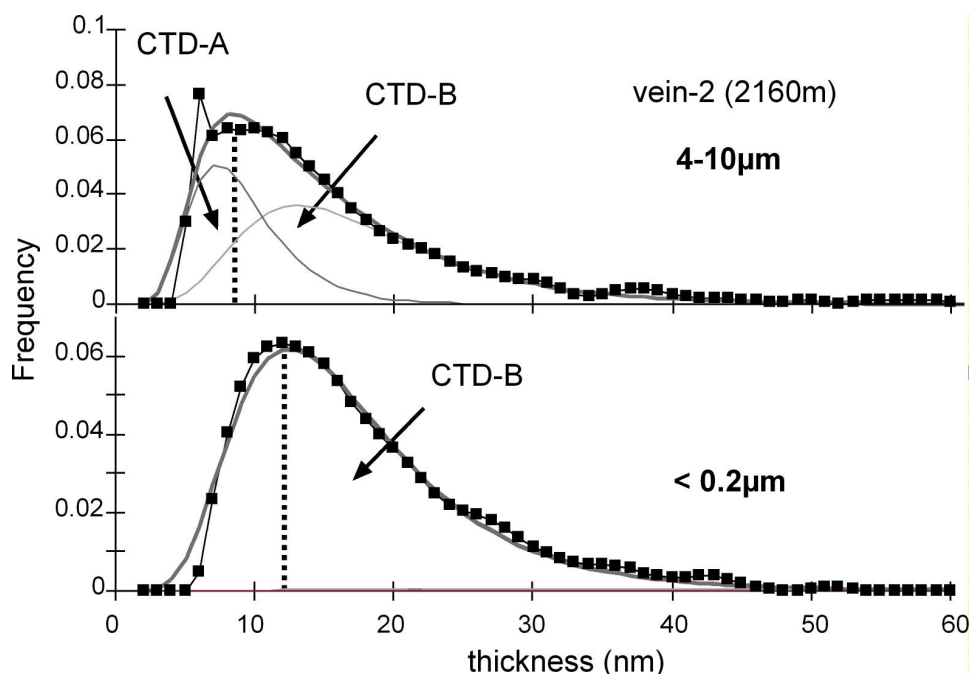


Fig. 4.6: Crystallite thickness distributions (CTDs) of two grain size fractions in the vein at 2160m, calculated using the MudMaster program. More complex asymmetrical distributions characterize the coarse fraction of the vein (4-10 μm), reflecting mixtures of different types of illite. The smallest grain sizes (< 0.2 μm) show more lognormal shapes and are considered to present the dominance of a single illite phase. A = poorly crystalline component, B = well crystalline component

Random powder preparations confirm the physical mixture of at least two different types of illite in all samples. The occurrence of distinct reflections at 3.07 \AA and 3.63 \AA indicate the presence of a 1M polytype of the trans-vacant variety (Drits et al. 1993), and the reflections at 2.91, 3.2 and 3.5 \AA characterize a 2M₁ illite (Moore & Reynolds 1997). The intensity of these diagnostic reflections shows consistent variations with grain size (Fig. 4.7). The 1M polytype peaks typically show a slight increase toward finer grain sizes, whereas the 2M₁ reflections show more pronounced changes, with significantly weaker reflections in the finest fractions and stronger reflections in the coarser fractions. These trends are most apparent in the illite-rich vein samples,

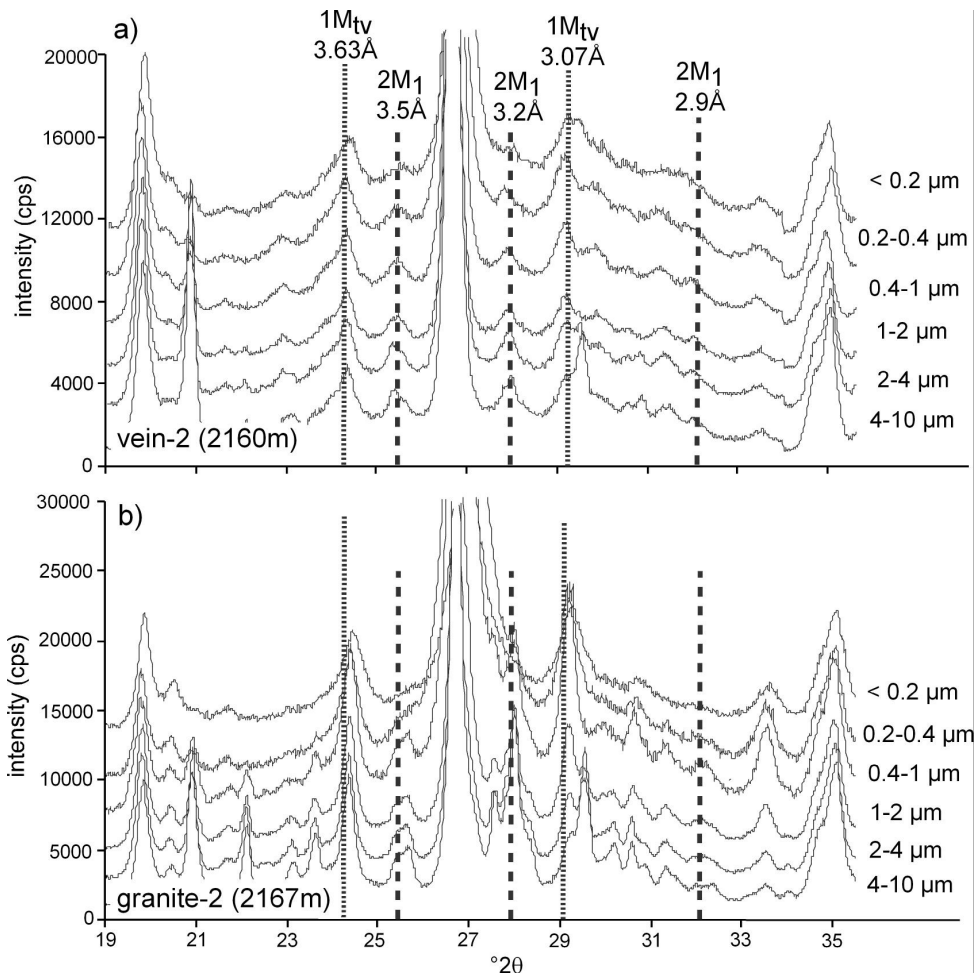


Fig. 4.7: Random powder preparations of the eight grain size fractions of a vein (2160m) and a granite (2167m) indicate the presence of a 1M polytype of trans-vacant variety, as well as 2M₁ illite polytype. The intensity of these diagnostic reflections show consistent variations with the grain sizes

but are more difficult to resolve in the polymineralic granite samples due to the complex overlap of hkl reflections.

4.2.4 K-Ar values of the different grain size fractions

A systematic decrease in K-Ar values with decreasing grain size can be recognized for most of the vein and granite samples (Tab. 4.1). This indicates that the mixtures of illite are of different ages, with the younger phase present in higher concentrations within the finer grain sized fractions and the older phase dominating the coarser separates. The K-Ar values of the separated grain sizes of the five samples studied (3 veins and 2 granites) are plotted together in Fig. 4.8 (see as well appendix page 92).

The oldest K-Ar values are recorded in the vein-3 sample from the deeper section of the borehole (2176m). Here, two groups of age values can be recognized, the oldest around 274-280 Ma in the $> 1\mu\text{m}$ fractions, and the youngest around 247-252 Ma in the $< 1\mu\text{m}$ sizes. In contrast, the other samples show a more continuous and progressive decrease in age values with decreasing grain size. The oldest value of vein-2 at 2160m in the coarsest fraction (4-10 μm) is ca. 256 Ma,

which corresponds well with the youngest group of values outlined for vein-3. The youngest value of this vein-2 is 211 Ma, which is recorded from the $<0.2\mu\text{m}$ fraction. Only two grain sizes ($<0.2\mu\text{m}$ and $<2\mu\text{m}$) were determined in the vein-1 sample from the upper part of the borehole (1431m depth). They provide a value at 182 Ma for the fine fraction and 232 Ma for the coarse fraction. The ca. 256 Ma end-member value of veins 2 and 3 is also present in the coarse 4-10 μm fraction of the pervasively altered granite-1 sample at 1570m. The lowest values of this sample are younger than the sequence of vein-2, forming a plateau at about 190-194 Ma in the fractions $<0.4\mu\text{m}$. A significantly younger range of K-Ar values characterizes the fractured host rock granite at 2167m. The oldest values within the coarser fraction (4-10 μm) again show a small plateau at ca. 153-156 Ma, whereas the youngest end-member occurs in the finest ($<0.2\mu\text{m}$) fraction at ca. 94 Ma.

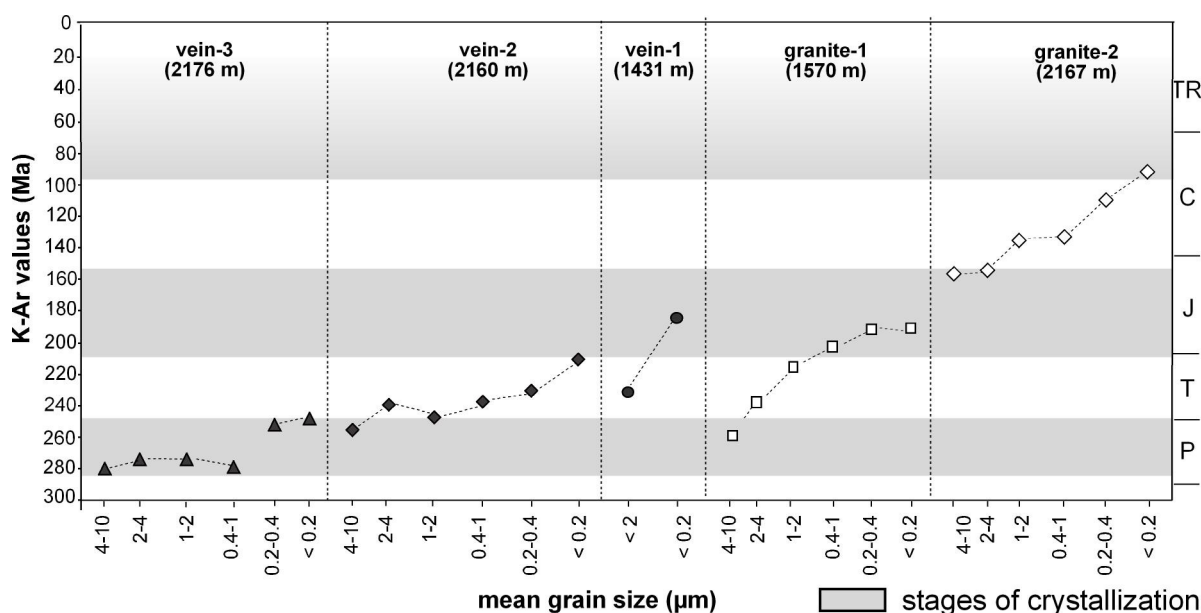


Fig. 4.8: K-Ar values of the separated grain size fractions of three vein samples and two granite samples showing the principle stages of illite crystallization. Based on the distributions of K-Ar values with varying grain size, five groups can be recognized. The oldest group (ca. 247-280 Ma) corresponds to a Permian age and are dominant in the veins. A second group correspond to Jurassic ages (ca. 153-194 Ma) and are present in both veins and granite. The youngest age group is present in the finest fraction of the granite-2 sample, and is Cretaceous ($<$ ca. 94 Ma) or younger in range. P= Permian, T= Triassic, J= Jurassic, C= Cretaceous, TR= Tertiary

Based on the described distribution of K-Ar values with varying grain sizes, three principle age groups can be recognized from the sample suite (gray bands in Fig. 4.8). The oldest K-Ar age group (ca. 247-280 Ma) corresponds to Permian ages, preserved in vein-3 and in the coarsest fraction of vein-2 and granite-1. A second K-Ar age group of Jurassic age (ca. 153-194 Ma) is best defined in the finest fraction of granite-1 and the coarsest fraction of granite-2. The youngest age group recognized in this study is of Cretaceous age ($<$ 94 Ma), here recorded only in the $<0.2\mu\text{m}$ fraction of granite-2.

4.2.5 Analysis of illite mixtures based on K-Ar values, polytypes and crystallite thickness distributions

To decipher the contributions of the individual illite populations from the described mixtures, and to evaluate the end member age values of the involved components, the K-Ar results are plotted against both the abundance of polytypes ($1M$ and $2M_1$) and the fitted CTDs (components A and B) in Fig. 4.9. Plotting the %- $2M_1$ polytype content against K-Ar values of vein-3 (Fig. 4.9a) confirms well the values previously estimated based on the variations of K-Ar results for the different grain size fractions (Fig. 4.8). Two equivalent apparent plateaus can be recognized in vein-3, implying that two separate phases of Permian crystallization occurred. However, each plateau consists of a mixture of both types of polytype crystals, indicating that they may have formed during single crystallization events. Two equivalent plateaus of Permian age are also observed when plotting the K-Ar age values against CTDs (Fig. 4.9b), but the estimated mixtures are not equal to those determined by polytype content. According to the UNMIXER-program, all coarse fractions $> 1\mu\text{m}$ in size contain just one population of illite crystallites, despite containing different polytypes.

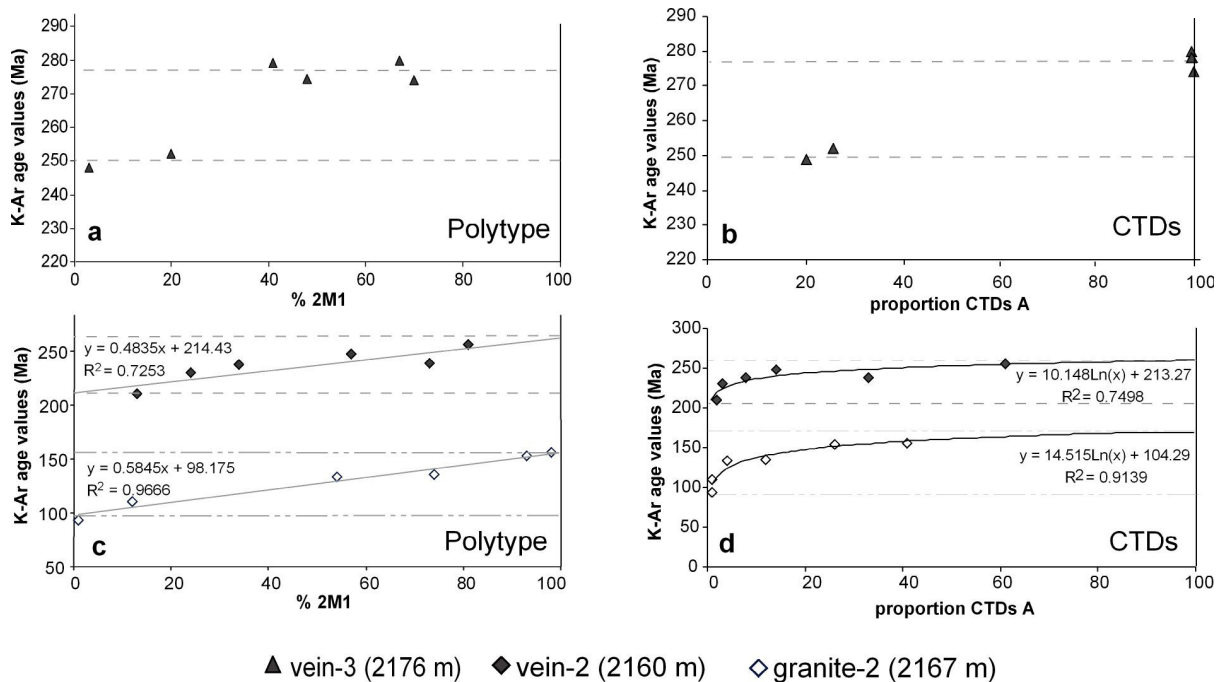


Fig. 4.9: K-Ar values plotted against the abundance of polytypes ($1M$ and $2M_1$) and CTDs (phases A and B) for vein-3, vein-2 and granite-2. Horizontal lines mark position of end member age

The vein-2 and granite-2 samples both show mixtures of polytypes and CTDs for the different measured grain sizes (Fig. 4.9c,d). The vein-2 sample (2160m), for instance shows a continuous mixture of the $1M_{TV}$ and $2M_1$ polytypes (Fig. 4.9c). Only the coarsest and finest fractions of the host granite (2167m) contain just one of the two polytypes. Fitting linear regressions to the polytype mixtures give reasonable correlation coefficients ($R^2=0.72-0.96$), with intercepts of the axis representing either the $1M_{TV}$ or the $2M_1$ end member. They indicate ages in accordance to those estimated from the K-Ar grain size data of the sample suite. Using this approach, the vein-2 sample contains a pure $1M_{TV}$ end member age value of ca. 215 Ma and a pure $2M_1$ age value of

ca. 260 Ma. In contrast, the granite-2 sample contains a mixture of the same two polytypes, but with younger age values of ca. 100 Ma and 160 Ma, respectively. The calculated CTDs of these sample fractions produce similar results as those obtained from the polytype data, with correlation coefficients of $R^2=0.75-0.91$ when fitting logarithmic curves. The vein-2 sample shows intercepts at ca. 225 Ma and 280 Ma for the $1M_{tv}$ and $2M_1$ end member polytypes (Fig. 4.9d), and the granite host sample (2167m) has intercepts at ca. 95 Ma and 165 Ma. With the CTD data, linear fits produced statistically unreliable results.

4.3 DISCUSSION

4.3.1 The timing and mechanism of episodic illite crystallization

The main argillaceous product of the hydrothermally altered Soultz-sous-Forêts granite studied here is illite, which is generally $< 10\mu\text{m}$ in size and comprises ca. 3-11% of the total rock weight (Tab. 4.1). On the basis of the combined XRD, SEM, TEM and isotopic results, a number of episodic illite crystallization events can be recognized in each of the granite and vein samples. In general, these are characterized by differences in crystal size, shape, microstructure, polytype, composition and K-Ar age values. Information concerning the timing and mechanism of these episodic events can be deduced from the eight grain size separates prepared for each sample, with mixtures of two principle types of illite crystals: platy $2M_1$ and fibrous $1M$ trans-vacant varieties (Figs. 4.2, 4.3). The pattern of K-Ar values for the two granites and the three veins studied reveals different combinations of three age groups to be present: Permian, Jurassic and Cretaceous (or younger) (Fig. 4.8).

Permian aged illite is largely of the $2M_1$ polytype and occurs in the coarse fraction of all samples, except granite-2. This polytype is well known to form under hydrothermal conditions in the $125-350^\circ\text{C}$ temperature range (Velde 1965). Despite similar appearance, a range of illite compositions occur in samples dominated by the $2M_1$ polytype, with significant variations in both K and octahedral cation content (Fig. 4.4). These variations indicate a link between the total Mg-Al-Fe content in the octahedral sites and the interlayer K content. However, there is no clear indication that these variations are related to the temperature of illite formation. For example, K-depleted platy illite occurs in one of the deeper vein samples at 2160m. The observed compositional variations are thus considered more likely to reflect variations in fluid compositions and the fluid-rock ratio experienced by the various parts of the granite body (Durst & Vuataz 2000, Pauwels et al. 1993). The characteristic Mg-Al-rich and Fe-poor octahedral content, with low to moderate amounts of interlayer K (0.35–0.75) of the vein and the granite samples, dominated by coarser platy illite, therefore probably reflect the composition of post-Variscan Permian fluids.

The deepest vein sample (2176m) of similar composition contains thick, platy $2M_1$ illite crystals of Permian age that are split up into numerous sub-grains, forming domains as small as 10nm in thickness (Fig. 4.2c). The high-contrast fringes mark the sites of planar defects and do not represent low-charged smectitic layers. Sub-grain formation implies relatively enhanced temperature conditions accompanied by intracrystalline strain, presumably associated with the

formation of the vein rock fabric (Warr & Peacor 2002). This Permian illite may well be related to the circulation of a late- to-post-Variscan, hydrothermal CO₂-rich fluids of high temperatures (180 to 340°C) and moderate salinity (2-7 wt% eq. NaCl) preserved as inclusions in quartz veins at similar depths within the borehole (Dubois et al. 1996).

This lower vein sample (2176m) actually shows two plateaus or age populations of apparent Early and Late Permian ages. Each population contains a mixture of 2M₁ and 1M polytypes of the same isotopic age. This feature could be viewed as two separate crystallization events occurring in response to the inflow of episodic Permian hydrothermal fluids. In such a scenario, the progressive cooling history of each fluid pulse, or changes in the saturation state of the fluid, could explain the transition of 2M to 1M polytypes observed in each population. Another possible explanation for the Late Permian cluster in this sample is the presence of younger illite occurring only in the < 0.4µm fraction of this sample. However, extrapolation of the end member ages from the pure 1M phase based on the K-Ar vs polytype plot gives an intercept modelled age of ca. 250 Ma, implying of no younger illite in this sample (Fig. 4.8).

Jurassic or Cretaceous (or younger) aged illite is present in most samples as either 2M₁ or 1M polytypes. The latter polytype occurs as fine-grained, elongated fibrous to lath-shaped crystals (< 1µm broad) of the trans-vacant variety (Fig. 4.3, 4.7). Such trans-vacant 1M polytypes are typical for pure hydrothermal illite and have been described in a number of case studies (Grathoff & Moore 2002, Rosenberg 2002). This polytype is generally considered to form under lower temperature conditions than 2M₁ varieties, and probably formed during migration of younger brines of around 130°C to 170°C, associated with the main alteration of biotite and plagioclase in the granite (Aquilina et al. 1997, Dubois et al. 1996). The younger 1M fibrous illite varieties also grew partly at the expense of older, platy illite. It is therefore a possibility that some inherited argon may have become incorporated into newly crystallized phases. Younger illite of Cenozoic Tertiary age (N. Liewig, *pers comm.*) has been reported in the finest grain sized fractions extracted from fracture coatings of the Soulz-sous-Forêts granite.

The composition of the 1M illite can only be estimated from the granite samples abundant in these phases. Here, fine-grained fractions yield a similarly broad range of K and Fe/Mg variations, as described for the platy 2M₁ crystals, but the K-content of the fibrous varieties in the fractured granite host rock is notably high (Fig. 4.4). Similar types of diagenetic fibrous illite are well documented in the Permian Mesozoic sediments of the North Sea Basins and northern Germany (Zwingmann et al. 1998, Wilkinson & Haszeldine 2002), and are considered to form under lower temperature diagenetic conditions. The pore-filling fibrous varieties of illite are clearly younger and are probably related to partial dissolution of the older 2M₁ platy phases, as well as plagioclase crystals.

Whereas the Permian age of illite appears to be relatively well established, the true age of the younger Mesozoic (or younger) illite is more difficult to define accurately on the basis of K-Ar ages alone. In considering both polytype results and the timing of illite crystallization it becomes apparent that the transition from 2M to 1M polytypes has occurred at least 3 or 4 times over a

period of ca. 200 Ma. Each transitions could be viewed as a hydrothermal event representing the progressive cooling of fluids. This may be applicable to the Permian events, where the different polytypes have similar K-Ar age values, but this mechanism of formation alone is unlikely to apply to the polytype transitions that show large age differences between end member K-Ar values. It is considered more probable that the rock permeability was a key factor controlling the polytype transition, which in turn influenced the saturation state of the pore fluids. It is evident that the 1M trans-vacant variety grew largely as fibrous illite in the restricted pore space of both veins and granite matrix. The reduced rock permeability conditions (Surma & Geraud 2003) were favorable for concentrating supersaturated pore fluids and the rapid growth of lath or fibrous crystals (Mullin 1961), similar to those documented in sandstones of the North Sea (Wilkinson & Haszeldine 2002). A strong permeability and fluid saturation control on the illite crystallization would explain the large range of illite compositions recorded in the alterations of the Soultz-sous-Forêts granite.

4.4 CONCLUSIONS

- 1) At least three episodes of hydrothermal illite crystallization occurred in the veins and fractured granite of the Soultz-sous-Forêts granite. Based on assessment of grain size dependent K-Ar values, and the modelled end member ages determined from K-Ar versus polytype plots, illitization events are suggested to have occurred during Permian, Jurassic and Cretaceous (or younger) times. K-Ar age determinations based on crystal thickness distributions confirmed these results, even if the method does not appear to be so reliable as age estimates based on polytype analyses
- 2) Each vein and granite sample studied contains two principle types of illite: a higher temperature pseudo-hexagonal 2M₁ polytype and a lower temperature 1M trans-vacant variety. The latter polytype occurs largely as lath to fibrous shaped crystals
- 3) K-Ar analyses reveals all samples contain different mixtures of illite ages. The differences observed in the distribution of illite ages, polytypes and compositions could be related to variations in burial depth. The primary influence on the nature of illite crystallization appears to have been temperature and composition of the percolating hydrothermal fluids, as well as factors related to changes in rock permeability. The transition from platy 2M to more fibrous 1M polytype structures appears to correspond with the progressive sealing of both vein and fracture granite matrix
- 4) The argillite veins are suggested to have formed during a high temperature Permian hydrothermal event related to CO₂-rich fluids. Additional sealing events also occurred during Mesozoic and Cenozoic times, which corresponded with the percolation of lower temperature saline brines.

5 ALTERATION HISTORY OF THE SCHAUBURG FAULT, UPLIFTED RHINE RIFT MARGIN

ABSTRACT

A retrograde sequence of fluid-controlled, low-temperature mineral reactions has been preserved along an E-W striking, dextral-oblique-slip fault in the uplifted Rhine Graben flank. This fault (the Schauenburg Fault, near Heidelberg), juxtaposes Permian rhyolite against Carboniferous (Variscan) granite and shows syn- or post-rift displacement of the N-S trending, eastern boundary fault of the rift basin. Both mineral texture and rock fabric indicate that the fault forms a site of high rock permeability and fluid flow, and records the exhumation and fluid-rock history of the rift shoulder since the Mesozoic. The reaction sequence and mineral composition of the clay minerals within the cataclasite and adjacent granite and rhyolite lithologies, document progressively decreasing fluid temperatures, with back-reactions of pure $2M_1$ illite to $1M_d$ (R3) illite-smectite, and eventually smectite and kaolinite assemblages. Compositional variations are attributed to Tertiary to recent fluid flushing of the fault zone associated with rift flank uplift, and with progressive dilution of the electrolyte-rich, acidic to neutral hydrothermal brines by down-flowing electrolyte-poor, meteoric waters.

5.1 INTRODUCTION

Uplifted rift flanks play an important role in influencing the regional flow of fluids within intracontinental extensional basins (Person & Garven 1994, Stanislavsky & Gvirtzman 1999). The localized areas of higher topography create a hydro-dynamic gradient that drives waters downward into aquifers within the syn-rift sequence (Abebe 2000, Lampe et al. 2001, Clauser et al. 2002). This understanding of the regional hydrodynamic behavior of rift shoulders and their evolution through time has been advanced by modelling fluid flow, taking into account permeability, thermal gradients, topography, crustal stress and fluid chemistry (van Balen & Cloetingh 1993, Bartels et al. 2000, Pribnow & Clauser 2000). An important aspect of such studies is to predict the physical and chemical properties of faults in the uplifting graben shoulders, which have implications for understanding and exploiting water, thermal and mineral resources in sedimentary basins (Carlé 1958, Evans 1990, Sibson 1994, May et al. 1996, Lampe et al. 2001), as well in the safety assessment of underground waste repositories (Gautschi, 2001).

The formation of clay minerals in faults have been shown to play a particularly important role in influencing the flow of fluids in sedimentary basins (Knipe 1993). Clay growth influences anisotropy, permeability and porosity as well as fault strength (Morrow et al 1984, Wintsch et al. 1995, Wibberley 1999, Warr & Cox 2001, Solum et al. 2003). Clay minerals also provide important information concerning fluid composition, temperature and the degree of fluid-rock interaction (Velde 1985, Inoue et al. 2004). However, in contrast to the well studied continuous, prograde clay mineral reactions from smectite to illite-smectite to illite-muscovite within burial diagenetic, low temperature metamorphic and hydrothermal environments (Srodon & Eberl 1984, Hunziker et

al. 1986, Dong et al. 1997), the nature of retrograde illitic and smectitic mineral reactions in fault rocks (Zhao et al. 1999, Abad et al. 2003), and in particular within the uplifted flanks of rift basins, has received much less attention.

In this chapter the nature of fluid-related clay mineral reactions within faulted crystalline basement rocks along the eastern uplifted flank of the Rhine rift, in the vicinity of Heidelberg, is examined. Based on X-ray and electron microscopy studies of reaction textures, mineral compositions and clay fabrics across the Schauenburg Fault, the exhumation and fluid-rock history of the rift flank is assessed. The Rhine rift provides an excellent region for such a study, because of the young age of the rift system, its well defined uplifted shoulders, and the availability of water chemistry from various depths in and around the rift system (e.g. Carlé 1975).

5.1.1 Sample material and field relationships of the Schauenburg Fault

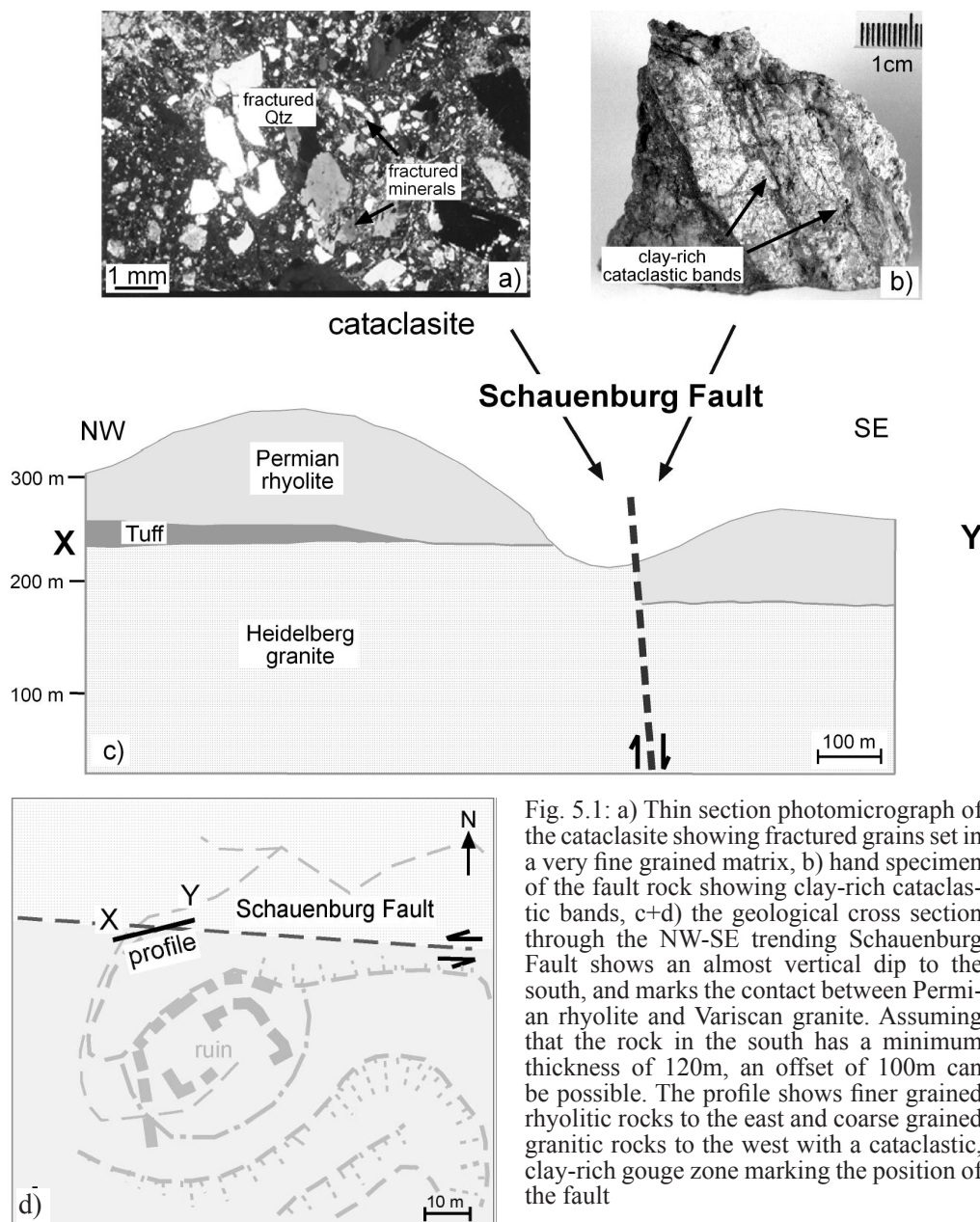


Fig. 5.1: a) Thin section photomicrograph of the cataclasite showing fractured grains set in a very fine grained matrix, b) hand specimen of the fault rock showing clay-rich cataclastic bands, c+d) the geological cross section through the NW-SE trending Schauenburg Fault shows an almost vertical dip to the south, and marks the contact between Permian rhyolite and Variscan granite. Assuming that the rock in the south has a minimum thickness of 120m, an offset of 100m can be possible. The profile shows finer grained rhyolitic rocks to the east and coarse grained granitic rocks to the west with a cataclastic, clay-rich gouge zone marking the position of the fault

A total of 18 samples were collected from a surface outcrop across a ca. 50m profile, traversing the fault zone (Fig. 2.2 page 7, 5.1, appendix page 87). Three segments could be recognized based on mesoscopic appearance: a rhyolitic wall rock zone to the south, with coarse-grained K-feldspar and quartz phenocrysts set in a fine-grained, felsic matrix; a finer grained cataclasite along the fault plane, characterized by strongly altered feldspar grains and thin, dark veins filled with cataclastic material (Fig. 5.1); and a highly fractured granitic wall rock to the north of the fault, with notably friable coarse-grained alkali feldspars and abundant biotite.

5.1.2 Analytical procedure

Samples were investigated by optical microscopy, XRD and SEM. Representative specimens were then selected for more detailed studies using XTG, HRTEM and AEM. The XRD work was partly conducted as part of the diploma thesis of Schleicher (2001). Additionally results were obtained using random powder and oriented texture samples (appendix page 93). Preparation of rocks followed the analytical methods described by Moore & Reynolds (1997). To aid the identification of the clay minerals, the samples were measured in a variety of states, including Ca-saturated, ethylene-glycol treatment and heating up to 480° C for 1 hour. The d-values were calibrated against the position of quartz reflections, and the FWHM parameter calibrated using the standards of Warr & Rice (1994). Selected samples were used for measuring the crystallographic-preferred orientation of illite by XTG (e.g. Oertel 1985, Schmid & Casey 1986). Normalized intensity data are expressed in multiples of random distribution (m.r.d.; Wenk 1985), where higher m.r.d values represent a larger degree of mineral preferred orientation.

SEM study was undertaken on gold- or carbon-coated samples prepared as small rock pieces (for secondary electron images) and thin sections (for backscattered images). Qualitative analyses of mineral composition were obtained by EDS. Three representative samples were also investigated by HRTEM and AEM following the analytical procedure outlined by Peacor (1992) and Warr & Nieto (1998). Samples were vacuum impregnated with L.R. White resin, to prevent collapse of smectite interlayers, following the procedure of Kim et al. (1995). Small sections (1mm diameter) were picked from the more homogenous and representative areas of the thin sections, then ion milled and carbon coated (appendix, page 88/89). TEM study of the material combined lattice-fringe imaging and SAED patterns of selected sites of interest, using the same methods as for the Soultz-sous-Forêts granite samples. Microscopy was also undertaken using a Philips CM 12 scanning-transmission electron microscope (STEM) with a Kevex Quantum solid-state detector, operating at 120kV and a beam current of 20mA. Further details can be found in the appendix (page 89/95). Compositional data were calibrated using the k-values of available laboratory standards.

5.2 RESULTS

5.2.1 Sample characteristics and mineral assemblages

The granite and rhyolite collected across the Schauenburg Fault are predominantly coarse-grained, except for a ca. 4m wide intensely deformed fine-grained cataclastic zone, developed along the fault plane (Fig. 5.1). The primary mineral components of both rock types are quartz, K-feldspar, plagioclase and biotite. Secondary minerals are plagioclase, sericite and a number of accessory minerals, notably hematite and rutile. Hand specimens of the less altered granite and rhyolite lithologies have an isotropic texture, which becomes increasingly overprinted by a brittle cataclastic fabric toward the fault plane.

Characteristically, the rhyolite is dominated by various phenocrysts (> 2-3mm) in a fine-grained matrix. Optical microscopy reveals 30-35% of anhedral, undulose quartz grains with strongly sutured, sometimes recrystallized rims. Large altered K-feldspars (20-25% of grains) show typical Carlsbad twinning and perthitic textures, but in contrast, the plagioclase and also biotite are strongly altered, and show signs of localized intracrystalline deformation. Open fractures within large quartz and feldspar grains are partly in-filled with granular, fine-grained quartz and later Fe-oxide phases (particularly hematite). The degree of brittle deformation increases toward the center of the fault plane, where the rocks are intensely fractured.

In contrast, the granite is coarser grained with characteristically large phenocrysts of K-feldspar, quartz and biotite. Quartz, which makes up ca. 40% of the rock, shows only minor degrees of intracrystalline deformation, expressed by undulose extinction. The cracks in these minerals are usually unmineralized, but the sericite alteration of feldspars is notably more intense than in the rhyolite, with almost complete alteration of plagioclase grains.

The 4m wide cataclastic zone is marked by a transitional increase in the degree of rock alteration, whereby the fault material becomes notably incohesive, forming a clay-bearing cataclasite. It is composed of a mixture of angular, small-sized (< 1mm) granitic and rhyolitic derived clasts, set in a heavily altered, very fine-grained clay matrix (Fig. 5.1). Anhedral quartz clasts (40-45%) show intensely dissolved mineral rims with a strong intracrystalline deformation, but almost no recrystallization. Strongly altered and fractured feldspar (30-40%) and deformed biotite crystals also occur. Whole rock geochemical investigations confirm the mixed origin of material in the cataclasite, but show a stronger similarity with the granite (Marbach et al. in press).

5.2.2 X-ray diffraction analysis

The whole rock powder XRD analysis confirms the mineralogical assemblage determined from thin section study. In addition to quartz, mica and feldspar (K-feldspar and albite) as main components, apatite, calcite and hematite are identified as typical accessory phases. In contrast, the clay-sized fraction (< 2 μ m) is dominated by illite, kaolinite, mixed-layered illite-smectite and occasional smectite. Comparing the basal (001) reflection of clay mineral XRD patterns of the different rock types reveal differences in air-dried, glycolated and heat-treated preparations,

indicating the presence of mixed-layered smectite (Fig. 5.2). In air-dried samples, the XRD pattern typically has a ca. 10.3 Å peak that shifts to ca. 10 Å when treated with ethylene glycol, with a weaker reflection appearing at ca. 11.1 Å. These characteristics suggest a R3 illite-smectite polytype as the dominant illitic phase, characterized by long-ranged ordering. The presence of smectite interlayers is confirmed by heating up to 480°C, causing the collapse of layers and the formation of sharp illite reflections at ~10 Å. Similar mineral assemblages were detected in the fault zone, with broad reflections of illite and illite-smectite mixtures. Discrete smectite reflections were observed in only a few granite samples.

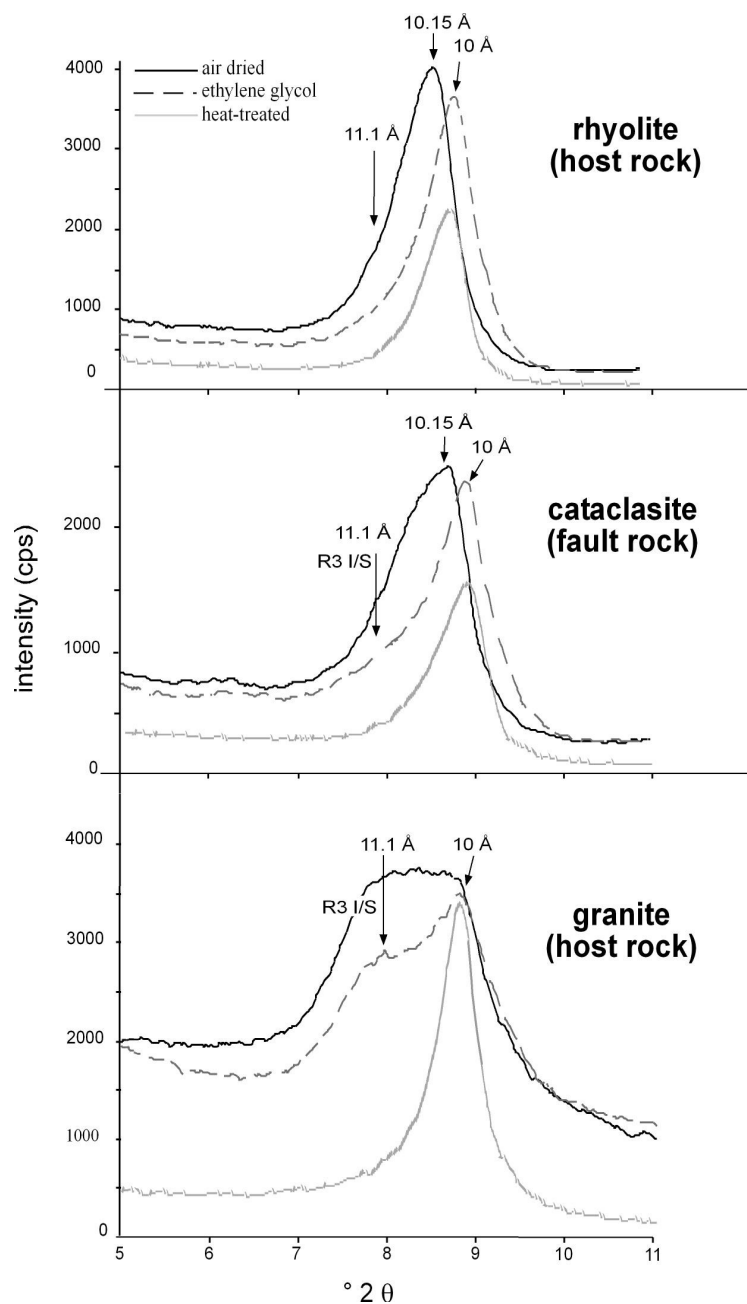


Fig. 5.2: XRD characteristics of the rhyolite, cataclasite and granite rocks from the Schauenburg Fault. The clay mineral (001) reflections of illite and illite-smectite, occurring between 5 and 11°2θ are shown for air-dried, glycolated and heat-treated preparations.

All samples contained significant amounts of kaolinite, with a basal reflection at 7.1Å. This mineral phase becomes thermally unstable at 500-550°C, indicating to be the kaolinite polytype (*sensu stricto*), as opposed to the higher temperature polytype of dickite (Brindley & Brown 1980, Ehrenberg et al. 1992). Fig. 5.3 shows intensity (cps) variations and FWHM values for the (001) illite and (001) kaolinite reflections across the fault zone.

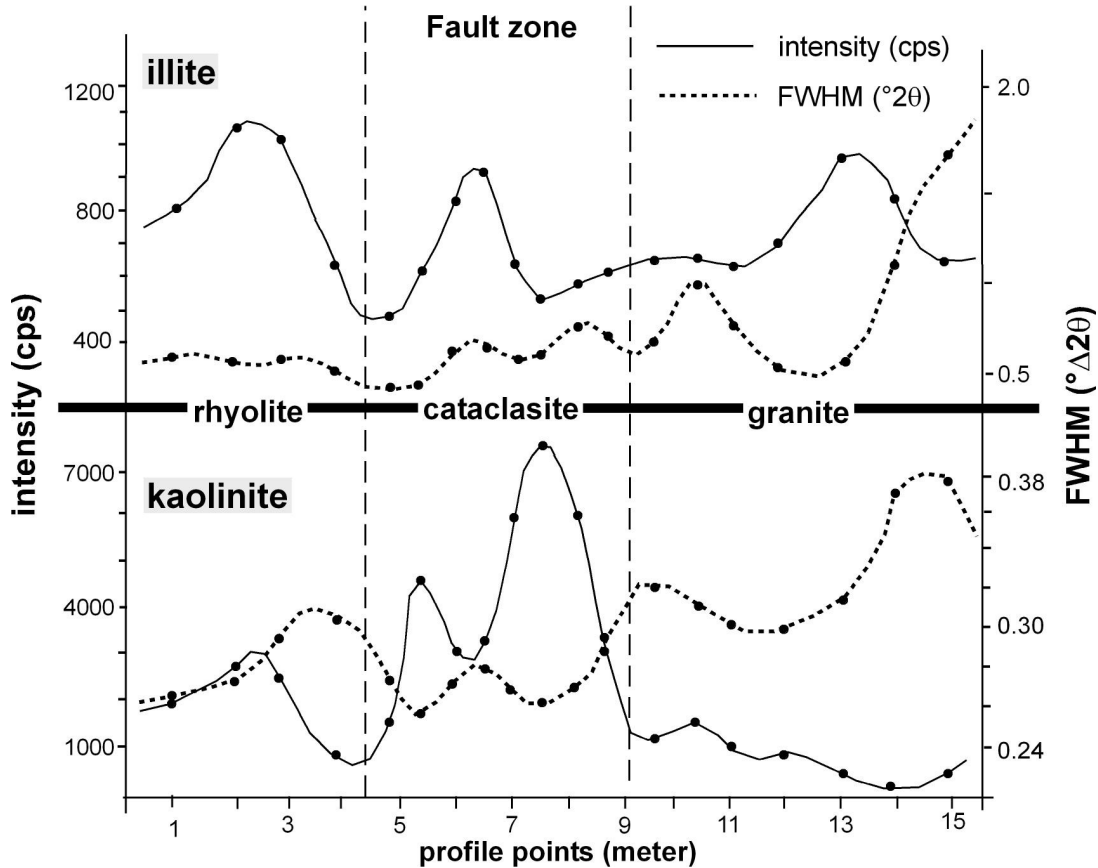


Fig. 5.3: Peak breadth (FWHM, dashed line) and intensity (cps, solid line) results of the (001) illite and (001) kaolinite reflections, which are plotted against the profile transect. The samples contain significant amounts of kaolinite in the cataclastic fault plane, whereas there are three specific illite peaks in all rock types, defining some probably pre-rift structures. Both illite and kaolinite crystallite sizes increase toward the granitic rocks

Differences in peak intensity are considered to largely reflect relative changes in mineral abundance, as the texture slides were prepared using constant amounts of clay, with consistent and reproducible degrees of particle orientation and heterogeneity. Three intensity maxima can be recognized for illite across the fault zone. Each maximum is characterized by a continuous increase in peak height, with a surprisingly low degree of fluctuation between samples. Although the precise amount of illite in these samples have not been quantified, the areas of enrichment occur both in fractured wall-rock and in the center of the fault zone. The maxima, therefore, seem to correspond to the position of highly fractured rupture zones or minor faults; however, due to poor exposure, the exact position of displacement planes could not be recognized in the field.

Variations in the FWHM of illite also occur across the fault profile. The lowest values occur

in the rhyolite (0.69 to $0.82^\circ 2\theta$), the highest values in the granite (mean= $1.2^\circ 2\theta$), whereas the fault zone is intermediate between the two (mean= $0.82^\circ 2\theta$). Notably higher degrees of fluctuation occur both in the fault zone and the granite. As these variations are maintained following treatment with ethylene glycol, the FWHM values are considered to largely reflect differences in mean crystallite size with lesser influence from the presence of mixed-layered smectite.

A mixture of $1M_d$ and $2M_1$ illite polytypes could be recognized by visual examination of the random powder XRD patterns, following the methods described in Grathoff & Moore (1996). The dominant polytype in all samples is a $1M_d$ illite variety with distinct peaks at 3.66 and 3.07\AA , whereas a $2M_1$ illite is present only in minor quantities, with diagnostic reflections at 2.98 , 2.86 and 2.80\AA , and is most abundant in the rhyolite. A quantification of illite polytypes was not conducted due to the large degree of overlapping reflections from other mineral phases, making reliable measurement of peak areas and intensities difficult. The intensity and FWHM variations of kaolinite across the fault zone show a simpler pattern than the illitic phases (Fig. 5.3).

Based on the high kaolinite peak intensities within the cataclasite, this mineral can be inferred to be most abundant along the fault zone. In contrast, kaolinite is least abundant in the granite. The low FWHM values of the (001) kaolinite reflection of fault zone samples also reflect thicker crystallite packets within the fault core. The highest FWHM values, reflecting small mean crystallite thickness, correspond with the lower amounts of kaolinite in the granite unit.

5.2.3 Rock texture

The preferred orientations of illite crystallites for the three representative samples (rhyolite, cataclasite and granite) measured using the (001) reflection at 10\AA , are plotted as contoured X-ray intensity data on equal-area, lower hemisphere projection pole-figures (Fig. 5.4).

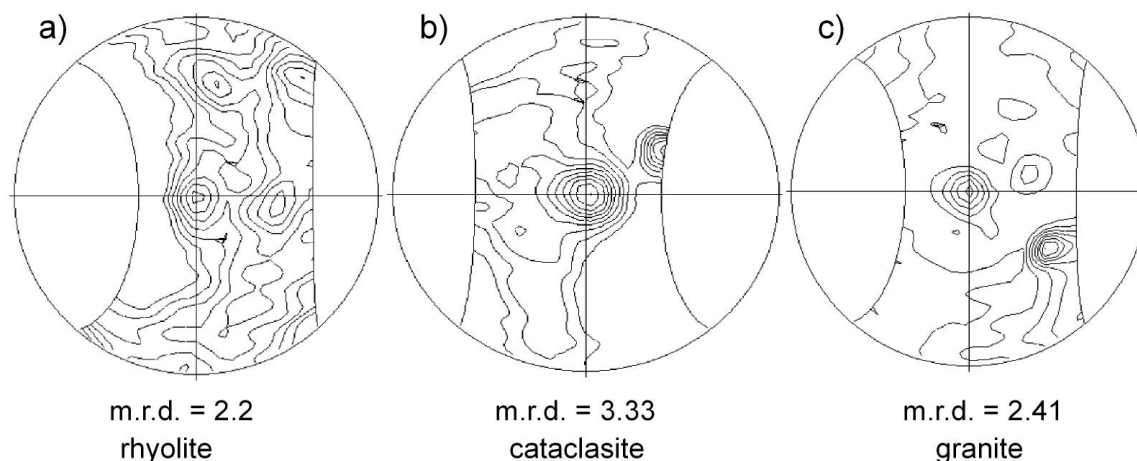


Fig. 5.4: Examples of X-ray texture goniometer (XTG) pole figures from three selected samples of the Schauenburg transect. The figures show the clay preferred orientation for a) rhyolite, b) cataclasite and c) granite, where each contour represents multiples of random distribution (m.r.d.)

The maxima for each sample have been rotated to the centre of the projection to reveal the shape and the intensity of fabric elements. The X-ray goniometry plots reveal complex fabrics

across the fault zone. The textural patterns of the rhyolite are characterized by four several closely spaced maxima attributable to the presence of relatively large stacks of illite (and kaolinite) as observed by electron microscopy (Fig. 5.4a). The poorly defined maxima (up to m.r.d of 2.2) reflect the variable orientation of clay stacks in the sample. In contrast, the cataclasite sample contains two tightly grouped maxima, defining a better-developed fabric (m.r.d. of 3.33; Fig. 5.4b). Microscopic observations similarly reveal the orientation of illite and kaolinite stacks to vary in the cataclasite samples with their basal planes lying subparallel to the fault plane. A well-defined fabric is absent in the granite sample (Fig. 5.4c), similar to the texture of the rhyolite (Fig. 5.4a).

5.2.4 Microstructure and chemical analysis

5.2.4.1 Scanning electron microscopy

Secondary and back-scattered electron microscopy images combined with EDS analyses reveal a variety of illite and kaolinite particle shapes, sizes and microstructural features, which vary across the fault zone (Fig. 5.5).

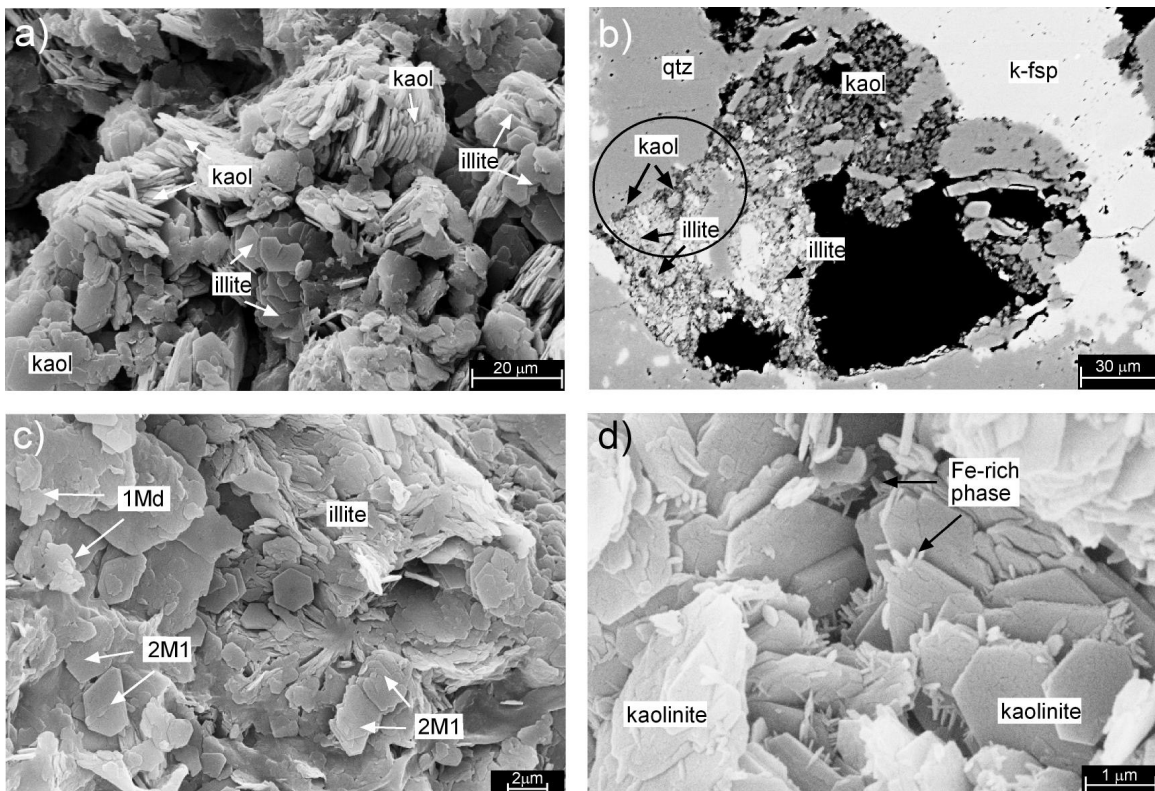


Fig. 5.5: SEM illustrations of the rhyolitic, the granitic and the cataclastic samples of the Schauenburg Fault region, a) vermiform stacks of illite and kaolinite grow side by side in feldspar pore spaces, b) BSE image of a pore filling in the cataclasite, with a feldspar to illite reaction appearing to be post-dated by the younger growth of kaolinite crystals in association with the dissolution of quartz, c) larger, pseudo-hexagonal 2M₁ illite polytypes grow together with smaller, slightly dissolved 1M_d illites in a pore spaces, d) hexagonal crystallites of kaolinite are overgrown with small, Fe-rich minerals

The cataclasite minerals are generally 0.5 to 4 μm in size and occur mainly as pore fillings associated with areas of high porosity (Fig. 5.5a). Some vermiform packets of blocky kaolinite are observed, stacked linearly up to 10 μm in length. Pores appear to have formed primarily by

the dissolution of quartz and feldspar, whereby plagioclase appears to be dissolved completely in the clay-sized fraction. A number of reaction textures can be observed, with the feldspar to illite reaction appearing to be post-dated by the younger growth of kaolinite crystals in association with the dissolution of quartz (Fig. 5.5b).

A range of illite crystal shapes can be observed by SEM in all units across the fault zone. Relatively large subhedral to euhedral crystals of illite occur within pore fillings (Fig. 5.5c), together with smaller illite particles having characteristic irregular edges. The latter are grouped together within larger aggregates. The well-crystallized euhedral kaolinite within the pores of the cataclasite has an average grain size of ca. $2\mu\text{m}$, and is post-dated by neocrystallization of smaller Fe-oxide particles (Fig. 5.5d).

5.2.4.2 High-resolution electron microscopy

Representative HRTEM images showing typical mineral assemblages and their microstructural characteristics of the rhyolite, cataclasite and granite samples are given in Figs. 5.6 to 5.8. At low magnification, the rhyolite contains packets of 15-30nm thick illite crystallites stacked together with ca. 100nm thick kaolinite (Fig. 5.6a). The contacts between illite and kaolinite packets are planar and commonly characterized by low-angle crystallite boundaries. Here, kaolinite is not the most abundant clay mineral observed.

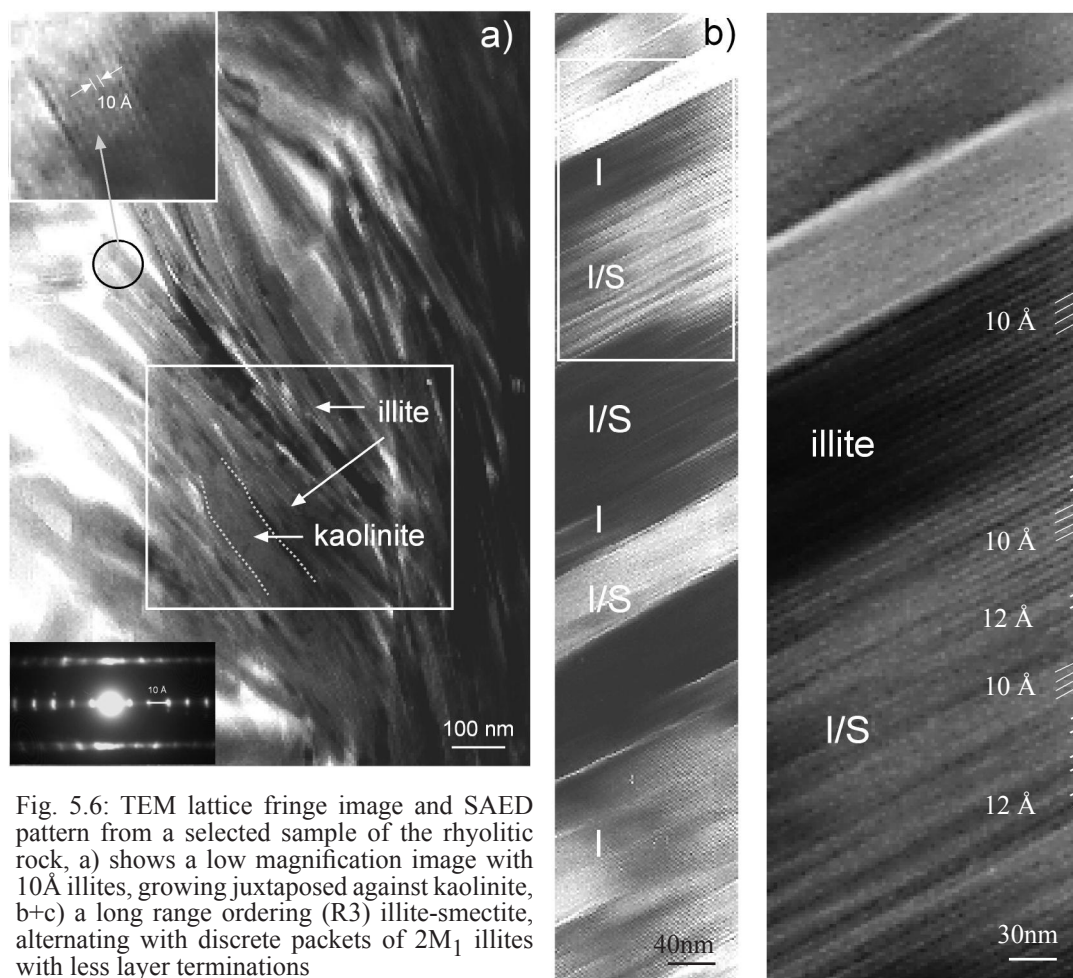


Fig. 5.6: TEM lattice fringe image and SAED pattern from a selected sample of the rhyolitic rock, a) shows a low magnification image with 10 Å illites, growing juxtaposed against kaolinite, b+c) a long range ordering (R3) illite-smectite, alternating with discrete packets of $2M_1$ illites with less layer terminations

Dominant are the packets of discrete illite and illite-smectite mixed-layered phases, which show relatively low concentrations of intracrystalline defects (e.g. layer terminations and lattice distortion) and a variety of crystallite thicknesses (Fig. 5.6b,c). Straight packets of discrete illite, at least 80nm long and 20nm in thickness, occur with a constant d-value. The occurrence of some 20Å periodicity in both fringe images and SAED patterns indicate these packets to be of the 2M₁ polytype. Illite-smectite mixed-layered minerals are also common in the rhyolite samples. These layers are stacked optically parallel with discrete illite packets (Fig. 5.6c). Smectite layers can be recognized by their higher contrast, irregular lattice fringes and ca. 12Å thicknesses. Long-range ordering, presumably R3, is evident by the reoccurrence of single smectite layers stacked optically parallel between 2 to 5 illite layers. The SAED patterns of the illite-smectite indicate a 1M_d polytype, with marked streakings in non-00 l reflections.

Four distinctly different minerals can be recognized in the cataclasite sample (Fig 5.7).

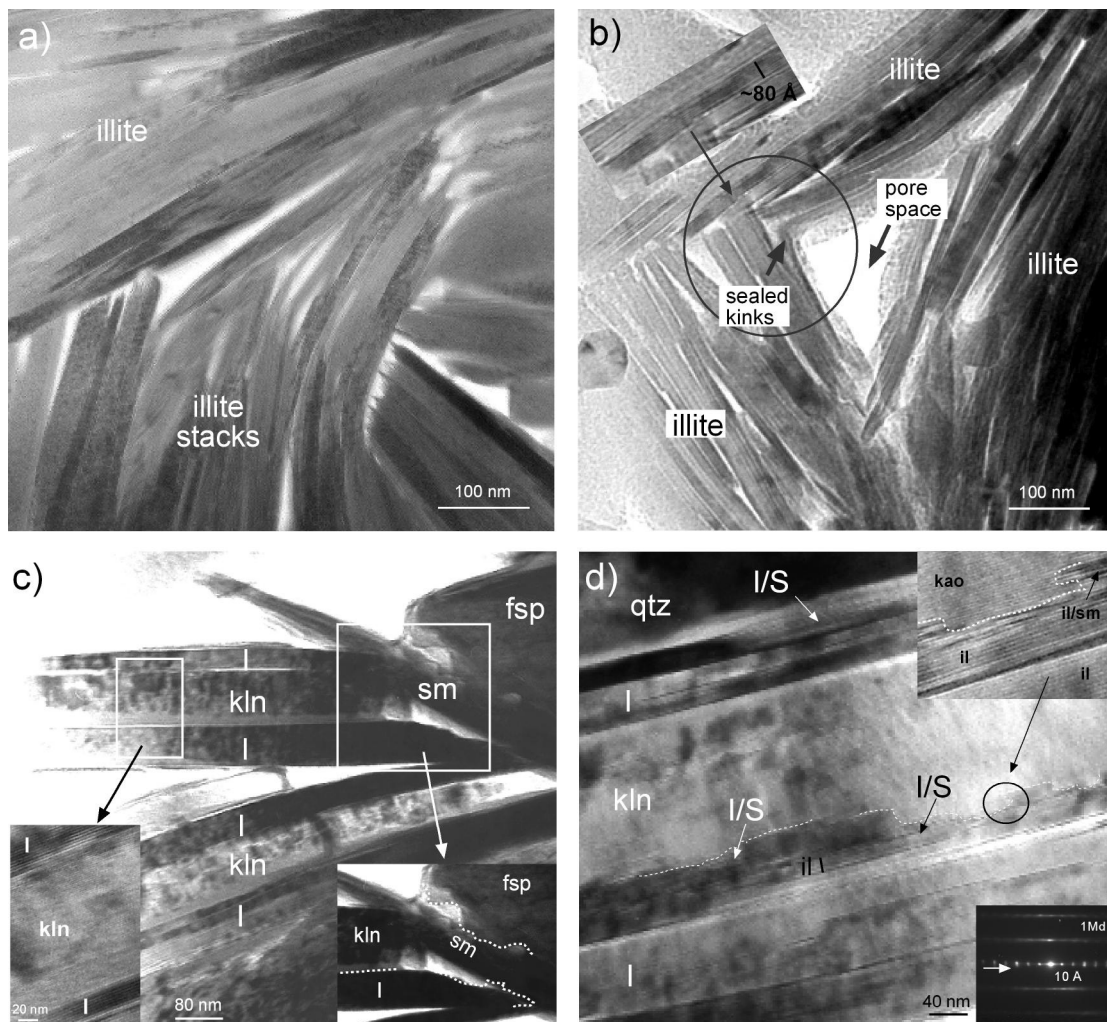


Fig. 5.7: Lattice fringe images and SAED pattern of the cataclastic fault plane. a) and b) show characteristically irregular 1M_d illite with frayed margins, which juxtapose against curved illite grains. Remnants of kink bands developed in illite packets are observed, c) and d) reveal the relationship between illite, illite-smectite and kaolinite. Kaolinite packets have formed by replacement of the illite and illite-smectite packets, and the contact between kaolinite and illite layers are often planar. Kaolinite and illite-smectite grain contacts are notably uneven, reflecting dissolution surfaces. The streaked hkl reflections on the SAED pattern indicate that stacking along (00 l) is disordered.

(i) abundant illite with typical 10Å layers, (ii) illite-smectite mixed layers that are more common than in the rhyolite sample, (iii) discrete particles of smectite, with typical anastomosing 12-14Å layers, and (iv) large quantities of thick kaolinite crystallites. All these mineral phases occur in crystallite packets commonly stacked parallel or subparallel to their basal planes. High angle grain boundaries also occur, with intersections between clay edges and particle surfaces (Fig. 5.7a,c,d). The edges of 1M_d illite crystallites, 10 to 20nm in thickness, show characteristically irregular, frayed margins, which juxtapose against curved illite grains, probably formed during rock deformation (Fig. 5.7a). Remnants of kink bands developed in illite packets are also observed (Fig. 5.7b), whereby the illite is interpreted to post-date kink formation. These structures are associated with significant pore space within fold hinge regions.

The formation of kaolinite packets (on average ca. 80-100nm thick) is commonly seen to replace illite and illite-smectite packets (Fig. 5.7c,d). The contacts between kaolinite and illite layers are often planar, whereas the kaolinite, illite-smectite grain contacts are notably uneven and reflect dissolution surfaces. Similar TEM replacement textures have been described by Robertson & Eggleton (1991) at kaolinite-muscovite contacts in altered granites of tin deposits in Australia. Smectite in the cataclasite occurs exclusively as individual particles, which have formed between pre-existing clay packets, and likely reflect neocrystallization in pore spaces.

Smectite particles with similar characteristics and origin are also observed in the granite sample. Areas of discrete smectite (Fig. 5.8a) have discontinuous, wavy layers with variable spacing between 12 and rarely 14Å, reflecting structural or compositional heterogeneities (Kim

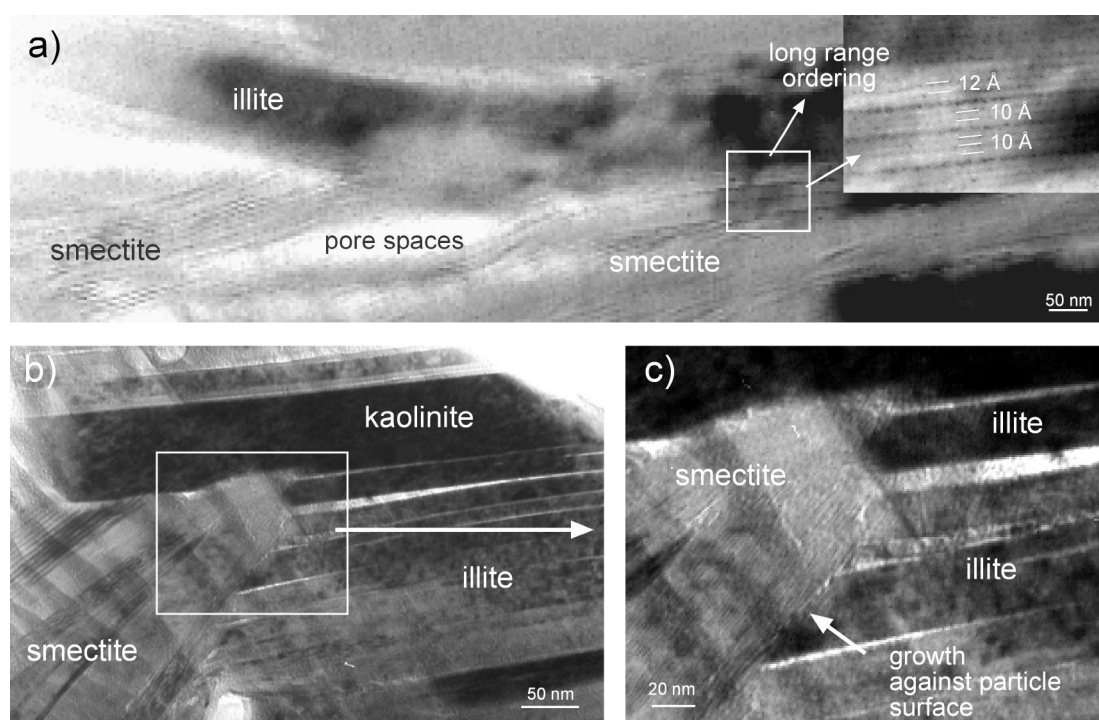


Fig. 5.8: a) low and b+c) high magnification images of the granitic rock sample. Discrete smectite has discontinuous, wavy layers with variable spacing between 12 and rarely 14Å. As in the rhyolite sample, the illite-smectite mixed layered structures are characterized by long-ranged orderings

et al. 1995). Defect-rich areas with abundant dislocations (layer terminations) are seen to have grown against both particle surfaces and edges of illite and illite-smectite crystallites (Fig. 5.8b, c), although precipitation of smectite layers does appear to have been associated with dissolution of both illite and kaolinite particle surfaces. As in the rhyolite sample, the illite-smectite mixed-layered structures are characterized by long-ranged ordering.

5.2.5 Compositions of illitic minerals

The structural formulae of illites (normalized to $O_{10}(OH)_2$) based on AEM analyses of the rhyolite, cataclasite and granite samples are listed in Tab. 5.1, and significant cations are plotted against Si content in Fig. 5.9. As Ca is absent or only present in trace amounts, it is not included here. Each of the samples can be distinguished on the basis of their octahedral and interlayer cation content. The rhyolite contains illite with compositions comparable to the Silver Hill illite (1Mt-1) of Hower & Mowatt (1966) as open squares in Fig. 5.9 and the felsic volcanoclastic illite of Inoue et al. (2004) as open triangles in Fig. 5.9, with an average K content of 0.64 per unit formula. In contrast, the illitic phases in the cataclasite are characteristically Al-rich (Al^{IV} : 0.79 per formula unit) and Mg-Fe poor, suggesting significant substitution of octahedral cations by Al. The lower interlayer cation content reflects the abundant mixed-layered smectite as also observed by TEM.

Two compositions of illitic phases can be recognized in the granite sample. An Al-rich illite (G1), similar to that found in the cataclasite, but with less octahedral substitution of Al for Mg and Fe, and a Si-rich, Al-poor phase, with a high interlayer cation content (G2), reflecting a high layered charged mineral. The latter illitic phase has an average K and Na content of 0.28 and 0.37 per unit respectively, probably reflecting the presence of some paragonite interlayers.

Tab. 5.1: Microchemical data for illite in the Schauenburg Fault zone, normalized to $O_{10}(OH)_2$ with interlayer summary (Σ_{int}) and octahedral summary (Σ_{oct}). Illite standard: Silver Hill illite (2Mt-1)

illite composition normalized to $O_{10}(OH)_2$	Si	Al^{IV}	Al^{VI}	Mg	Fe	Σ_{oct}	K	Na	Σ_{int}
rhyolite	3.53	0.47	1.4	0.31	0.23	0.54	0.64	0.08	0.72
cataclasite	3.21	0.79	2.06	0.06	0.05	0.11	0.24	0.02	0.26
granite 1	3.88	0.12	1.42	0.18	0.01	0.19	0.74	0.2	0.95
granite 2	3.14	0.86	1.67	0.32	0.19	0.52	0.28	0.37	1.66
Illite standard	3.39	0.62	1.35	0.26	0.41	0.67	0.69	0.00	0.69

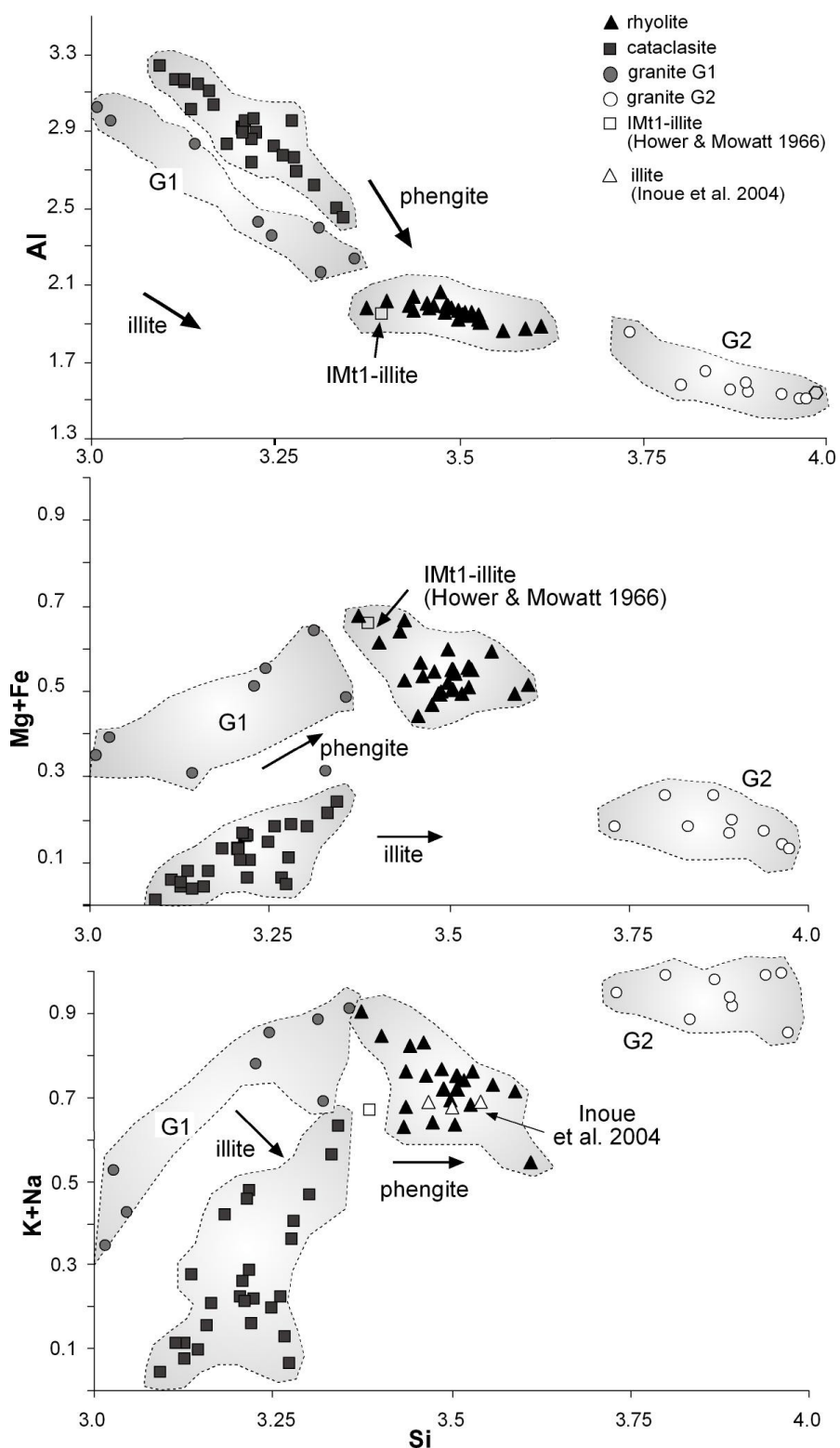


Fig. 5.9: Chemical composition diagrams of illite from the different lithologies. The symbols indicate the illite compositions in the different rock types, whereas Al and the octahedral and interlayer cations are plotted against silicon.

5.3 DISCUSSION

Fault rocks along the Schauenburg Fault are enriched in clay minerals with reaction textures representing a retrograde sequence of back-reactions from $2M_1$ illite polytypes to $1M_d$ (R3) illite-smectite to discrete smectite and kaolinite. The cataclasite, marking the fault plane, is particularly enriched in pseudo-hexagonal vermiform kaolinite stacks and illite-smectite assemblages. These patterns are interpreted to reflect fault-controlled circulation of low temperature hydrous fluids that were responsible for clay mineral formation. Based on the XRD, XTG and electron microscopy study, this retrograde history of clay mineral reactions is discussed in terms of initial hydrothermal illitization of feldspars, followed by exhumation and focused fluid flow along the fault zone within the uplifting rift shoulder. A schematic reconstruction of the mineral textures and rock fabrics of the Schauenburg Fault is presented in Fig. 5.10.

5.3.1 Hydrothermal illitization of feldspars

The first stage of alteration within the fault rocks was the crystallization of well-developed pseudo-hexagonal $2M_1$ illite crystals (sericite), formed predominantly by the dissolution of feldspar grains (Fig. 5.10a). The plagioclase feldspar has been completely altered in the clay-sized fractions of most rock types across the fault zone, and dissolution and illite crystallization in pore spaces is common within K-feldspar grains (Fig. 5.5b, 5.10a).

This $2M_1$ illitic phase shows features typical of fluid-dominated, hydrothermal mineral growth. The sharp illite peaks (XRD) of the rhyolite samples reflect well-ordered crystals (Fig. 5.5c), with a tendency toward K-phengitic (Si-rich) compositions (Fig. 5.8a). The stage of illite formation, dated to be of late Jurassic age (Marbach et al. in press), took place in an environment of regional scale fluid flow during Mesozoic extension. This tectonic setting is associated with the breakup of Pangaea and the initial stages of Atlantic rifting and burial by platform sediments across the peneplained Variscan basement (Clauer et al. 1995, Brockamp et al. 2003). The occurrence of pure illite in all rock types across the Schauenburg Fault zone, and its common occurrence in the more impermeable Permian rhyolite unit implies that this stage of hydrothermal alteration was more pervasive and occurred prior to Tertiary rifting. Although this initial stage of extensive rock alteration was fracture related, there is little indication to suggest that the Schauenburg Fault existed as a distinct fault at this time.

The phengitic composition of the pure illite phase is comparable with a number of low temperature illite formed under a range of diagenetic, low temperature metamorphic and hydrothermal conditions (Hunziker et al. 1986, Bove et al. 2002, Inoue et al. 2004). Yoder & Eugster (1955) and Velde (1965) determined that the $1M_d$ to $2M_1$ white mica transformation occurs experimentally in the temperature range of 125°C (400MPa) to 350°C, and in natural prograde metamorphic sequences this transition occurs predominantly under anchizonal conditions (200-300°C) and is complete by the beginning of the greenschist facies (Frey 1987). The direct dissolution of feldspar and precipitation of pure illite (sericite) is a reaction driven by proton attack and therefore triggered by the circulation of acid or neutral solutions (Brockamp et al. 2003) likely

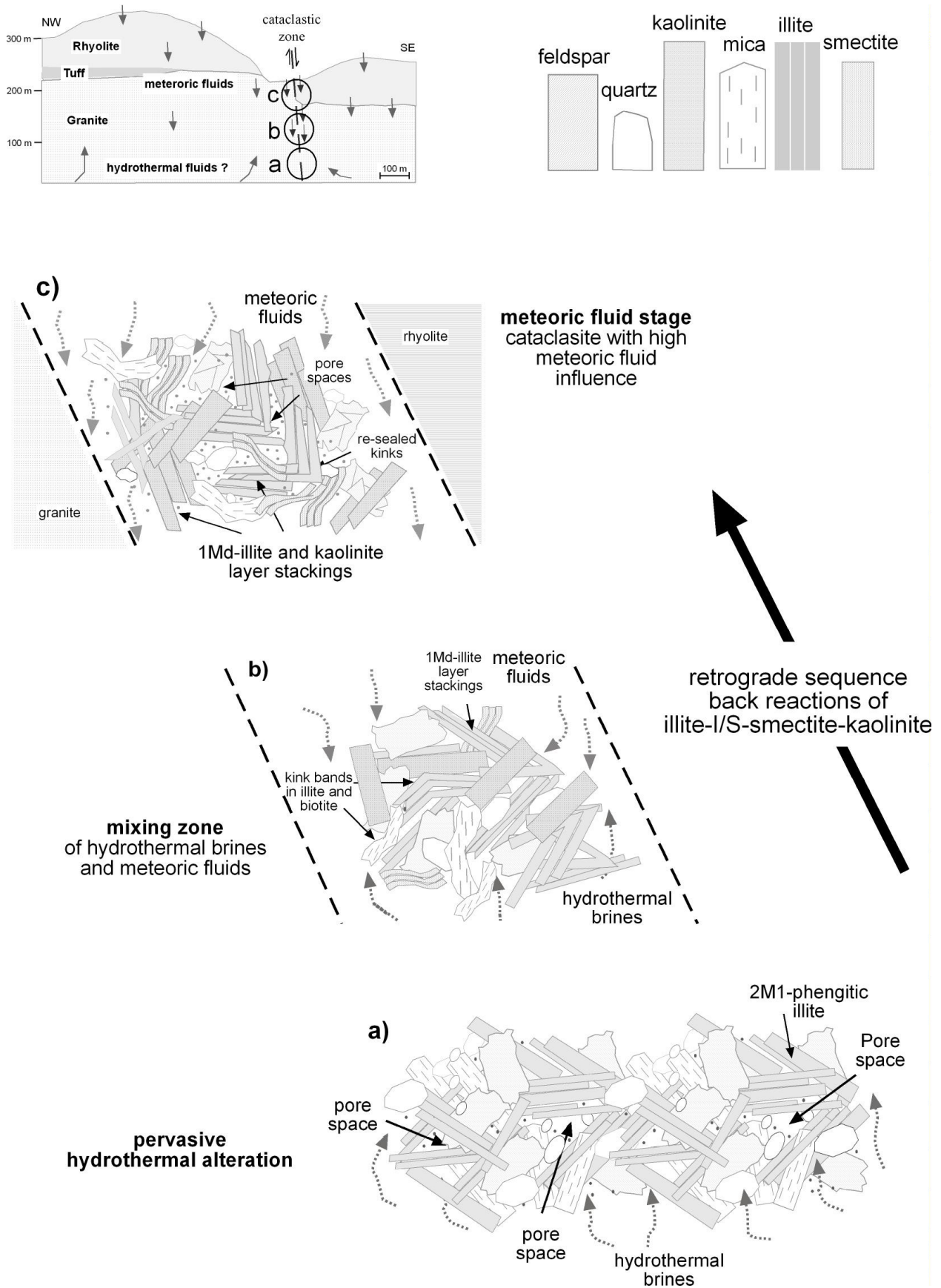


Fig. 5.10: Schematic representation of the development of the minerals in the cataclastic fault plane, under the influence of hydrothermal and meteoric fluids and the uplift of the Rhine graben shoulders

originating from granite fluids of the graben region. It is suggested that the Jurassic Schauenburg fluids were similar in composition to the mildly acidic hot thermal brines that have been recovered from depths in the basement of the rift and in adjoining areas (Soultz, Cronenburg, Urach 3). Such fluids are typical of high $p\text{CO}_2$ contents, where the lower carbonate content of granitic crystalline rocks give a low buffering capacity, hence yielding neutral to slightly acidic solutions (Appelo & Postma 1999). These fluids differ from the more alkali concentrated brines of the Heidelberg borehole, which result from percolation through young Miocene evaporites (Carlé 1975).

The compositions of the 2M_1 Schauenburg illites are also very similar to those described in felsic volcanoclastic rocks of the Kakkonda active geothermal system of Japan by Inoue et al. (2004), where phengitic Mg + Fe rich R3 illites were formed at depths $> 750\text{m}$ ($> 174^\circ\text{C}$) under the influence of circulating NaCl-rich brines (pH of ~ 7.3), which were considered to represent a mixture of meteoric and fossil seawater that was trapped in the sediments.

5.3.2 Exhumation and flushing of the fault

A fault-related stage of alteration is recognizable in the layer-by-layer transformation from 2M_1 illite to 1M_d (R3) illite-smectite (Fig. 5.6c, 5.10b). This reaction was formed by new illite-smectite crystallites that overgrow kinked white mica structures, but are themselves only slightly deformed (Fig. 5.7a, b). As the fault cuts the Permian rhyolite, and slightly offsets the main N-S striking Rhine Graben boundary fault, this stage of alteration is attributed to exhumation and uplift along the fault during Tertiary or post-Tertiary times.

These Al-rich illite-smectite are most predominant within the cataclasite, and have compositions notably depleted in K, Mg and Fe. They are similar to some of the illite described by Inoue et al. (2004) formed from near neutral pH- and Na-rich solutions generated by progressive hydrolytic reactions between felsic glass and groundwater formed at temperatures $> 133\text{-}160^\circ\text{C}$. In the Schauenburg Fault, these Al-rich illites are attributed to cooling hydrothermal basinal brines that were diluted by infiltration of meteoric waters. Such zones of mixing have been documented in the present day chemistry of ground waters along the Rhine Graben margin (Bender 1995, Durst & Vuataz 2000) and have been reported in fluid inclusion studies of diagenetic minerals (Behr et al. 1987).

The significant quantities of kaolinite along the fault, which formed mainly by the replacement of illite-smectite (Fig. 5.7d), reflect the final stage of fault zone flushing and implies the circulation of large volumes of dilute waters of meteoric origin. The alteration textures observed in the cataclasite are very similar to those documented in granites of Trial Hill in east Queensland by Robertson & Eggleton (1991). The layer-by-layer transformation process involves the replacement of K^+ ions by H_3O^+ ions in the mica interlayer sites and, therefore, involves the release of cations into solution. The reaction of white mica to kaolinite is well documented and is particularly well known from the hydrothermal or supergene alteration of granites (Robertson & Eggleton 1991). Key factors controlling this reaction are low temperatures $< 120^\circ\text{C}$, large fluid-to-rock ratios and acidic conditions. This stage of alteration was therefore enhanced by the influx of fresh, potentially

organic-rich meteoric waters as the fault was exhumed to near surface levels.

Similar alteration was observed along the main eastern boundary fault, during the construction of the train tunnel in Heidelberg (V. Schweizer, *pers. comm.*), supporting the interpretation of percolation of these younger waters to be fault-controlled. The enhanced fabrics and permeabilities of these faults allowed a down-flowing fluid movement along older (pre-existing) fractures of the eastern half graben shoulder. This stage of fluid flow likely corresponds to the stage of REE and Pb-enrichment within the fault and the Th-U disequilibrium modeled age supports a young timing (10^5 – 10^6 years) for this final event.

5.4 CONCLUSIONS

- 1) A retrograde sequence of fluid-controlled, low temperature clay mineral back-reactions have occurred along the Schauenburg oblique-slip fault of the uplifted eastern shoulder of the Rhine Graben.
- 2) The initial stage of alteration was marked by the dissolution of plagioclase and K-feldspar under the influence of hot, but mildly acidic Jurassic hydrothermal brines.
- 3) Alteration to K-illite of phengitic composition is attributed to regional, pervasive fluid-flow, best preserved in the Permian rhyolite.
- 4) Subsequent cooling and a dilution of waters passing through the fault zone during Tertiary uplift of the rift shoulders, formed successively cation-depleted clays which produced illite-smectite mixed-layers, pure smectite and finally pure kaolinite.
- 5) This study identifies the Schauenburg Fault as a primary location for the mixing of basement brines and meteoric waters with fault zone flushing corresponding to uplift and exhumation of the Rhine Graben flanks.

6 A SYNTHESIS AND DISCUSSION

ABSTRACT

This chapter synthesizes and discusses the type of clay mineral reactions and crystallization mechanisms that occurred in the faulted and fractured granitic rocks of the presented case studies. Based on their mineral abundance, crystal shapes, polytypes, chemistry and fabric development, the analyzed faulted crystalline rocks of the Rhine Graben basin and uplifted shoulder were compared and integrated to reconstruct an alteration history for the basement of the Rhine rift system. K-Ar isotopic age value analyses of the various grain-size fractions reveal at least three episodes of fluid-dominated illite mineralization occurred during Permian, Jurassic and Cretaceous (or younger) times in the hydrothermally mineralized Soultz-sous-Forêts granite. Repeated transitions from pseudo-hexagonal platy $2M_1$ illite to lath and fibrous $1M$ trans-vacant illite occurred as the mineralized veins and fracture granite was progressively sealed by episodic and heterogeneously distributed crystallization events. These reactions were related to the extensive breakdown of feldspar (plagioclase and K-feldspar) and biotite, although the younger phases of illite also crystallized at the expense of older illite crystals. In contrast, the Schauenburg Fault shows a single Jurassic hydrothermal event forming platy $2M_1$ illite followed by a retrograde series of back-reactions related to exhumation and uplift of the rift shoulders and the influx of electrolyte-poor meteoric waters. These back-reactions produced a disordered $1M_d$ illite-smectite, as well as significant quantities of kaolinite and some smectite. The differences in fluid-related episodic clay mineral formation between the two localities can be related to the different history of faulting, burial, exhumation and fluid-rock interaction.

6.1 INTRODUCTION

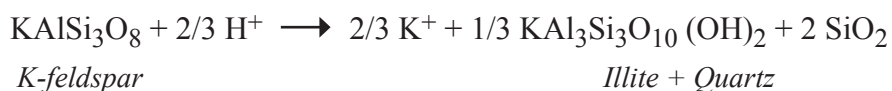
Fluid flow within faulted and fractured rocks is known to cause local mineral reactions by both dissolution and crystallization of unstable mineral phases (Sausse 2002, Solum et al. 2003, Thyne et al. 2001, Wilkinson & Haszeldine 2002). These changes invariably influence both rock porosity and permeability, and thus are of central importance in influencing fluid flow by sealing or opening of fluid pathways (Sausse 2002). The most important set of mineral reactions occurring in crystalline (igneous) basement rocks of the upper crust involve incongruent dissolution and hydration of high temperature, high pressure minerals and the formation of clay minerals along fractures and adjacent wall rock material (e.g. Evans 1990, Warr & Cox 2001, Imber et al. 1997). The current challenge is to understand the alteration mechanisms that influence such mineral reactions in both time and place, and to resolve their dependence on thermal history, fluid activity and rock deformation in fractured crystalline rocks.

The following chapter synthesizes and discusses the nature of clay minerals formed in such fractured and faulted crystalline rocks of the Rhine Graben basin and its uplifted shoulder (Chapters 4 and 5). The primary motive here is to evaluate the characteristics of the alteration products and to assess their importance in the fluid-rock history of the region. Particular attention will be given to

discussing the reactions and crystallization processes that took place in these faulted rocks based on evaluation of clay mineral abundance, crystal shape, polytype structure, chemistry and fabric development. It is shown that these features are related to the tectono-thermal history of the region, and formed during stages of burial, exhumation and uplift related to recognized geological events occurring pre-, syn- and post-rift formation.

6.2 Mineral reactions and clay formation

The kinetic controls of fluid-mineral reactions are of critical importance in the formation of clay minerals. An important aspect is the supply of ions derived from minerals or circulating fluids (Small et al. 1992), which continuously vary as old minerals dissolve and new ones crystallize. In the two case studies presented in this thesis, the hydration of feldspar (both plagioclase and K-feldspar) is the main reactant altering to clay minerals in the crystalline rocks. The two dominant reactions are listed below:



Both these alterations occur under weakly acidic conditions and represent incongruent dissolution of high temperature alkali-alumino-silicates by proton (H^+) attack (Meunier & Velde 2004, Brockamp et al. 2003). The precipitation of quartz and illite occurs with increasing ionic concentrations, and is associated with the release of alkali cations (Na and K) into solution (Shijun et al. 2001).

In the Soultz-sous-Forêts borehole the illite neo-crystallization occurs via two principle mechanisms involving the alteration of feldspar. In the matrix illite is formed largely by dissolution of plagioclase crystals (ca. 39.5% content in fresh granites, Tab. 6.1) and minor K-feldspar (ca. 18-20% in fresh granite). In the fractured granite sample (2167m), the matrix plagioclase is much more extensively altered (ca. 15%) than the K-feldspar (ca. 10%), and optically shows extensive illitization along the lamellae twin planes of albitized feldspar grains. In the pervasively altered granite sample (1570m), plagioclase and K-feldspar are notably less altered (ca. 40% plagioclase and ca. 15% K-feldspar). In these cases the source of K^+ could also reflect extensive biotite alteration (ca. 9% in fresh granites), which can react to chlorite by the following equation (after Veblen 1992):



Strong alteration of biotite (ca. 6%) to chlorite is observed in the pervasively altered granite

at 1570m depth. In contrast, the fractured granite at 2160m depth is characterized by intense alteration of biotite directly to illite, with only local occurrence of chlorite. Such reactions were also documented by L  desert (1999) in the hydrothermally active cataclastic zone at ca. 2158m depth, along with the coeval occurrence of tosudite (a mixed-layer smectite-chlorite mineral).

Tab. 6.1: Mineral content (%) of the Soultz-sous-For  ts granite and the Schauenburg Fault samples determined from thin sections

	Soultz-sous-For��ts samples							Schauenburg Fault samples		
	Fresh granite(1)	Fresh granite(2)	vein 1431m	granite 1570m	granite 2167m	vein 2160m	vein 2176m	rhyolite	cataclasite	granite
Qtz	29.4	25.9	30	20	15	50	40	30	40	30
Plg	39.9	39.4	--	40	15	--	--	max.5	max.5	10
K-fls	18.8	19.8	2	15	10	1	1	20	15	20
Bt + Chl	8.4	9.4	--	6	3	--	--	3	1	6
Hbl	4.5	3.5	--	1	--	--	--	--	--	--
Carb	--	--	10	1	1	--	--	--	--	--
Kln	--	--	--	--	--	--	--	20	30	15
Il	--	--	58	12	63	45	38	10	8	9
Hem	--	--	3	--	--	--	--	1	1	3

(1) Ledesert 1996 (2) Genter 1989

In contrast, illite mineralization in the veins resulted from direct precipitation from an inflowing of highly saline solutions rich in Na⁺ and Cl⁻ (Pauwels et al. 1992, Durst & Vuataz 2000). The present day Soultz brines of similar composition (Pauwels et al. 1993) indicate these solutions to be relatively rich in K⁺ (ca. 3.36g/l), however the activity is reduced by the high concentrations of Na (ca. 28.3g/l) and Ca (ca. 8g/l), as seen in Tab. 6.2.

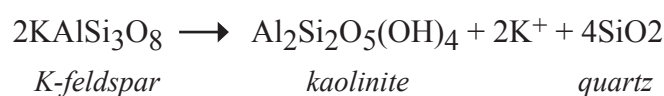
Tab. 6.2: Composition of present day Soultz-sous-For  ts brines and fluids (mg/l) from two granite wells in the Black Forest margin

locality	author	Na	K	Mg	Ca	Fe	Cl	depth (m)	temp. (��C)
Soultz-sous-For��ts EPS-1 borehole	Pauwels et al. (1993)	28300	3360	122	7990	20.4	59800	2000	150
Black Forest margin granite well	Bender (1995)	3	1.2	1.7	6.3	0.01	2.6	--	9.1
granite well	Bender (1995)	1.4	2.0	2.1	5.8	0.04	3.2	--	7.5

Whereas a certain quantity of the K⁺ in these brines may also be derived from feldspar breakdown in the granite, as outlined above, the high rates of fluid circulation imply additional external K⁺ sources. The occurrence of organic acids in solutions collected from 2160-2176m depth provide clear indications that waters have percolated down through the sedimentary cover and into the granite basement (L  desert et al. 1996, 1999). This source of H⁺ derived from the decomposition of organic matter is considered to be an important factor leading to enhanced

feldspar dissolution and extensive crystallization of both fissure illite and quartz (Lédesert et al. 1999, Shijun et al. 2001). An external source of K^+ from outside the granite could therefore be simultaneously contributing to the large amounts of illite in this hydrothermally altered granite.

Similar feldspar reactions can be recognized in the Schauenburg Fault within the uplifted margin of the rift as the main mechanism of illite formation. On the north side of the E-W striking fault both plagioclase (5-10%) and K-feldspar (15-20%) of the Heidelberg-granite (Tab. 6.1) has been intensely altered within the fault zone, with notable dissolution of albite crystals and the formation of micro-porosity (Chapter 5, Fig. 5.1, appendix page 87). In contrast to the Soultz-sous-Forêts granite, a number of other illitic minerals occur, as well as pure kaolinite and smectite phase forming reactions. The fault-related stage of alteration is dominated by the reactions:



I/S mixed-layers are notably depleted in K^+ and are attributed to the mixing of hydrothermal basinal brines and meteoric waters (Fig. 5.9, page 47). The chemistry of these solutions was probably similar to present day ground waters described along the Rhine Graben margin (Bender 1995; Tab.6.2). The formation of kaolinite along the fault was formed mainly by the replacement of illite-smectite minerals and reflect the final stage of fault zone flushing, implying the circulation of large volumes of dilute waters of meteoric origin associated with the uplift of the Rhine Graben flanks. The layer-by-layer transformation process observed (Fig. 5.6-5.8, page 44-46) involves the replacement of K^+ by H_3O^+ ions in the mica interlayer sites, thus releasing cations (K^+ , Na^+ , Ca^{2+}) into the solution.

Biotite also occurs in the rocks of the Schauenburg Fault, but only in the coarser grain-sized fractions (ca. 1-6%; Tab.6.1). In contrast to the Soultz-sous-Forêts granite, no chlorite was observed in the fault rocks of the Schauenburg structure, indicating different reaction paths for the alteration of the biotite. Although the mechanism of magmatic mica alteration has not been determined in this study, it is considered likely that the biotite altered directly to either illite or kaolinite phases.

Significant quantities of illite (here 8-63% of rock volume; Tab. 6.3) occur in the granite of the rift basin and adjacent areas, formed by the reactions outlined above. The mineralized argillite veins of the crystalline basement below the rift sediments (Soultz-sous-Forêts borehole at 1431m, 2160m and 2176m depth) contain abundant illite, with 38 to 58% occurring in the illite-quartz

Tab. 6.3: Quantification of illite and quartz components in selected study samples based on the mineral standard mixtures and calibration curve of Rügner (2000)

	Soulz-sous-Forêts granite					Schauenburg Fault rocks		
	1431 m (vein)	1570 m (granite)	2160 m (vein)	2167 m (granite)	2176m (vein)	rhyolite	cataclasite	granite
whole rock	~ 58 %	~12 %	~45 %	~63 %	~38 %	~10%	~8 %	~9 %

mineral veins studied (Tab.6.3). However, it is the fractured granite which contains the most illite, with 63% recorded at 2167m depth. The abundance of illite in this rock type is particularly concentrated in the matrix and in the finer grain-size fractions, where the 0.4 to 1 micron size range consists of an almost pure illite fraction (Chapter 4, page 22). This high content is attributed to the strong alteration of feldspar and biotite-rich lithologies. In contrast, the non-fractured pervasive granite rock type at 1570m depth contains only ca. 12% illite, reflecting a low permeability and lower intensity of fluid-rock interaction (Genter & Traineau 1991, Surma & Geraud 2003).

The high abundance of pure illite in the crystalline basement beneath the Rhine rift sediments is quite typical for hydrothermal argillite alterations associated with igneous bodies (Jaquemont 2002, Lédésert 1999). In the Soultz-sous-Forêts borehole site the local geothermal gradient today reaches up to ca. 100°C/km (Pribnow & Schellschmidt 2000), and is clearly of importance in

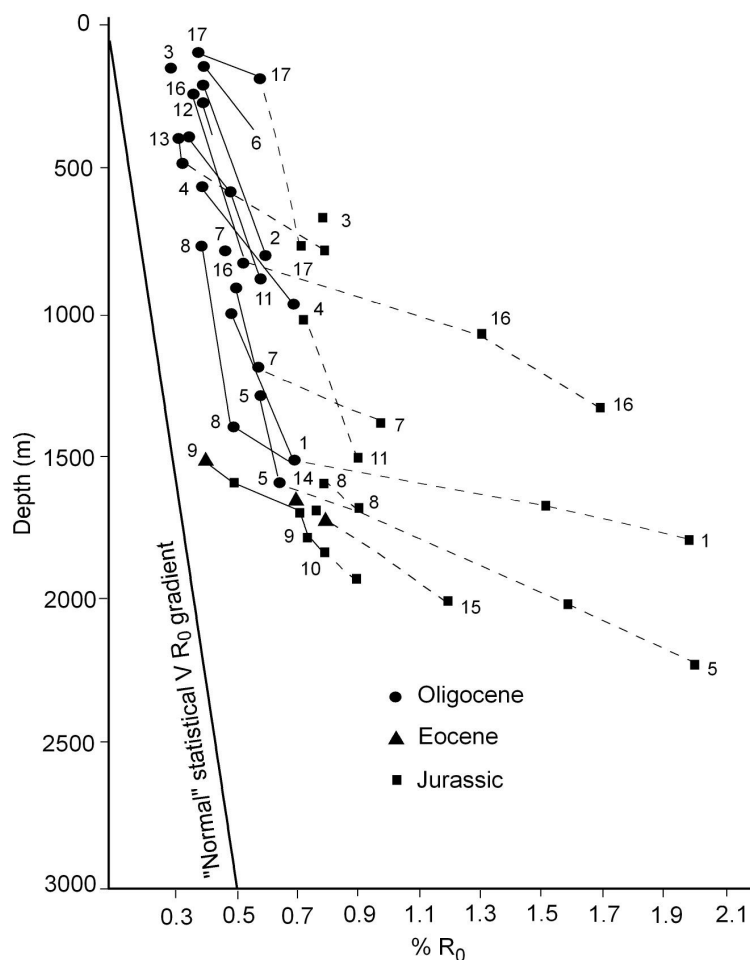


Fig. 6.1: Vitrinite reflectance versus burial depth. Oligocene data (circles) indicate a distribution roughly following the normal thermal gradient, whereas the Eocene (triangles) and the Jurassic (squares) data show a higher geothermal gradient (Teichmüller 1970)

driving young rock alteration (Komninou & Yardly 1997). However, the regional thermal history of the Upper Rhine Graben sediments, as reconstructed by plotting the vitrinite reflectance versus burial depth plots (Fig. 6.1) of Teichmüller (1970) shows normal geothermal gradients (25-30°C/km) to have characterized the basin throughout most of Oligocene.

A higher geothermal event was postulated around the Eocene-Oligocene boundary, to explain the significantly higher reflectance values of Jurassic to Eocene rocks. However, the occurrence of illite of Permian and Jurassic ages in the Soultz-sous-Forêts granite (Chapter 4, page 40) do reveal additional hydrothermal events have occurred, at least along the western margin of the rift basin. Such thermal events in the Mesozoic can be related to known episodes of lithospheric extension: notably the Permian volcanic activity and the Mid-Jurassic stages of Atlantic rifting, both of which are well documented throughout western Europe (Flick 1986, Littke et al. 2000). The enhanced states of organic maturation in the pre-Eocene rocks of the Upper Rhine Graben documented by Teichmüller (1970) could also partly reflect such a Jurassic thermal event.

The amount of illite in the Schauenburg Fault zone of the rift shoulder is notably lower than in the Soultz-sous-Forêts granite, ranging between 8 to 10% for all felsic lithologies (granite, cataclasite and rhyolite, Tab. 6.3). This is despite the fact that the whole rock composition of the less altered Heidelberg granite and rhyolite (some km's away of the Schauenburg Fault) contains on average about twice the concentration of K^+ (4-10%) than the Soultz-sous-Forêts granite (ca. 3%), as documented in Fig. 6.2 and Tab. 6.4.

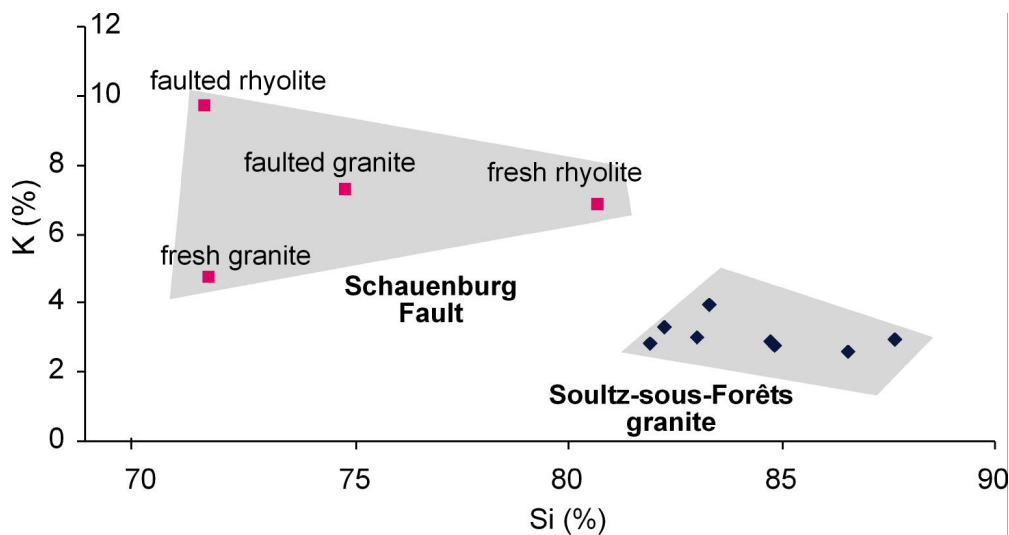


Fig. 6.2: K versus Si plot for representative whole rock study samples. Depending on the lithology, the Schauenburg Fault rocks contain about twice the concentration of K^+ than in the Soultz-sous-Forêts granite

The occurrence of K-poor illites in relatively K-rich granites can be explained by proposing differences in fluid compositions. Either the Jurassic hydrothermal fluids were characterized by lower K activity than the equivalent Soultz brines, or more likely that much of the more K-rich mica phases have been leached during younger fluid flushing of the fault, to produce more K-poor, clay mineral phases (Chapter 5, page 49).

Tab. 6.4: Whole rock composition (%) selected of Soultz-sous-Forêts granite and the Schauenburg Fault rocks measured by ICP-MS

	Si	Al	Mg	Fe	K	Na	Ca
vein (1431m)	83.3	7.95	1.17	1.95	3.94	0.19	1.5
granite (1570m)	82.23	7.39	0.7	2.00	3.32	3.06	1.3
granite (2167m)	84.81	7.53	0.28	1.24	2.76	0.96	2.42
vein (2160m)	87.64	6.42	0.26	0.86	2.96	0.13	1.73
vein (2176m)	84.76	7.8	0.68	2.24	2.89	0.08	1.55
fresh (4666)	81.91	7.52	0.76	2.13	2.81	2.95	1.92
fault rhyolite	71.48	14.23	0.51	1.58	9.72	0.18	0.05
fault granite	74.8	13.6	0.08	0.5	7.29	2.61	0.49
"Stift Neuburg" granite	71.6	15.4	1.09	2.2	4.74	3.47	0.78
"Quarry Vatter" rhyolite	80.8	9.8	0.05	0.8	7.61	0.19	0.09

A Jurassic age of illitization has also been recognized in the Schauenburg Fault, along the eastern uplifted margin of the rift (Marbach 2002, Lippolt & Leyk 2004), as well as many other localities in Mesozoic sediments around the Rhine area (Knudsen 2001, Liewig et al. 1987). Although today the heat flow of this portion of the rift is considered to be relatively low (Clauser et al. 2002), the occurrence of pure 2M₁ illites described in chapter 4 do indicate hydrothermal conditions during the Jurassic event. Fission track studies of apatite in the crystalline basement of the Heidelberg Odenwald (Wagner & Storzer 1972, 1975) reveal healing ages between 70 and 105 Ma, indicating a clear post-Variscan thermal event during late Mesozoic times with temperatures of at least 150°C. This implies high geothermal gradients in the Odenwald area in the range of 80-150°C/km. The lower abundance of pure illite in the Schauenburg Fault rocks could also be explained by the younger, retrograde mineral reactions that occurred in these rocks. Here, significant quantities of illite-smectite mixed-layered minerals, discrete smectite phases and kaolinite formed partly at the expense of illite during the downward circulation of meteoric waters accompanying exhumation and uplift of the graben shoulder. Although it is not possible to quantify the precise amounts of illite involved in these reactions, the formation of kaolinite does imply strong leaching of cations into solution during fluid flushing of the fault zone (Schleicher et al. in press).

6.3 Mechanisms of illite crystallization

In addition to the variety of mica mineral reactions and the variations in clay abundance described, there is a range of interesting illite crystal shapes developed in the studied fault rocks (Fig. 6.3). The control on crystal size and shape is considered to be largely a function of chemical constraints (Small et al. 1992) and temperature (Inoue et al. 1994), in particular reaction kinetics (Ehrenberg & Nadeau 1989, Berger et al. 1997, 1992, Wilkinson & Haszeldine 2002), solute supply (Hamilton et al. 1992), porefluid composition and flow velocity (Darby et al. 1997). The crystalline

rocks of both localities investigated contain mixtures of illite of different sizes and shapes, with platy illites dominating the hydrothermal veins in the Soultz-sous-Forêts granite and all rock types of the Schauenburg Fault. The younger, fibrous varieties are typical for the fractured granite matrix of the drilled basement rocks, whereas hexagonal kaolinite, illite-smectite mixed-layers and discrete smectite are abundant in the Schauenburg rocks (Fig. 6.3). Güven (2001) explained

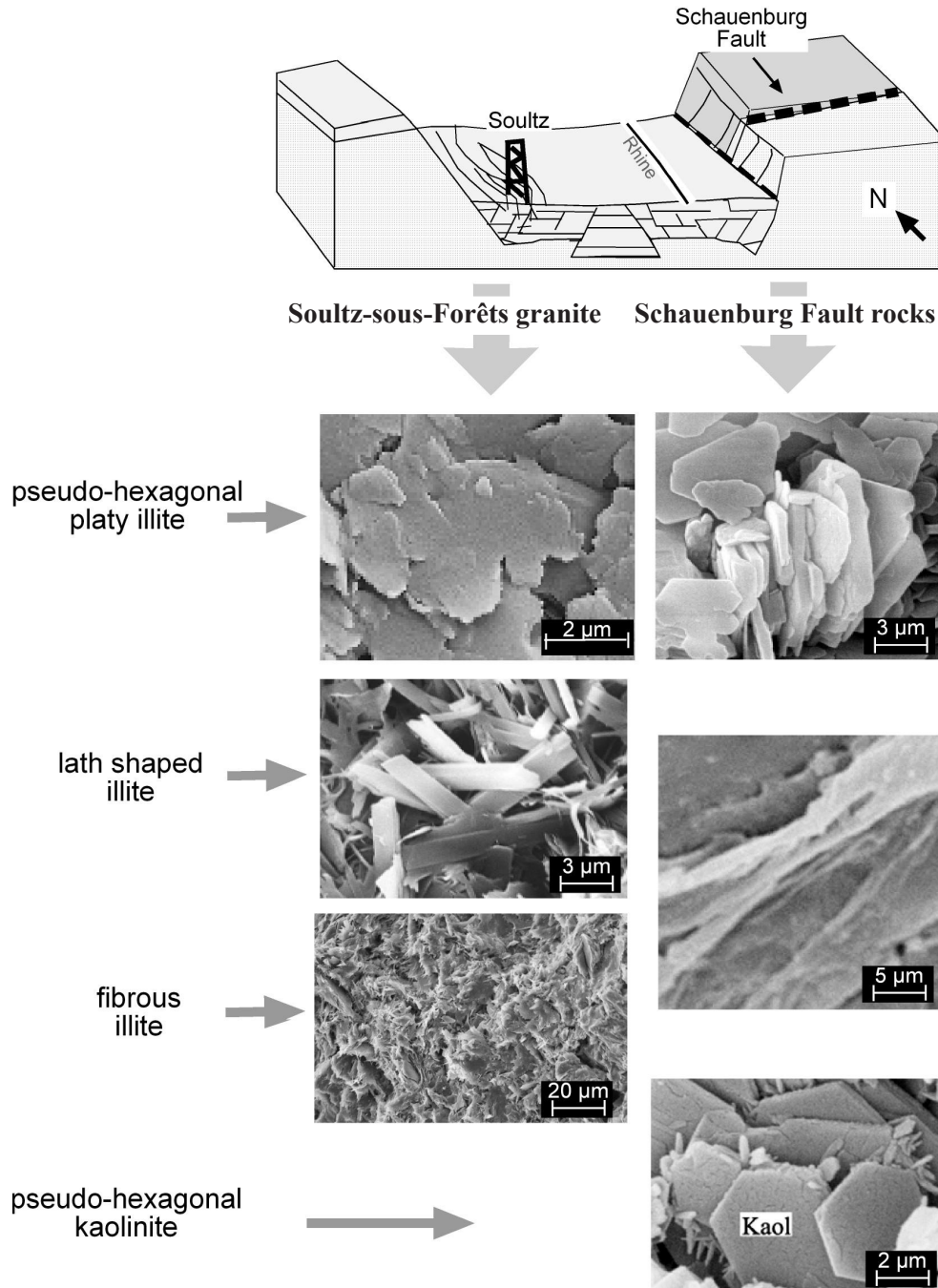


Fig. 6.3: Different morphologies of illite and kaolinite crystals observed in the Soultz-sous-Forêts granite and the Schauenburg Fault. Pseudo-hexagonal platy illite are abundant in the veins of the Soultz-sous-Forêts granite and in all rocks of the Schauenburg Fault. Lath shaped and fibrous illite present dominates the granite host rocks of the Soultz-sous-Forêts granite with only minor amount in the Schauenburg Fault. Pseudo-hexagonal stacks of kaolinite could only be recognized in the Schauenburg rocks

the formation of different crystal habits by different growth rates in the [100], [110] and [-1-10] directions for fibrous, lath and hexagonal crystals, suggesting that the position of the vacant site may be the critical factor influencing the growth process.

6.3.1 Development of platy hexagonal illite

Well crystallized, large pseudo-hexagonal illite in the veins of the hydrothermal Soultz-sous-Forêts granite and the Schauenburg Fault were formed mainly under hydrothermal conditions at the 125-350°C temperature range (Velde 1965). In the Soultz veins, they directly precipitated from fluids with probable different K-sources, as outlined above. Such crystal shapes are considered to form when the nucleation rate is so slow that most excess dissolved material is consumed by crystal growth on a limited number of critical nuclei (Berner 1981). Alternatively slow growth may be driven by low levels of supersaturation, in comparison to fibrous morphologies (Wilkinson & Haszeldine 2002).

The hydrothermal illites in the Schauenburg Fault were formed predominantly by the dissolution of feldspar grains, showing features typical of fluid-dominated, hydrothermal mineral growth (Chapter 5.2.4). Zöller & Brockamp (1997) and Zöller (1994) considered such hexagonal shaped particles corresponding to the $2M_1$ polytypes to show no clear differences in chemical compositions. Although abundant $2M_1$ illite is observed in the Soultz veins, polytype analysis of veins dominated by platy habits do indicate that these crystals are not exclusively $2M_1$, but represent a mixture of both 1M and $2M_1$ varieties. This is illustrated, for example, by the argillite vein at 2176m depth where the mixed illite assemblage of this sample shows quite consistent compositions (Fig. 4.4 page 26). This is also documented in the Schauenburg Fault, where hexagonal shaped crystals are mostly of the $1M_d$ polytype, but with minor amounts of $2M_1$. Mixtures of different polytypes were also documented by Grathoff et al. (2001) for the Paleozoic Illinois basin.

6.3.2 Development of lath and fibrous illite

The very small, lath to fibrous and flaky illites that dominate the hydrothermal granite of the Soultz-sous-Forêts granite probably formed at lower temperatures (max. 150°C) and are related to younger fluid events in the Rhine rift, as documented by the fluid inclusion studies of Dubois et al. (1996). The fibrous illites replaced mainly plagioclase, which served as the primary mineral substrate (Chapter 4.2.1). However, partial solution of platy illite and K-feldspar is also observed, suggesting that some of the fibrous illite grew partly at the expense of previously crystallized hydrothermal illite. According to Mullin (1961) and Wilkinson & Haszeldine (2002) a high degree of pore fluid supersaturation is the probable cause of the lath or fibrous crystal forms due to rapid crystal growth. The growth continues until enough material is removed from solution so that supersaturation is relieved and equilibrium is attained (Berner 1981). It is generally considered in the literature that the fibrous and lath shaped particles correspond to a 1M polytype (Srodon & Eberl 1984, Zöller & Brockamp 1997, Zöller 1994).

Despite all of the fibrous illites described in both fault rocks of this study are of the

1M polytype, the XRD and electron microscopy results show different types of 1M structures characterizing each locality. A 1M trans-vacant illite polytype dominates the strongly fractured granitic matrix in the Soultz-sous-Forêts borehole (e.g. 2167m, Chapter 4), as described by Kyser et al. (2000) for hydrothermal illite of elongated and lath-shaped crystals in sedimentary basins. A transition from 1M polytypes with octahedral trans-sites vacant ($1M_{TV}$) to a 1M polytype with the octahedral cis-sites vacant ($1M_{CV}$) has been investigated in diagenetic sandstones (Drits et al. 1993, Reynolds & Thomson 1993). Here, the $1M_{TV}$ polytype is considered to represent the higher temperature structure of the two varieties. However, such a transition has not yet been well investigated in hydrothermal environments, and it is not clear whether temperature is the determining factor. In the Soultz-sous-Forêts site, the fibrous and flaky crystals of the hydrothermal granite consist solely of the $1M_{TV}$ polytype and show no indication for a $1M_{CV}$ modification.

In contrast, a $1M_D$ illite polytype occurs in the fractured rocks of the Schauenburg Fault. This polytype exhibits a large degree of disorder in the stacking sequence (01/ directions) and generally exhibits a lower interlayer charge (Eberl et al. 1987). Reynolds (1980) showed the degree of ordering increases with the amount of interlayer K^+ . Smectite for example, with a lower potassium interlayer content reveals a typical turbostratic structure, with a highly disordered stacking arrangement. As the Schauenburg Fault contains a number of discrete smectite and illite-smectite mixed-layers with a lower K-content, the occurrence of more K-poor illitic varieties does explain the more abundant disorder and occurrence of $1M_D$ polytypes. However, it is not always the case that 1M and $1M_D$ polytypes have a lower interlayer charge. 1M illite with a 0.9 unit layer charge have also been identified in active hydrothermal systems (Lonker & Fitz Gerald 1990).

6.4 Fabric development

An additional aspect of understanding clay formation in faults is to study the fault rock fabric and to assess the anisotropy of permeability based on the textural orientation of particles. For this purpose, the XTG patterns of illite crystallites have been compared for the Soultz-sous-Forêts granite and the Schauenburg Fault rocks (Fig. 6.4). Both localities show characteristically poor fabrics, which are generally considered to be typical of fault rocks (Solum et al. 2003). In the Soultz-sous-Forêts drilling, the fabric of the illite crystallites reveal a better textural development in the granite (3.12-3.43 m.r.d.) than in the veins (2.14-2.82 m.r.d.). Similar patterns occur in the cataclasite and granite of the Schauenburg, and probably reflect the growth of crystal stacks along pre-existing orientated grains, such as earlier crystallized platy micas, or the dissolved cleavage planes of feldspar crystals (Fig. 5.4 page 41).

Although the illite fabric is less developed in the veins than in the granite, they do tend towards more girdle distributions (Fig. 6.4). The particles orientations in these mineralized fissures presumably represent crystallization with the basal planes oriented roughly parallel to the fractured wall-rock. The girdle distributions reflect the poorly developed microfolds observed in SEM images (Fig. 4.2a, page 24), which are associated with a secondary hinge porosity. The occurrence of such girdle patterns can therefore be associated with the development of local, deformation related

porosity. This indicates that rock deformation of the veins may have led to some enhancement of fluid migration. However, the intensity of fabrics developed in both granite and vein samples does imply that the granite developed a better permeability anisotropy than the veins. The vein mineralizations were more successfully sealed during Mesozoic crystallization events.

These features are in accordance with the porosity measurements of Surma & Geraud

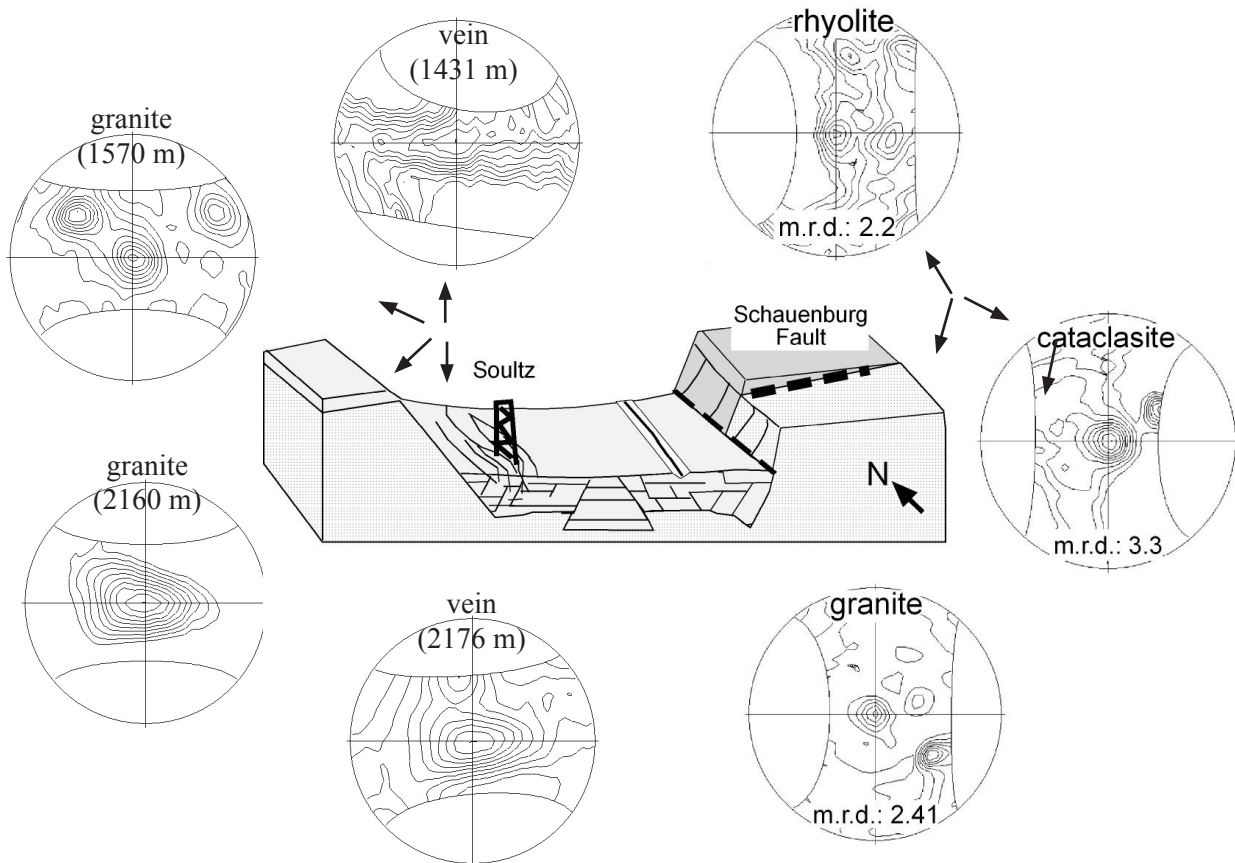


Fig. 6.4: X-ray texture goniometry pole figures from the Soutz-sous-Forêts granite and the Schauenburg Fault show similarities in textural development of the fractured and fault rocks, and the host rock samples

(2003), which showed the porosity of the granite matrix to be higher than the porosity of the veins. Bearing in mind that the younger, fibrous illites are concentrated in the matrix of the granite and the older (Permian and Jurassic) platy illites in the mineralized fissures, it appears that the rock permeability and rock fabrics were both important in influencing the sites of mineralization.

6.5 History of alteration and fluid-rock interaction

In this final section the established history of rock alteration determined from the two studied localities, representative of both buried rift basement and Tertiary uplifted shoulder, is placed within the geological context of the Rhine Graben area. On the basis of clay mineral assemblages, K-Ar isotope characteristics and the well studied nature of fluid-rock interactions (e.g. Dubois et al. 1996, Pauwels 1993, Durst & Vuataz 2000), three schematic reconstructions are presented (Figs. 6.5–6.8) and outlined in order to highlight recognized Permian, Mesozoic and Cenozoic events.

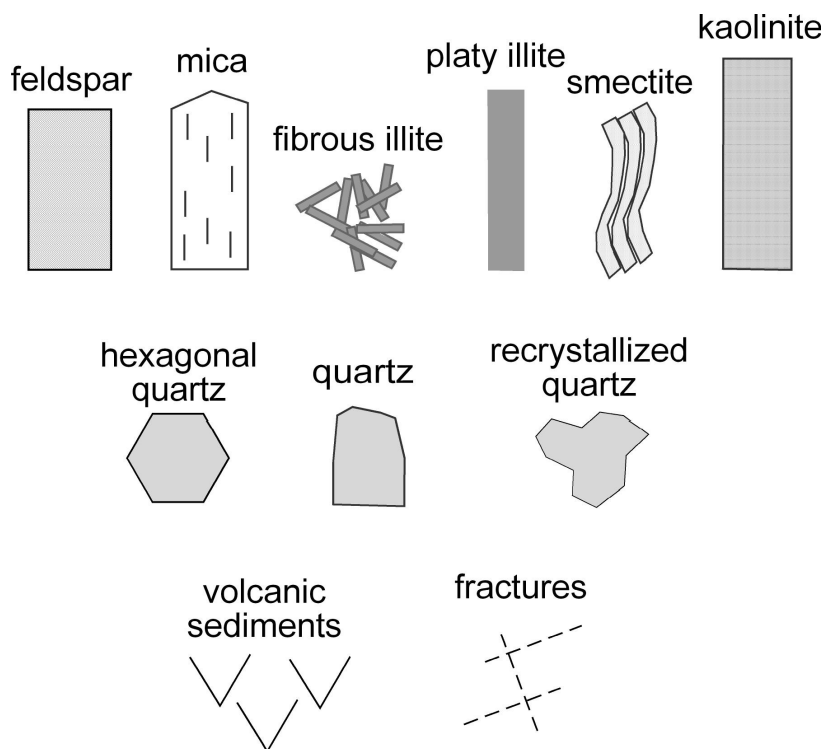


Fig. 6.5: Legend to the mineral components and structures used in the geological reconstruction (Fig. 6.6-6.8)

6.5.1 Permian mineralization (Fig. 6.6)

The oldest argillite vein mineralization investigated in this study occur in the deepest vein (at 2176m depth) and is ca. 50 Ma younger than the emplacement of the 331 ± 9 Ma old (U/Pb) Soultz-sous-Forêts granite (Alexandrov et al. 2001). At this time, the granite pluton was already affected by a well documented pervasive alteration related to the circulation of residual igneous fluids (e.g. Jaquemont 2002), with early fracture related mineralizations of magnetite grains (Just 2005). During a subsequent hematite forming event recognized to occur during Late Carboniferous and Early Permian times by paleomagnetic investigations (Just 2005), the granite was strongly affected by unloading and exhumation, with brittle deformation and reactivation of pre-existing fractures. It is during this event that the veins where most likely formed, with dilation and cogenetic Early Permian illite mineralizations within open fissures.

The Permian aged illite, which dominates the coarse fractions of all three studied veins, as well as crystallizing in the pervasive granite, are suggested to have formed from the highly saline (enriched in Na, Ca and K) and hot (180-340°C) CO₂-rich fluid inclusions preserved in quartz that percolated through the granite at this time (Pauwels 1992, Dubois et al. 1996, Smith et al. 1998). Well developed hydrothermal quartz crystals in the vein-3 sample also contain some fragments of illite, implying a cogenetic crystallization of these minerals. However, the vein-2 sample (just 16 metres above) shows notable signs of both quartz and illite recrystallization, suggestive of enhanced temperatures and syn-or post-tectonic deformation. The micro-folding of the illite fabric observed in this sample resulted in some hinge porosity as a result of local dilations (Fig. 4.2 page 24). It is this porosity which provided the sites for the younger crystallization events observed in this vein, in contrast to the lower vein-3 sample, that was completely sealed during Permian crystallization. A similar history is suggested for the vein-1 sample located just 30m from the Permian unconformity.

Similar illite mineralization is also recognized in the pervasively altered granite, ca. 600m above the vein sample (at 1570m depth). In this granite, which contains no visible fractures, the larger illite crystals were formed during the Early Permian stage, mainly due to the alteration of the K-bearing minerals, in particular K-feldspar and biotite. It is also assumed that some alteration of the plagioclase occurred at this stage, with particle orientations indicating preferential growth of illite along albite cleavage lamellae. Overall, this episode of hydrothermal mineralization can be related to relatively high temperatures, with crystallization of 2M illite polytypes, local recrystallization effects and the high temperatures of fluid inclusions trapped in cogenetic quartz crystals. Such conditions can be explained by the intense Permian volcanic activity in this region, which was probably accompanied by higher thermal gradients and regionally enhanced heat flow conditions (Flick 1986, Lippolt et al. 1990, Hess & Lippolt 1996). In the reconstruction presented, the additional occurrence of 1M Permian illite in the deepest vein (2176m) probably reflect the cooling of these hydrothermal fluids, together with possible changes in fluid composition accompanying crystallization. In contrast to the Soultz-sous-Forêts granite, no Permian alteration history has been recognized in the Schauenburg Fault rocks.

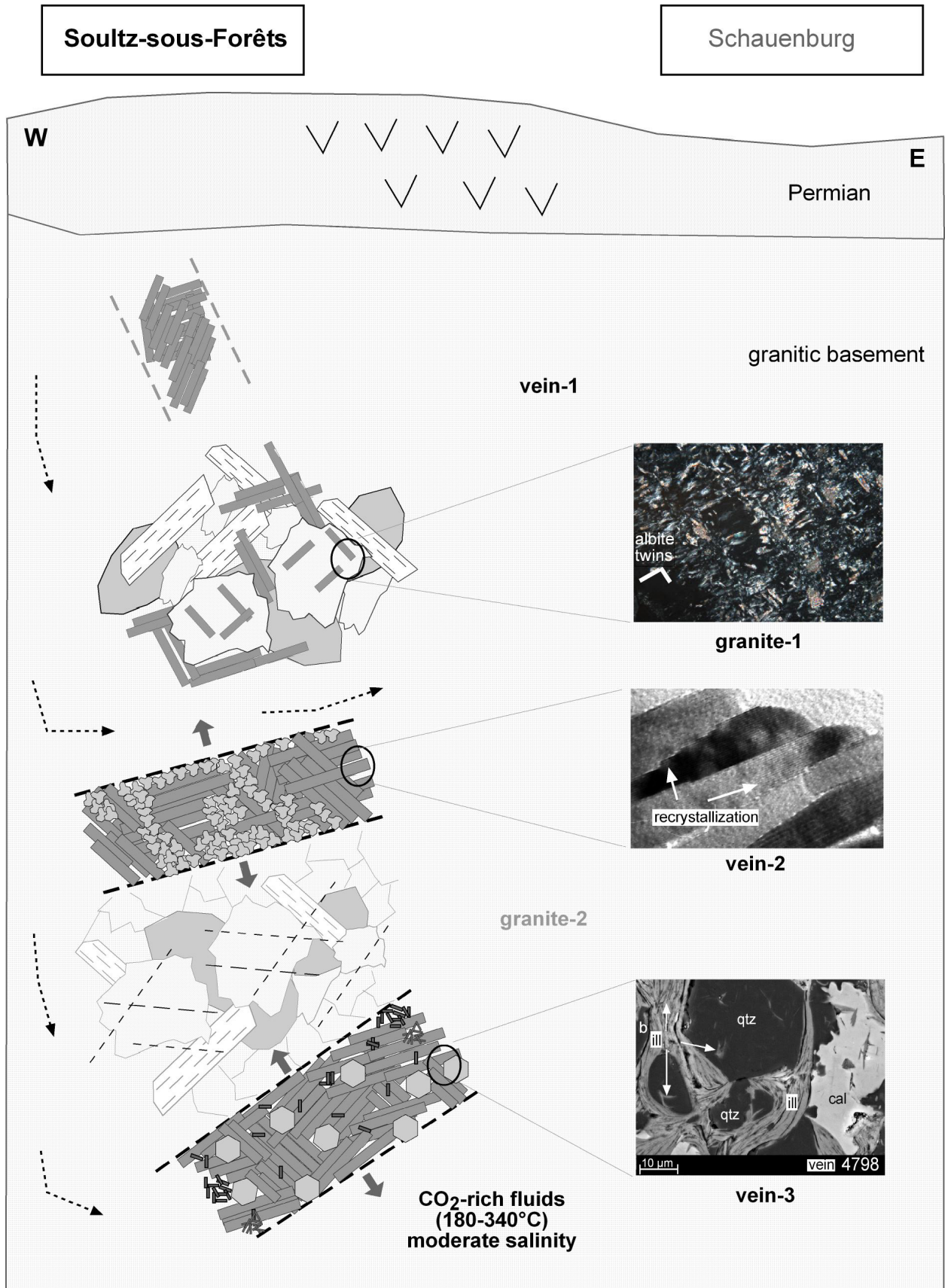


Fig. 6.6: Permian argillite mineralization history. See text for explanation

6.5.2 Mesozoic mineralization (Fig. 6.7)

Illite crystallization of Jurassic age is recognized in vein-1 and vein-2, as well as in both granite samples of the Soultz borehole. Widespread illite crystal growth of this age is well known in the North Atlantic seaboard of western Europe, and occurred in response to intense fluid-rock interaction associated with the breakup of Pangaea and the initial stages of Atlantic rifting and burial (Clauer et al. 1995, Brockamp et al. 2003). It is evident that this phase of fluid-rock alteration also influenced the Soultz-sous-Forêts granite, leading to localized illite crystallization in both granite matrix and unsealed mineralized veins. Based on the study of younger fluid inclusions it is considered that the temperatures did not vary significantly from those of present day conditions, and ranged between 130°C to 170°C. Although the fluids are strongly saline, the concentration of salts in solution does appear to have been quite variable. It is, however, unclear whether these fluid conditions apply to the Jurassic hydrothermal circulations, or reflect only younger Tertiary events.

Jurassic illite also occurs both as $2M_1$ and $1M$ trans-vacant varieties. In granite-2, the $2M_1$ illite of this age group forms the oldest mineralization phase recorded in this sample. In contrast, all overlying samples show secondary Jurassic illite of the $1M_{TV}$ polytype. These relationships are suggested to partly reflect temperature gradients during the cooling of hydrothermal fluids and also possibly fluid composition changes due to the restricted secondary porosity and permeability of these rocks. In addition to the Jurassic illite, a younger Mesozoic (Late Cretaceous) value was obtained on the basis of the $1M_{TV}$ polytype end member age (Fig. 4.9 page 31). This illite characterizes the finest fraction of the granite-2 sample, however, if any inherited argon was acquired from the dissolution of older Jurassic illite, this modelled age value may be older than its true crystallization ages.

Jurassic illite has also been shown to be present in the Schauenburg Fault rocks (Marbach et al. in press). Here, crystallization occurred in the form of a well-developed pseudo-hexagonal $2M_1$ illite, predominantly by dissolution of feldspar grains. However, it is considered that this alteration was probably widespread, and there is little evidence to indicate that the Schauenburg Fault existed at this time (Chapter 5, page 49). The well developed crystal shapes are typical of fluid-dominated, hydrothermal mineral growth, taking place in an environment of regional scale fluid flow during Mesozoic extension. A Cretaceous thermal event, documented by fission track dating in the vicinity of the Schauenburg Fault (Wagner et al. 1975) can also be related to this stage of Mesozoic hydrothermal activity.



Fig. 6.7: Mesozoic argillite mineralization history. See text for explanation

6.5.3 Cenozoic mineralization (Fig. 6.8)

It is well recognized that the present day features of the Upper Rhine Graben system resulted largely from Cenozoic tectonic activity, in particular extensive Tertiary rifting during Eocene-Oligocene times. The rifting not only resulted in higher geothermal gradients and syn-rift sedimentary thickness approaching 3.5 km, but also resulted in thermal and flexure uplift of the rift shoulders (Laubscher 2001).

Although in the studied samples of this work no Tertiary K-Ar age values were recorded, even in the finest grain sizes containing near-to-pure end member 1M illite, the occurrence of such Tertiary ages have been recognized in other Soultz-sous-Forêts granite samples by other researchers. For example, a young Tertiary age value was measured from a fissure coating (N.Liewig, *pers. comm.*), and similarly from an altered granite sample (E. Laverret, *pers. comm.*). It is therefore evident that Tertiary illite also occurs in the Soultz-sous-Forêts granite, but was not encountered in this sample set. Additional signs of younger clay mineral formation come from the active fluid zone at ca. 2150-2190m, where mixed-layered chlorite-smectite (tosudite) has been recorded in fracture granite from this depth (Leddesert 1996). As in this study no tosudite mineral was recorded in the three samples investigated from this zone, it is considered that this phase is of very restricted occurrence. The K-Ar age values of these three samples actually give no indications of this recent stage of fluid-rock interaction.

Although not directly dated, more extensive Cenozoic fault-related alteration is considered to have occurred in the uplifted rift shoulder rocks of the Schauenburg Fault. A young stage of Quaternary (within the last 10^6 years) alteration, with REE and Pb-enrichment along the fault, has been suggested by Marbach et al. (in press) on the basis of Th-U disequilibrium model. A clear retrograde sequence of fluid-controlled, low-temperature mineral reactions can be recognized in this zone. The illite-smectite, smectite and kaolinite formed along the fault are considered to be the retrograde mineral products of Cenozoic age (Chapter 5, page 49). This stage of alteration is attributed to the exhumation and uplift along the fault during Tertiary or post-Tertiary times. The strong leaching of this zone reflects the infiltration of more dilute, meteoric waters, documented in the present day chemistry of ground waters along the Rhine Graben margin (Bender 1995, Durst & Vuataz 2000).

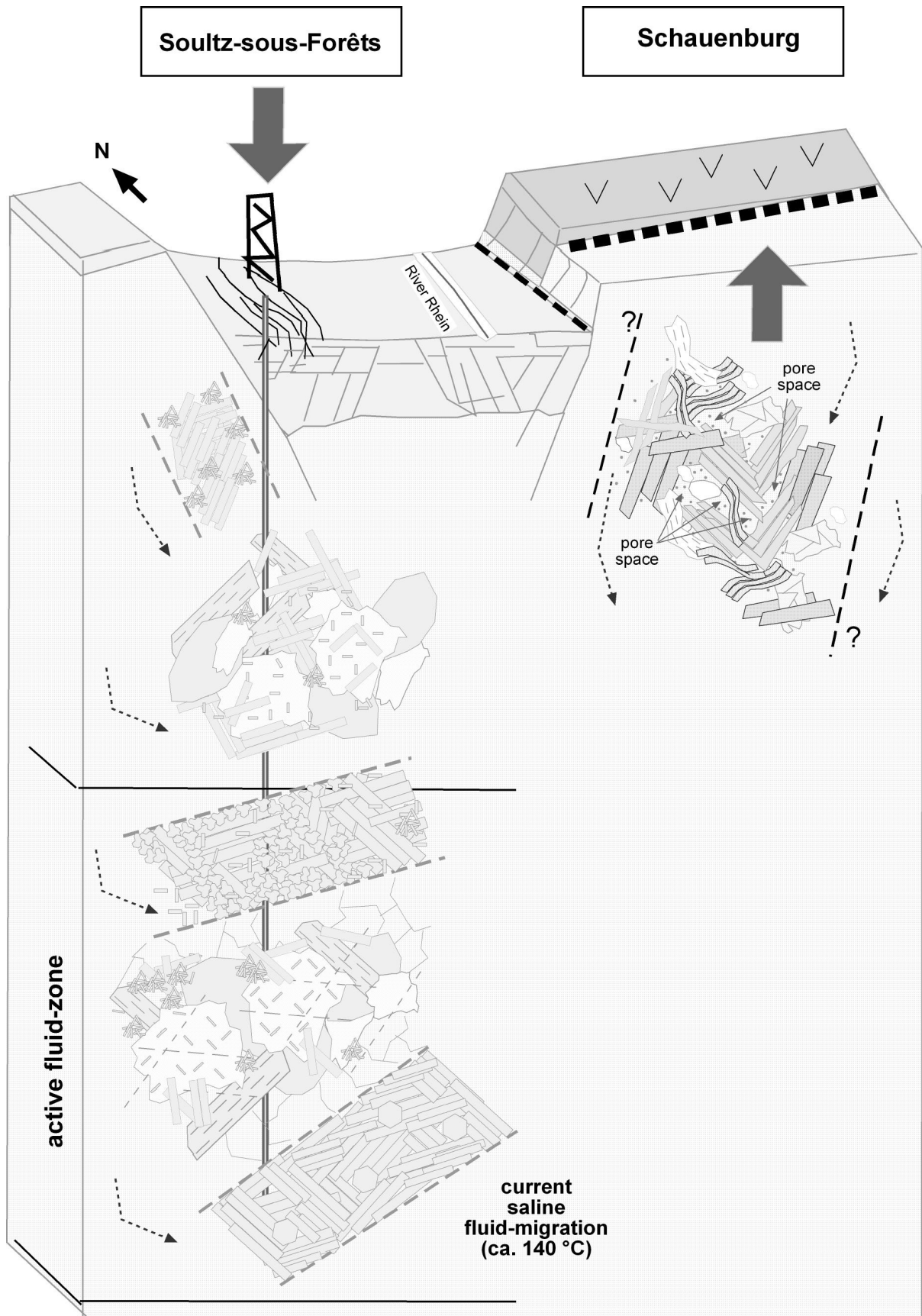


Fig. 6.8: Cenozoic clay mineral formation. See text for explanation

6.6 CONCLUDING REMARKS

On the basis of this study, it is evident that the two localities representing buried and exhumed granitic fault zones show a contrasting rock alteration history, despite general similarities in the two Variscan granites. Such differences clearly reflect the variable thermal and fluid-rock interactions that have occurred in the crystalline basement beneath the Rhine rift basin and its uplifted flank. A large proportion of the clay formation, particularly illite crystallization, actually occurred before the development of the current day Tertiary rift system during Permian and Mesozoic episodes of hydrothermal activity. The lower temperature, retrograde alteration that formed other types of clays, such as illite-smectite, smectite and kaolinite was focused along faults of the uplifted rift shoulder. All events are considered to have been episodic in nature and influenced strongly by the permeability and porosity development of the fraction and fault zones. This study highlights the significantly long time over which these crystallization events occurred and shows how episodes of faulting and fluid flow are closely interlinked with the formation of clay minerals in fractured crystalline rocks.

- 1) Episodic hydrothermal alteration of the Soultz-sous-Forêts granite resulted in the development of pure illite with little influence from surface conditions. In contrast, the Schauenburg Fault within the uplifted shoulder, experienced extensive retrograde alteration with the fluid flushing of meteoric waters, resulting in low temperature, near surface assemblages of illite-smectite, smectite and kaolinite
- 2) Argillaceous clays formed mainly by the hydration of feldspars (K-feldspar and plagioclase), mica, although some external cation sources of K^+ are predicted for the hydrothermal Soultz-sous-Forêts granites. The transition from 2M to younger 1M illite polytypes was partly achieved by direct dissolution of large platy 2M illite crystals and the neocrystallization of thin fibrous 1M varieties. In the Schauenburg Fault rocks, dissolution of pure illite also occurred, but in this case was directly replaced by kaolinite
- 3) The two study sites show different types of illite polytypes, that also reflect variations in fluid-rock history. The Soultz-sous-Forêts granite displays episodic transitions from platy shaped, higher temperature, 2M₁ illite to younger, fibrous lower temperature, 1M trans-vacant polytype varieties. In contrast, the Schauenburg Fault, contains a 2M₁ illite and a younger disordered 1M illite-smectite variety, which formed in association with other backreactions to low temperature smectite and kaolinite
- 4) Assessment of the fault rock fabric based on X-ray textural measurements of particle orientation of illite reveal better textural development was achieved in the granitic host rocks than in the veins or the cataclastically deformed Soultz or Heidelberg granites. However, the fabric intensity does imply that the granite developed a better permeability anisotropy, due to the

preferred orientation of particles. Such fabrics are not well developed in the vein samples, which are generally better sealed. In both localities, rock permeability and porosity seems to be a key controlling factor influencing the sites of mineralization

5) At least three regionally recognized episodes of fluid-controlled hydrothermal mineralization occurred in the Soultz-sous-Forêts granite during the Permian, Jurassic and Cretaceous (or younger) times. The Jurassic stage of illite growth has also been documented along the Schauenburg Fault, but here subsequent cooling and dilution of waters passing through the fault zone appears to have been the dominant alteration event accompanying uplift of the rift shoulders.

LITERATURE LIST

- Abad I., Nieto F., Peacor D.R., Velilla N. (2003) Prograde and retrograde diagenetic and metamorphic evolution in metapelitic rocks of Sierra Espuna (Spain). *Clay Minerals*, 38, 1-23
- Abebe T. (2000) Geological limitations of a geothermal system in a continental rift zone: example the Ethiopian rift valley: Proceedings World Geothermal Congress, Kyushu-Tohoku, Japan
- Alexandrov P., Royer J.J., Deloule E. (2001) 331 ± 9 Ma emplacement age of the Soultz monzogranite (Rhine Graben basement) by U/Pb ion-probe zircon dating of samples from 5 km depth. *Earth and Planetary Sciences*, 332, 747-754
- Allen P.A., Allen J.R. (1990) *Basin analysis: Principles and Applications*. Cambridge, Massachusetts, USA, Blackwell Science Inc., 491 p.
- Altaner S.P., Ylagan R.F., Savin S.M., Aronson J.L., Belkin H.E., Pozzuoli A. (2003) Geothermometry, geochronology, and mass transfer associated with hydrothermal alteration of a rhyolitic hyaloclastite from Ponza Island, Italy. *Geochim. et Cosmochim. Acta*, 67, 2, 275-288
- Altherr R., Henes-Klaiber U., Hegner E., Satir M., Langer C. (1999) Plutonism in the Variscan Odenwald (Germany): from subduction to collision. *Int. Journ. Earth Sciences*, 88, 422-443
- Andrae A., Osann A. (1893): *Erläuterungen zur Geologie des Blattes Heidelberg*. 5. Auflage von Hans Thürach (1995) *Mitt. Bad. Geol. L.-Anst.* 2: 345-388.
- Appelo C.A.J., Postma D. (1999) *Geochemistry, groundwater and pollution*. A.A. Balkema/Rotterdam/Brookfield, 536 p.
- Aquilina L., Pauwels H., Genter A., Fouillac C. (1997) Water-rock interaction processes in the Triassic sandstone and the granitic basement of the Rhine Graben: Geochemical investigation of a geothermal reservoir. *Geochim. et Cosmochim. Acta*, 61, 20, 4281-4295
- Bailey S.W., Hurley P.M., Fairbairn H.W., Pinson Jr. W.H. (1962) K-Ar dating of sedimentary illite polytypes. *Geological Society of America Bulletin*, 73, 1167-1170
- Bartels J., Kühn M., Pape H., Clauser C. (2000) A new aquifer simulation tool for coupled flow, heat transfer, multi-species transport and chemical water-rock-interaction. Proceedings World Geothermal Congress, Kyushu-Tohoku, Japan
- Bailey S.W. (1980) Structure of layer silicates. In: G.W. Brindley and G. Brown (eds), *Crystal structure of clay minerals and their X-ray identification*. Mineralogical Society, London, 1-124
- Behr H.-J., Horn E.E., Frenzel-Beyme K., Reutel C. (1987) Fluid inclusions characteristics of the Variscan and post-Variscan mineralizing fluids in the FRG. *Chem Geol* 61, 273-285
- Bender K. (1995) Herkunft und Entstehung der Mineral- und Thermalwässer im nördlichen Schwarzwald. *Heidelberger Geowissenschaftliche Abhandlungen*, 85, Ruprecht-Karls-Universität Heidelberg: 145 p
- Benek, R., Kramer, W., McCann T., Scheck M., Negendank J.F.W., Koric D., Huebscher H.-D.,
-

Bayer U. (1996) Permo-Carboniferous magmatism of the Northeast German basin. *Tectonophysics*, 266, 379-404

Berger G., Lacharpagne J-C., Velde B., Beaufort D., Lanson B. (1997) Kinetic constrains on illitization reactions and the effects of organic diagenesis in sandstone/shale sequences. *Appl. Geochem.*, 12, 23-35

Berger G., Turpault M.P., Meunier A. (1992) Dissolution-precipitation processes induced by hot water in a fractured granite. Part2: Modellin gof water-rock interaction. *Eur. J. Mineral* 4, 1477-1488

Berner R.A. (1981) Kinetics of weathering and diagenesis. In: A.C. Lasaga and R.J. Kirkpatrick (Editors) *Kinetics of geochemical processes. Reviews in Mineralogy* 8, 111-134, Miner. Soc. Amer., Washington D.C.

Blès J.L., Bonijoly D., Castaing C., Gros Y. (1989) Successive post-Variscan stress fields in the French Massif Central and its borders (Western European plate): comparison with geodynamic data. *Tectonophysics*, 169, 79-111

Bonhomme M., Thuizat R., Pinault Y., Clauer M., Wendling R., Winkler R. (1975) Methode de datation potassium-argon. Appareillage et techniques. Note Technique de l'Institute de Géologie de Strasbourg, 3, 53 p.

Bove D.J., Eberl D.D., McKarty D.K., Meeker G.P. (2002) Characterization and modeling of illite crystal particles and growth mechanisms in a zoned hydrothermal deposit, Lake City, Colorado. *American Mineralogist* 87, 1546-1556

Bradley W.F. (1945) Diagnostic criteria for clay minerals. *Am. Miner.* 30, 704-713

Brindley G.W., Brown G. (1980) Crystal structures of clay minerals and their X-ray identification. Monograph 5: Mineralogical Society London, 326

Brockamp O., Clauer N., Zuther M. (2003) Authigenic sericite record of a fossil geothermal system: the Offenburg trough, central Black Forest, Germany. *Int. Journal of Earth Science*, 92, 843-851

Brockamp O., Clauer N., Zuther M. (1994) K-Ar dating of episodic Mesozoic fluid migrations along the fault system of Gernsbach between the Moldanubian and Saxothuringian (Northern Black Forest, Germany), *Geol. Rundschau*, 83, 180-185

Buseck P.R. (1993) Principles of transmission electron microscopy. In: P.R Buseck (ed.), *Minerals and reactions at the atomic scale: Transmission Electron Microscopy*, Mineralogical Society of America

Carlé W. (1975) Die Mineral- und Thermalwässer von Mitteleuropa. Wissenschaftliche Verlagsgesellschaft mbH, 643

Carlé W. (1958) Rezente und fossile Mineral- und Thermalwässer im Oberrheintalgraben und seiner weiteren Umgebung. *Jber. Mitt. Oberrh. Geol. Ver.*, 40, 77-105

Chester F., Evans J.P., Biegel R.L. (1993) Internal structure and weakening mechanisms of the San

-
- Andreas Fault. *Journal of Geophysical Research*, 98, 771-786
- Chester F.M., Logan J.M. (1986) Implications for mechanical properties of brittle faults from observations of the Punchbowl Fault zone, California. *Pure Appl. Geophys.*, 124, 79-106
- Clauer N., Liewig N., Pierret M., Toulkeridis T. (2003) Crystallization conditions of fundamental particles from mixed-layer illite-smectite of bentonites based on isotopic data (K-Ar, Rb-Sr and delta (super 18)O), *Clays and Clay Minerals*, 51, 6, 664-674
- Clauer N., Chaudhuri S. (2001) Extracting K-Ar ages from shales: the analytical evidence. *Clay minerals* 36, 227-235
- Clauer N., O'Neil J.R., Furlan S. (1995) Clay minerals as record of temperature conditions and duration of thermal anomalies in the Paris Basin, France. *Clay Minerals* 30, 1-13
- Clauer, N., Chaudhuri, S. (1995) *Clays in crustal environments; isotope dating and tracing*, Springer-Verlag, Berlin, Federal Republic of Germany (DEU)
- Clauer N., Naoual R., Schaltegger U., Piqué A. (1995) K-Ar systematics of clay-to-mica minerals in a multi-stage low-grade metamorphic evolution, *Chemical Geology*, 124, 305-316
- Clauer C., Griesshaber E., Neugebauer H. (2002) Decoupled thermal and mantle helium anomalies: Implications for the transport regime in continental rift zones. *Journal of Geophysical Research* 107 B11,1-1 - 1-16
- Clauer C., Villinger H. (1990) Analysis of convective and conductive heat transfer in a sedimentary basin, demonstrated for the Rhine Graben. *Geophys. J. Int.*, 100, 393-414
- Clifton J., McDonald P., Plater A., Oldfield F. (1999) An investigation into the efficiency of particle size separation using Stokes' Law, *Earth Surface Processes and Landforms*, 24, 8, 725-730
- Cloetingh S., Kooi H. (1992) Intraplate stresses and dynamical aspects of rifted basins. *Tectonophysics*, 215, 167-185
- Dallmeyer R.D., Franke W., Weber K. (1995) *Pre-Permian Geology of Central and Eastern Europe* (eds). Springer, 604 pages
- Darby D., Wilkinson M., Fallick A.E., Haszeldine R.S. (1997) Illite dates record deep fluid movements in petroleum basins. *Petroleum Geoscience* 3, 133-140
- Dietl, C. (2000) *Structural and petrologic aspects of the emplacement of granitoid plutons: case studies from the western margin of the Joshua Flat-Beer Creek-Pluton (White-Inyo Mountains, California) and the Flasergranitoid zone (Odenwald, Germany)*. Ph-D thesis, University of Heidelberg
- Dong H., Peacor D.R., Freed R.L. (1997) Phase relations among smectite, R1 illite-smectite and illite. *American Mineralogist* 82, 379-391
- Drits V., Srodon J., Eberl D.D. (1997) XRD measurement of mean crystallite thickness of illite and illite/smectite: Reappraisal of the Kübler index and the Scherrer equation. *Clays and Clay*
-

Minerals, 45, 461-475

Drits V., Weber F., Salyn A.L., Tsipursky S.I. (1993) X-ray identification of one layer illite varieties: application to the study of illites around uranium deposits of Canada. *Clays and Clay Minerals*, 41, 389-398

Dubois M., Ayt Ougoudal M., Meere P., Royer J., Boiron M., Cathelineau M. (1996) Temperature of paleo- to modern self-sealing within a continental rift basin : The fluid inclusion data (Soultz-sous-Forêts, Rhine Graben, France), *Eur. J. Mineral.*, 8, 1065-1080

Dudek T., Srodon J., Eberl D.D., Elsass F., Uhlik P. (2002) Thickness distribution of illite crystals in shales. I: X-ray diffraction vs. high-resolution transmission electron microscopy measurements; *Clays and Clay Minerals*, 50, 5, 562-577

Durst P., Vuataz F.D. (2000) Fluid-rock interactions in hot dry rock reservoirs. A review of the HDR sites and detailed investigations of the Soultz-sous-Forets system. *Proceedings World Geothermal Congress 2000, Kyushu-Tohoku, Japan, May 28 - June 10*

Eberl D.D., Nueesch R., Sucha V., Tsipursky S. (1998) Measurement of fundamental illite particle thicknesses by X-ray diffraction using PVP-10 intercalation, *Clays and Clay Minerals*, 46, 1, 89-97

Eberl D.D., Drits V.A., Srodon J., Nueesch R. (1996) MUDMASTER; a program for calculating crystallite size distributions and strain from the shapes of X-ray diffraction peaks, *Open-File Report- U.S. Geological Survey, Report: OF 96-0171*, <ftp://brrcrftp.cr.usgs.gov/pub/ddeberl/>

Eberl D.D., Velde B. (1989) Beyond the Kubler index. *Clay Minerals*, 24, 571-577

Eberl D., Srodon J., Mingchou L., Nadeau P.H., Northrop H. (1987) Sericite from the Silverton Caldera, Colorado; correlation among structure, composition, origin, and particle thickness, *American Mineralogist*, 72, 9-10, 914-934

Echtler H-P., Altherr R. (1993) Variscan crustal evolution in the Vosges Mountains and in the Schwarzwald; guide to the excursion of the Swiss Geological Society and the Swiss Society of Mineralogy and Petrology, 73,1, 113-128

Edel J.B., Schulmann K., Holub F.V. (2003) Anticlockwise and clockwise rotations of the Western Variscides accommodated by dextral lithospheric wrenching: paleomagnetic and structural evidence. *Journal of the Geological Society*, 160, 209-218

Egashira K., Matsuo K., Gibo S., Nakamura S., Zhou Y., Inoue H., Sasaki K. (2000) Clay mineralogical approach to the slip-surface formation in the O'dokoro Landslide, Niigata, central Japan. *Clay Science*, 11, 2, 107-113

Ehrenberg S.N., Aagaard P., Wilson M.J., Fraser A.R., Duthie D.M. (1992) Depth-dependent transformation of kaolinite to dickite in sandstones of the Norwegian continental shelf. *The Mineralogical Society*, 325-352

Ehrenberg S.N., Nadeau P.H. (1989) Formation of diagenetic illite in sandstones in the Garn formation, Haltenbanken area, mid-Norwegian continental shelf. *Clay Minerals*, 24, 233-253

-
- Elsass P., Aquilina L., Beauce A., Benderitter Y., Fabriol H., Genter G., Pauwels H. (1995) Deep structures of the Soultz-sous-Forêts HDR site. Proc. World Geothermal Congress, Florence, Italy, 2543-2647
- Engelhardt W. (1955) Möglichkeiten der quantitativen Röntgenanalyse von Mineralgemischen (abgekürzte Zusammenfassung). Geol. Rdsch. 43, 2, 568-572
- Evans J.P. (1990) Textures, deformation mechanisms and the role of fluids in the cataclastic deformation of granitic rocks. In: R.J. Knipe, E.H. Rutter (eds.), Deformation mechanisms, rheology and tectonics. Geological Society Special Publication 54, 29-39
- Flick H. (1986) Permokarboner Vulkanismus im südlichen Odenwald. Heidelberger Geowiss. Abhandl., 6, 121-138
- Fisher D., Byrne T. (1990) The character and distribution of mineralized fractures in the Kodiak Formation, Alaska: implications for fluid flow in an underthrust sequence. Journ. of Geophys. Research, 95, 9069-9080
- Flick H. (1986) Permokarboner Vulkanismus im südlichen Odenwald. Heidelberger Geowissenschaftliche Abhandlungen 6, 121-138
- Flöttmann T., Oncken O. (1992) Constraints on the evolution of the Mid Crystalline Rise –a study of outcrops west of the river Rhine. Geologische Rundschau, 81, 2, 515-543
- Flores-Marquez E.L., Royer J.J. (1993) Convective heat transfer around the Soultz-sous-Forêts geothermal site (Rhine Graben). Doc. BRGM 223, 5th International Symposium on Continental Scientific Drilling Programs, Paris, April 1992, 155-170
- Frey M. (1987) Very low-grade metamorphism of clastic sedimentary rocks. In: M. Frey (Editor), Low temperature metamorphism. Blackie, Chapman and Hall, 9-58
- Gautschi A. (2000) Hydrogeology of a fractured shale (Opalinus clay): Implications for deep geological disposal of radioactive wastes. Hydrogeology Journal 9, 97-107
- Geng A. (1995) Diagenesis of the Middle Triassic Muschelkalk, Southwestern Germany. Diss. Univ. Heidelberg, 86p
- Genter A., Traineau H., Ledesert B., Bourguine B., Gentier S. (2000) Over 10 years of geological investigations within the HDR Soultz project, France. Proceedings World Geothermal Congress 2000, Kyushu-Tohoku, Japan, May 28-June 10, 2000
- Genter A., Traineau H. (1996) Analysis of macroscopic fractures in granite in the HDR geothermal well EPS-1, Soultz-sous-Forêts, France. Journal of Volcanology and Geothermal Research, 72, 121-141
- Genter A., Traineau H. (1991) Geological survey of the HDR borehole EPS-1, Soultz-sous-Forêts, Alsace-France. BRGM, R 32433
- Gérard A., Menjoz A., Schwoerer P. (1984) L'anomalie thermique de Soultz-sous-Forêts. Géothermie Actualités, 3, 35-42
-

Glasmacher U.A., Tschernoster R., Clauer N., Spaeth G. (2001) K-Ar dating of magmatic sericite crystallites for determination of cooling paths of metamorphic overprints, *Chemical Geology*, 175, 3-4, 673-687

Grathoff G.H., Moore D. (2002) Characterization of the Waukesha illite: a mixed-polytype illite in the Clay Mineral Society repository, *American Mineralogist*, 87, 1557-1563

Grathoff G.H., Moore D.M., Hay R.L., Wemmer K. (2001) Origin of illite in the lower Paleozoic of the Illinois Basin; evidence for brine migration, *Geological Society of America Bulletin*, 113, 8, 1092-1104

Grathoff G.H., Moore D.M. (1996) Illite polytype quantification using WILDFIRE calculated x-ray diffraction patterns. *Clays and Clay Minerals* 44, 834-842

Greiling R.O., Verma P.K. (2001) Strike-slip tectonics and granitoids emplacement: an AMS fabric study from the Odenwald Crystalline Complex, SW Germany. *Mineralogy and Petrology* 72, 165-184

Güven N. (2001) Mica structure and fibrous growth of illite. *Clays and Clay Minerals* 49, 189-196

Guthrie G.D., Veblen D.R. (1989) High-resolution transmission electron microscopy of mixed-layer illite/smectite: Computer simulations. *Clays and Clay minerals* 37, 1-11

Hamilton P.J., Giles M.R., Ainsworth P. (1992) K-Ar dating of illites in Brent Group reservoirs: a regional perspective. In: A.C. Morton et al. (eds.), *Geology of the Brent Group*. Spec. Publ. Geol. Soc. London 61, 377-400

Henes-Klaiber U. (1992) Zur Geochemie der variszischen Granitoide des Bergsträßer Odenwaldes. Unpubl. dissertation, TU Karlsruhe, 264 p.

Hess J.C., Lippolt H.J. (1996) Numerische Stratigraphie permokarbonischer Vulkanite Zentraleuropas. *Geol. Jb. Hessen III: Odenwald*, 124, 39-46

Hickman S.H., Evans B. (1992) Growth of grain contacts in halite by solution-transfer; implications for diagenesis, lithification, and strength recovery. *Fault mechanics and transport properties of rocks, a Festschrift in honor of W.F. Brace*. B.e.Evans and T.-f.e. Wong: 253-280

Honty M., Uhlik P., Sucha V., Caplovicova M., Francu J., Clauer N., Biron A. (2004) Smectite to illite alteration in salt-bearing bentonites; the East Slovak Basin. *Clays and Clay Minerals*, 52, 5, 533-551

Hower J., Mowatt T.C. (1966) The mineralogy of illites and mixed-layer illite/montmorillonites. *American Mineralogist* 51, 825-854

Hower J., Hurley P.M., Pinson W.H., Fairbairn H.W. (1963) The dependence of K-Ar age on the mineralogy of various particle size ranges in a shale, *Geochim. et Cosmochim. Acta*, 27, 405-410

Hunziker J.C., Frey M., Clauer N., Dallmeyer R.D., Friedrichsen H., Flehmig W., Hochstrasser K., Roggwiler P., Schwander H. (1986) The evolution of illite to muscovite: mineralogical and

isotopic data from the Glarus Alps, Switzerland. *Contrib. Mineral. Petrol.*, 92, 157-180

Illies J.H., Fuchs K. (1974) Approaches to Taphrogenesis. Inter-Union Commission on Geodynamics Scientific Report 8, Stuttgart

Illies J.H. (1968) Graben Tectonics as Related to Crust-Mantle Interaction. In: J.H. Illies, S. Mueller (eds.) Graben Problems. International Upper Mantle Project, Scientific Report 27

Illies J.H. (1965) Bauplan und Baugeschichte des Oberrheingrabens. *Oberrheinische Geologische Abhandlungen*, 20, 1-54

Illies J.H. (1963) Der Westrand des Rheingrabens zwischen Edenkoben (Pfalz) und Niederbronn (Elsass). *Oberrhein. Geol. Abh. Jg. 12*, 1-2, 1-23

Illies J.H. (1962) Prinzipien der Entwicklung des Rheingrabens, dargestellt am Grabenabschnitt von Karlsruhe. *Mitteilungen aus dem Geologischen Staatsinstitut in Hamburg*, 31, 58-121

Imaoka T., Nakashima K., Itaya, T., Okada T. (2001) Timing and duration of hydrothermal activity in the Oligocene Hamada Cauldron, SW Japan; evidence from K-Ar ages of sericites, *Resource Geology (Tokyo 1998)*, 51, 1, 55-62

Imber J., Holdsworth R.E., Butler C.A., Lloyd G.E (1997) Fault-zone weakening processes along the reactivated Outer Hebrides Fault Zone, Scotland. *J. of Geol. Soc. London*, 154, 105-109

Inoue A., Meunier A., Beaufort D. (2004) Illite-smectite mixed-layer minerals in felsic volcanoclastic rocks from drill cores Kakkonda Japan. *Clays and Clay Minerals* 52, 1, 66-84

Inoue A., Kitagawa R. (1994) Morphological characteristics of illitic clay minerals from a hydrothermal system. *Amer. Miner.*, 20, 69-79

Jaquemont B. (2002) Etude des interactions eaux-roches dans le granite de Soultz-sous-Forêts. Quantification et modélisation des transferts de matière par les fluides. Ecole et Observatoire des Sciences de la Terre, Centre de Géochimie de la France (UMR 7517)

Janecke S.U., Evans J.P. (1988) Feldspar-influenced rock rheologies. *Geology*, 16, 1064-1067

Jasmund K., Lagaly G. (1993) Tonminerale und Tone. Struktur, Eigenschaften, Anwendungen und Einsatz in Industrie und Umwelt. Steinkopf Verlag, Darmstadt, 490 p.

Just, J. (2005) Modification of magnetic properties in granite during hydrothermal alteration (EPS-1 borehole, Upper Rhine Graben). Ph-D thesis, University of Heidelberg, 92 p.

Kim J., Peacor D.R. (2002) Crystal-size distribution of clays during episodic diagenesis; the Salton Sea geothermal system, *Clays and Clay Minerals*, 50, 3, 371-380

Kim J.W., Peacor D.R., Tessier D., Elsass F. (1995) A technique for maintaining texture and permanent expansion of smectite interlayers for TEM observations. *Clays and Clay Minerals* 43, 51-57

Knipe R.J. (1993) The influence of fault zone processes and diagenesis on fluid flow. In: A.D.

Horbury, A.G. Robinson (eds.), Diagenesis and basin development. American Association of Petroleum Geologists: Studies in Geology 36, 135-148

Knudsen T.L. (2001) Contrasting provenance of Triassic/Jurassic sediments in North sea rift; a single zircon (SIMS), Sm-Nd and trace element study. *Chemical Geology* 171, 3-4, 273-293

Komninou A., Yardley B.W.D. (1997) Fluid-rock interactions in the Rhine Graben: A thermodynamic model of the hydrothermal alteration observed in deep drilling, *Geochim. et Cosmochim. Acta*, 61, 3, 515-531

Kooi H.S., Cloetingh S. (1992) Lithospheric necking and regional isostasy at extensional basins 2. Stress-induced vertical motions and relative sea level changes. *J. Geoph. Res.* 97, 17, 573-17,591

Kossmat F. (1927) Gliederung des variskischen Gebirgsbaues. *Abh Sächs Geol L-Anst*, 1, 1-39

Kyser K., Hiatt E., Renac C., Durocher K., Holk G., Deckart K. (2000) Diagenetic fluids in paleo- and meso- Proterozoic sedimentary basins and their implications for long protracted fluid histories. In: K. Kyser (eds.) *Fluids and basin evolution*. Mineralogical Association of Canada, Short Courses Series 28, 473-506

Lampe C., Person M., Nöth S., Ricken W. (2001) Episodic fluid flow within continental rift basins: some insights from field data and mathematical models of the Rhinegraben. *Geofluids* I, 42-52

Laubscher H. (2001) Plate interactions at the southern end of the Rhine graben. *Tectono-physics* 343 1-2, 1-19

Laverret E. (2002) Evolutions temporelles et spatiales des altérations argileuses des gisements d'uranium sous discordance, secteur de shea creek (bassin de L' Athabasca, Canada), unpublished thesis, Université de Poitiers

Lédesert B., Berger G., Meunier A., Genter A., Bouchet A. (1999) Diagenetic-type reactions related to hydrothermal alteration in the Soultz-sous-Forêts Granite, France. *European Journal of Mineralogy*, 11, 4, 731-741

Lédesert B., Joffre J., Ambles A., Sardini P., Genter A., Meunier A. (1996) Organic matter in the Soultz HDR granitic thermal exchanger (France): natural tracer of fluid circulations between the basement and its sedimentary cover. *Journ. of Volc. And Geoth. Res.* 70, 3, 235-253

Liewig N., Clauer N. (2000) K-Ar dating of varied microtextural illite in Permian gas reservoirs, northern Germany, *Clay Minerals*, 35, 271-281

Liewig N., Clauer N., Sommer F. (1987) Rb-Sr and K-Ar dating of clay diagenesis in Jurassic sandstone oil reservoirs, North Sea. *Assoc. Petrol. Geol. Bull.* 71, 1467-1474

Lippolt H.J., Leyk H.-J. (2004) Alterations-Alter des Heidelberger Granits aus Untersuchungen an Tonmineralanreicherungen aus dem Bergwerk am Branich in Schriesheim/SW Odenwald. *Jahreshefte des Landesamts für Geologie, Rohstoffe und Bergbau Baden-Württemberg*, 40, 187-230

Lippolt H.J., Kirsch H. (1994a) Ar/Ar- Untersuchungen an serizitisierten Plagioklasen des

-
- Frankenstein-Gabbros (NW-Odenwald) im Hinblick auf ihren Alterations-Zeitpunkt. *Geol. Jb. Hessen*, 122, 123-142
- Lippolt H.J., Kirsch H., Plein E. (1990) Karbonische und permische Vulkanite aus dem Untergrund des nördlichen Oberrheingrabens: Art, Altersbestimmung und Konsequenz. *Jber. Mitt. Oberrhein. geol. Ver.* 2, 227-242
- Littke R., Bueker C., Hertle M., Karg H., Stroetmann-Heinen V. (2000) Heat flow evolution, subsidence and erosion in the Rheno-Hercynian orogenic wedge of Central Europe. In: W. Franke, V. Haak, O. Oncken (eds.), *Orogenic processes; quantification and modelling in the Variscan Belt*. Geological Society Special Publications 179, 231-255
- Lonker S.W., Fitz Gerald J.D. (1990) Formation of coexisting 1M and 2M polytypes in illite from an active hydrothermal system. *Amer. Mineral.* 75, 1282-1289
- McCaffrey K., Lonergan L., Wilkinson J.J. (1999) Fractures, fluid flow and mineralization. *Geol. Soc. Spec. Publ.*, 155
- Marbach T., Kober B., Mangini A., Warr L., Schleicher A. (in press) Mobility of U-Th radionuclides connected with fault porosity: a case study of the Schauenburg Fault, Rhine Graben Shoulder, Germany. *Physics and Chemistry of the Earth* (in press)
- Marbach T. (2001) Fluid-rock interaction history of a faulted rhyolite-granite contact, eastern Rhine Graben Shoulder, SW-Germany: Alteration Processes determined by Sr-Pb-isotopes, Th-U-disequilibria and elemental distributions. Ph-D thesis, University of Heidelberg, 140 p.
- Maurin J-C., Niviere B. (2000) Extensional forced folding and decollement of the pre-rift series along the Rhine Graben and their influence on the geometry of the syn-rift sequences. In: J.W. Cosgrove, S.M. Ameen (eds.), *Forced folds and fractures*, Geological Society Special Publications, 169, 73-86
- May F., Hoernes S., Neugebauer H.J. (1996) Genesis and distribution of mineral waters as a consequence of recent lithospheric dynamics: the Rhenish Massif, Central Europe. *Geol. Rundschau*, 85, 782-799
- Mc Kenzie, D. (1978) Some remarks on the development of sedimentary basins, *Earth and Planetary Science letters*, 40, 25-32
- Merriman R.J., Frey D. (1999) Patterns of very low-grade metamorphism in metapelitic rocks In: M. Frey, D. Robinson (eds.) *Low-grade metamorphism*. Blackwell Science, 313p.
- Merriman R.J., Peacor D.R. (1999) Very low grade metapelites: mineralogy, microfabrics and measuring reaction progress. In: M. Frey, D. Robinson (eds.) *Low-grade metamorphism*. Blackwell Science, 313p.
- Meunier A., Velde B. (2004) *Illite*. Springer Verlag, 286p.
- Meyer M., Brockamp O., Clauer N., Renk A., Zuther M. (2000) Further evidence for a Jurassic mineralizing event in central Europe: K-Ar dating of hydrothermal alteration and fluid inclusion systematics in wall rocks of the Käfersteige fluorite vein deposit in the Northern Black Forest,
-

Germany. Mineral. Depos. 35, 754-761

Mitchell J.G., Halliday A.N. (1976) Extent of Triassic/Jurassic hydrothermal ore deposits on the North Atlantic margins. *Trans. Inst. Min. Metall.*, B85, 159-161

Montigny R., Faure G. (1969) Contribution au probleme de l'homogeneisation isotopique du strontium des roches totales au cours du metamorphisme. Cas du Wisconsin Range, Antarctique. *C R Acad Sci Paris* 268D, 1012-1015

Moore D.M., Reynolds R.C. (1997) X-ray diffraction and the identification and analysis of clay minerals. Oxford University Press: 378 p.

Morrow C.A., Radney B., Byerlee J.D. (1984) Permeability of fault gouge under confining pressure and shear stress. *Journal of Geophysical Research B* 89, 3193-3200

Mullin J.W. (1961) Crystallization. Butterworths, England

Oertel G. (1985) The relationship of strain and preferred orientation of phyllosilicates grains in rocks: a review. *Tectonophysics* 100, 413-447

Okrusch M., Schubert W., Stähle V. (2000) The Odenwald, Germany: Variscan metamorphic evolution and igneous events. *Beih. Z. Eur. J. Mineral.* 12, 2, 45-89

Oncken O. (1998) Evidence for precollisional subduction erosion in ancient collisional belts: The case of the Mid-European Variscides. *Geology*, 26, 1075-1078

Pauwels H., Fouillac C., Fouillac A.M. (1993) Chemistry and isotopes of deep geothermal saline fluids in the Upper Rhine Graben: origin of compounds and water rock interactions *Geochim. Cos. Acta* 57, 2737-2749

Pauwels H., Fouillac C., Criaud A. (1992) Water-rock interactions during experiments within the geothermal Hot Dry Rock borehole GPK1, Soultz-sous-Forêts, Alsace, France. *Applied Geochemistry*, 7, 243-255

Peacor D.R., Bauluz B., Dong H., Tillick D. Yan Y. (2002) Transmission and analytical electron microscopy evidence for high Mg contents of 1M illite: absence of 1M polytypism in normal prograde diagenetic sequences of pelitic rocks. *Clays and Clay Minerals* 50, 757-765

Peacor DR (1992) Diagenesis and low-grade metamorphism of shales and slates. In: P.R. Buseck (ed.), *Minerals and Reactions at Atomic Scale: Transmission Electron Microscopy*. *Rev. Mineral.* 27, 335-380

Person M., Garven G. (1994) A sensitivity study of the driving forces on fluid flow during continental-rift basin evolution. *Geol. Sci. Am. Bull.* 106, 461-475

Pribnow D., Clauser C. (2000) Heat and fluid flow at the Soultz hot dry rock system in the Rhine Graben. *Proceedings World Geothermal Congress Kyushu-Tohoku, Japan, May 28-June10, 2000*

Pribnow D., Schellschmidt R. (2000) Thermal tracking of upper crustal fluid flow in the Rhine Graben. *Geophys. Res. Lett.* 27, 13, 1957-1960

-
- Prier H. (1969) Das pyroklastische und sedimentäre Rotliegende im Bereich der Bergstraße des südlichen Odenwaldes. *Jh. Geol. Landesamt BW* 11, 279-298
- Prodehl C., Mueller St., Haak V. (1995) The European Cenozoic rift system: Continental rifts, evolution, structure, tectonics. In: K.H. Olsen (Editor), *Developments in Geotectonics* 25, 133-212
- Reuter A. (1985) Grain-size dependency of K-Ar dating and illite crystallinity determined on anchizonal metapelites and associated metatuffs from the eastern Rhenish Schiefergebirge; *Goettinger Arbeiten zur Geologie und Palaeontologie*, 27, 91 pp.
- Reynolds R.C. (1993) Three-dimensional X-ray powder diffraction from disordered illite: simulation and interpretation of the diffraction patterns. In: *Computer applications*
- Reynolds R.C., Reynolds R.C. (1996) NEWMOD: A computer program for the calculation of one-dimensional diffraction patterns of mixed-layered clays, Hanover, New Hampshire
- Reynolds R.C. jr., Thomson C.H. (1993) Illite from the Potsdam Sandstone of New York: A probable noncentro-symmetric mica structure. *Clays and Clay Minerals* 41, 66-72
- Reynolds R.C. (1980) Interstratified clay minerals. In: G.W. Brindley, G. Brown (eds.) *Monograph* 5, Mineralogical Society, 249-303
- Robertson I.D., Eggleton R.A. (1991) Weathering of granitic muscovite to kaolinite and halloysite and of plagioclase-derived kaolinite to halloysite. *Clays and Clay Minerals* 39, 2, 113-126
- Rosenberg P.E. (2002) The nature, formation and stability of end-member illite: A hypothesis; *American Mineralogist*, 87, 103-107
- Rousset D., Clauer N. (2003) Discrete clay diagenesis in a very low-permeable sequence constrained by an isotopic (K-Ar and Rb-Sr) study, *Contrib. Mineral. Petrol.*, 145, 182-198
- Rügner O. (2000) Tonmineral-Neubildung und Paläosalinität im Unteren Muschelkalk des südlichen Germanischen Beckens. Elektronisch publizierte Dissertation, Universität Heidelberg
- Rutter E.H., Maddock R.H., Hall S.H., White S.H. (1986) Comparative microstructure of natural and experimentally produced clay bearing fault gouges. *Pageoph.*, 124, 3-30
- Sausse J. (2002) Hydromechanical properties and alteration of natural fracture surfaces in the Soultz Granite (Bas-Rhin, France) In: P. Labaume, D. Craw, M. Lespinasse, P. Muchez (eds.), *Tectonic processes and the flow of mineralising fluids. Tectonophysics*, 348, 1-3, 169-185
- Sausse, J., Genter A., Leroy J.L., Lespinasse M. (1998) Description and quantification of vein alterations; paleopermeabilities in the Soultz-sous-Forêts granite (Bas-Rhin, France), *Bulletin de la Societe Geologique de France*, 169, 5, 655-664
- Schleicher A.M., Warr L.N., van der Pluijm B.A. (in press) Fluid focusing and back reactions in the uplifted shoulder of the Rhine rift system: a clay mineral study along the Schauenburg fault zone (Heidelberg, Germany), submitted to *International Journal of Earth Sciences*
-

Schleicher A.M. (2001) Niedrig temperierte Alterationsprodukte in felsischen Gesteinen am Beispiel der Schauenburgstörung, östliche Rheingrabenschulter bei Heidelberg. Unpublished Master thesis, University of Heidelberg, 115 p.

Schliephake R. W. (1970) Präparateträger für Röntgen-Diffraktometer-Aufnahmen an sehr dünnen Pulverpräparaten. N.Jb. Miner., Mh., 1, 24-26, Schweizerbart, Stuttgart

Schmidt S.M., Casey M. (1986) Complete fabric analysis of some commonly observed quartz c-axis patterns. In: B.E. Hobbs, H.C. Heard (eds.), Mineral and Rock Deformation: Laboratory Studies, Am. Geophys. Un. Geophys. Monogr. 36, 263-287

Schulz R., Schellschmidt R. (1991) Das Temperaturfeld im südlichen Oberrheingraben. Geol. Jahrbuch, E 48, 153-165

Schumacher M.E. (2002) Upper Rhine Graben: Role of preexisting structures during rift evolution. Tectonics 21,1: 6,1-6,17

Shijun N., Qing H., Jianwu T., Jiaduo L., Zeqin L. (2001) Kinetics of the fluid-mineral reactions in the Eocene lacustrine sandstone, Jiangnan basin, SE China. Abstract Goldschmidt conference Virginia, May 20-24

Sibson R.H. (1994) Crustal stress, faulting and fluid flow. In: J. Parnell (eds.), Geofluids: Origin, Migration and Evolution of Fluids in Sedimentary Basins. Geological Society Special Publication 78, 69-84

Sibson R.H. (1977) Fault rocks and fault mechanisms. J.Geol.Soc. London, 133, 191-213

Simon W. (1968) Mineralien und Gesteine als geologische Zeitmesser. Aufschluss Sonderdruck, Heidelberg, 7/8, 185-194

Small J.S., Hamilton D.L., Habesch S. (1992) Experimental simulation of clay precipitation within reservoir sandstones. 2: Mechanism of illite formation and controls on morphology. J. Sedim. Petrol. 62, 520-529

Smith M.P., Savary V., Yardley B.W.D., Valley J.W., Royer J.J., Dubois M. (1998) The evolution of the deep flow regime at Sault-sous-Forêts, eastern France: Evidence from a composite quartz vein. Journal of Geophysical Research, 103, B11, 27.223-27.237

Solum J.G., van der Pluijm B.A., Peacor D.R., Warr L.N. (2003) Influence of phyllosilicate mineral assemblages, fabrics, and fluids on the behavior of the Punchbowl fault, southern California. Journal of Geophysical Research 108, B5: 5-1 - 5-12

Srodon J., Clauer N., Eberl D. (2002) Interpretation of K-Ar dates of illitic clays from sedimentary rocks aided by modeling; American Mineralogist, 87, 11-12, 1528-1535

Srodon J., Eberl D. (1984) Illite. In: S.W. Baily (Editor), Micas. Reviews in Mineralogy 13, 495-544

Srodon J. (1984) X-ray identification of illitic materials. Clays and Clay Minerals, 32, 337-349
Stanislavsky E., Gvirtzman H. (1999) Basin-scale migration of continental-rift brines:

Paleohydrologic modeling of the Dead Sea basin. *Geology* 27, 9, 791-794

Steeds J.W., Morniroli J.P. (1992) Electron Diffraction- SAED and CBED. In: P.R. Buseck (eds.), *Minerals and Reactions at Atomic Scale: Transmission Electron Microscopy*. *Rev. Mineral.* 27, 37-83

Steiger R.H., Jäger E. (1977) Subcommittee on geochronology: convention on the use of decay constants in geo- and cosmochronology. *Earth Planet. Sc. Lett.*, 36, 359-352

Stein E. (2001) The Geology of the Odenwald Crystalline Complex. *Mineralogy and Petrology* 72, 7-28

Stober I., Bucher K. (2004) Fluids sinks within the Earth's crust. *Geofluids*, 4, 143-151

Stober I., Bucher K. (2000) Herkunft der Salinität in Tiefenwässern des Grundgebirges unter besonderer Berücksichtigung der Kristallinwässer des Schwarzwaldes. *Grundwasser*, 3/5, 125-140

Stokke P.R., Carson B. (1973) Variation in clay mineral X-ray diffraction results with the quantity of sample mounted. *J. Sedim. Petrol.*, 43, 4, 957-964

Surma F., Geraud Y. (2003) Porosity and thermal conductivity of the Soultz-sous-Forêts granite. *Pure Appl. Geophys.* 160, 1125-1136

Teichmüller M. (1970) Bestimmung des Inkohlungsgrades von kohligen Einschlüssen in Sedimenten des Oberrheingrabens: Ein Hilfsmittel bei der Klärung geothermischer Fragen. In: *Graben problems*. J.H. Illies, S. Müller (eds.) *Upper mantle Sci. Proj. Sci. Rept.*, 27, 124-142

Thyne G., Boudreau B.P., Ramm M., Midtbo E. (2001) Simulation of potassium feldspar dissolution and illitization in the Statfjord Formation, North Sea. *AAPG Bulletin* 85, 4, 621-635

Turcotte D.L. Oxburgh E.R. (1973) Mid-plate tectonics, *Nature*, 244, 337-339

van Balen R.T., Cloetingh S. (1993) Stress-induced fluid flow in rifted basins. In: A.D. Horbury, A.G. Robinson (eds.), *Diagenesis and Basin Development*. American Association of Petroleum Geologists, Tulsa, Oklahoma, 87-98

van der Pluijm B.A., Hall, C.M., Vrolijk P.J., Pevear D.R., Covey M.C. (2001) The dating of shallow faults in the Earth's crust, *Nature*, 412

van der Pluijm B.A. (1999) Clay-bearing fault gouge; processes and implications, *Goettinger Arbeiten zur Gologie und Palaeontologie*, Sonderband 4, 158p.

van der Pluijm B.A., Ho N., Peacor D. (1994) High-resolution X-ray texture goniometry. *Journal of Structural Geology* 16, 7, 1029-1032

Veblen D.R. (1992) Electron microscopy applied to nonstoichiometry, polysomatism and replacement reactions in minerals. In: P.R. Buseck (eds.), *Minerals and Reactions at Atomic Scale: Transmission Electron Microscopy*. *Rev. Mineral.*, 27, 181-223

Velde B. (1985) Developments in sedimentology: Clay Minerals, a physico-chemical explanation of their occurrence. Elsevier Amsterdam, 427 p.

Velde B. (1965) Experimental determination of muscovite polymorph stabilities. *American Mineralogist* 50, 436-449

Vrolijk P., van der Pluijm B.A. (1999) Clay gouge. *J. Struct. Geol.* 21, 1039-1048

Wagner G.A., Storzer D. (1975) Spaltspuren und ihre Bedeutung für die thermische Geschichte des Odenwaldes. *Aufschluß, Sonderband 27 (Odenwald)*, 79-85

Wagner G.A., Storzer D. (1972) Fission track length reductions and the thermal history of rocks. *Transact. Amer. Nucl. Soc.*, 15, 127-128

Warr L.N., Peacor D.R. (2002) Evaluation of X-ray diffraction methods for determining the crystal growth mechanisms of clay minerals in mudstones, shales and slates, *Schweizerische Mineralogische und Petrographische Mitteilungen*, 82, 2, 187-202

Warr L.N., Cox S. (2001) Clay mineral transformations and weakening mechanisms along the Alpine Fault, New Zealand. *Geological Society London, Special Publication 186*, 85-101

Warr L.N., Nieto F. (1998) Crystallite thickness and defect density of phyllosilicates in low-temperature metamorphic pelites: a TEM and XRD study of clay-mineral crystallinity-index standards. *The Canadian Mineralogist* 36, 1453-1474

Warr L.N., Rice A.H.N. (1994) Interlaboratory standardization and calibration of clay mineral crystallinity and crystallite size data. *J. Metamorphic Geol.*, 12, 141-152

Welton J. E. (1984) SEM petrology atlas. *AAPG methods in exploration series*, 4, 237p.

Wen B.P., Aydin A. (2003) Microstructural study of a natural slip zone; quantification and deformation history. *Engineering Geology* 68, 3-4, 289-317

Wenk H.R. (1985) Preferred orientation in deformed rocks (eds.). Academic Press, Orlando

Werner D., Doebel F. (1974) Eine geothermische Karte des Rheingrabenuntergrundes. In: J.H. Illies, K. Fuchs (eds.), *Approaches to taphrogenesis*. E. Schweizerbarth, Stuttgart, 182-191

Wibberley C. (1999) Are feldspar-to-mica reactions necessarily reaction-softening processes in fault zones? *Journal of Structural Geology* 21, 1219-1227

Wintsch R.P., Christoffersen R., Kronenberg A.K. (1995) Fluid-rock reaction weakening of fault zones. *Journal of Geophysical Research* 100, B7,13,021-13,032

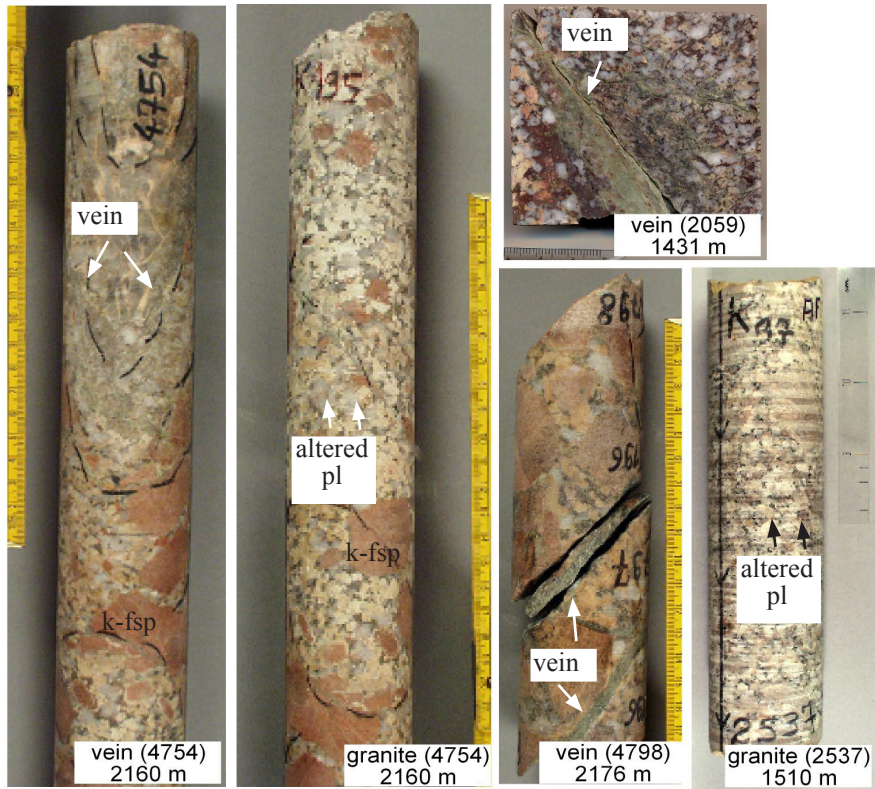
Wilkinson M., Haszeldine R.S. (2002) Fibrous illite in oilfield sandstones-a nucleation kinetic theory of growth. *Terra Nova*, 14, 56-60

WU F.T., Blatter L., Roberson H. (1975) Clay gouges in the San Andreas fault system and their possible implications. *Pure Applied Geophysics*, 113, 87-96

-
- Yan Y., Tillick D.A., Peacor D.R., Simmons S.F. (2001) Genesis of dioctahedral phyllosilicates during hydrothermal alteration of volcanic rocks II. The Broadlands-Ohaaki hydrothermal system, New Zealand. *Clays and Clay minerals*, 49, 141-155
- Yates D.M., Rosenberg P.E. (1998) Characterization of neoformed illite from hydrothermal experiments at 250 °C and Pv, soln: An HRTEM/ATEM study; *American Mineralogist*, 83, 1199-1208
- Ylagan R.F., Kim C.S., Pevear D.R., Vrolijk P.J (2002) Illite polytype quantification for accurate K-Ar age determination, *American Mineralogist*, 87, 1536-1545
- Ylagan, R.F., Altaner S.P., Pozzuoli A. (1996) Hydrothermal alteration of a rhyolitic hyaloclastite from Ponza Island, Italy. *Journal of Volcanology and Geothermal Research* 74, 215-231
- Yoder H.S., Eugster H.P. (1955) Synthetic and natural muscovites. *Geochimica et Cosmochimica Acta* 8, 5-6, 225-280
- Zhao G., Peacor D. R., McDowell S. D. (1999) Retrograde diagenesis of clay minerals in the Freda Sandstone, Wisconsin. *Clays and Clay Minerals* 47, 119-130
- Ziegler P.A. (1993) Late Paläozoic-Early Mesozoic plate reorganization: evolution and demise of the Variscan fold belt. In: J.F. von Raumer, F. Neubauer (eds.), *Pre-Mesozoic geology in the Alps*, Springer, Berlin 203-216
- Zöller, M.H., Brockamp O. (1997) 1M and 2M1-illites: different minerals and not polytypes. *Eur. J. Mineral.*, 9, 821-827
- Zöller M.H. (1994) Einkristalluntersuchungen an 1M und 2M1 illiten durch konvergente Elektronenbeugung. Dissertation Universität Bremen
- Zwingmann H., Clauer N., Gaupp R. (1998) Timing of fluid flow in a sandstone reservoir of the North-German Rotliegend (Permian) by K-Ar dating of related hydrothermal illite. In: J. Parnell (eds.), *Dating and duration of fluid flow events*, Geol. Soc. London Spec. Publ., 144, 91-106

APPENDIX

Soultz-sous-Forêts borehole



Schauenburg-Fault



Key study samples from the Soultz-sous-Forêts borehole and the Schauenburg Fault

Instruments and measuring parameters**X-ray diffractometer**

machine:	Siemens D500
X-ray:	CuK α
wavelength:	1.541nm
aperture slit:	1°
detector slit:	0.15°; MudMaster 0.05°
goniometer:	Bragg-Brentano-circle; $\theta/2\theta$
voltage:	40 kV
current:	30mA

Powder measurements

start angle:	2°
end angle:	70°
step size:	0.02°
step time:	1s

Texture measurement

start angle:	2°
end angle:	50°
step size:	0.02°
step time:	2s

MudMaster measurement

start angle:	4°
end angle:	10°
step size:	0.02°
step time:	10s

Polytype measurement

start angle:	19°
end angle:	36°
step size:	0.02°
step time:	10s

X-ray texture goniometer

machine:	Enraf-Nonius CAD4 single crystal X-ray diffractometer
X-ray:	MoK*
wave length:	0.929nm
1 theta:	2.03 (for mica)
voltage:	40kV
current:	20mA
program:	“XPGF” (Windows application)

Scanning electron microscopy parameter

Instrument:	Leo 440
EDX analysis:	Oxford, Link Isis 300

Transmission electron microscopy setting

Machine:	Philips CM 12
Detector:	KeveX Quantum solid-state
Accelerating voltage:	0-120kV
Beam current:	20mA
Filament:	Single crystal lanthanum hexaboride
Magnification:	100,000x
Resolution :	HTEM 0.2nm lattice, 0.34nm point-to-point

“Sedi-tool: Stoke’s gravity”:

Distance centrifuge axis to top water column:	7.6cm
Distance centrifuge axis to top sediment:	16cm
Rotations per minute:	1000-3000
Water temperature:	23°C
Spec. gravity grains:	2.65g/cm ³ (clay)
Range of grain sizes:	63-0.2µm

Preparation methods**Grain size separation for K-Ar dating**

The samples were crushed into small pieces and the green and white coloured illite in veins and granites carefully selected by hand. 25g of rock chips were then wetground in a rock-mill for 10sec at 700r/min. Wet grinding was necessary to avoid possible phase changes or microstrains occurring in the crystal structure, which may cause a XRD line broadening. About 100g of the ground material was suspended in 2 liters of distilled water. After 15 minutes treatment in an ultrasonic bath, the material was cooled down to ca. 23°C and stirred well before grain-size separation.

For K-Ar analysis up to 8 different grain size fractions (> 63µm, 10-63µm, 4-10µm, 2-4 µm, 1-2µm, 0.4-1µm, 0.2-0.4µm and < 0.2µm) were separated by sedimentation, centrifugation and filtering with specific temperatures (°C), rotation-speed (r/min) and running-times (min) calculated using Stokes law (“SediTools” (© R.Petschick, Geol.-Paläont. Institut, Universität Frankfurt; table 2). The calculated values were corrected for acceleration- and deceleration times.

After 0.75 min of sedimentation, the remaining > 63µm grain size fraction could be extracted, and the suspension (< 63µm) mixed again with distilled water. This procedure was repeated three times, and the resulting material (> 63µm) dried in an oven at 55°C. The remaining suspension (< 63µm) was used for separating the next grain size fractions. All further working steps followed the same procedure. Resulting powdered grain-size fractions were measured as powder-

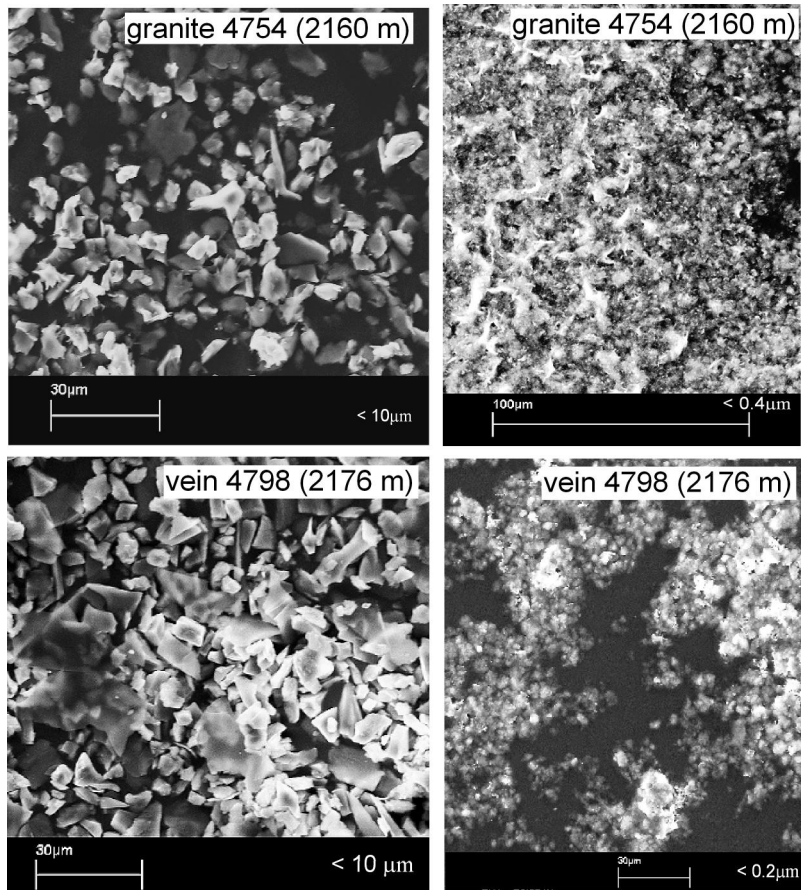
preparations (random oriented grains), and texture preparations (well oriented clay mineral flakes parallel to the substrate).

Weight of the extracted grain-size fractions

grain size (μm)	1570m depth granite (g)	2167m depth granite (g)	2160m depth vein (g)	2176m depth vein (g)
> 63	920.00	394.50	99.80	43.17
10-63	48.61	48.30	10.47	3.33
4-10	10.29	11.69	3.20	0.90
2-4	7.13	12.69	2.82	0.72
1-2	6.98	8.37	1.96	0.77
0.4-1	4.00	3.31	4.61	1.36
0.2-0.4	0.95	10.99	1.12	0.37
<0.2	0.41	4.10	1.64	0.30
sum	998.38	493.94	125.61	50.91
source material (g)	1000	600	136	52

Settings used to separate the different grain sizes

grain size (μm)	method	Temp. ($^{\circ}\text{C}$)	speed (r/min)	R1 (cm)	R2 (cm)	sed/cent-time (min)
> 63	sedimentation	23	-	-	-	0.75
> 10	sedimentation	23	-	-	-	30
> 4	centrifugation	23	1000	7.5	16	0.67
> 2	centrifugation	23	1000	7.5	16	2.4
> 1	centrifugation	23	1000	7.5	16	10.45
> 0.4	centrifugation	23	3000	7.5	16	7.3
> 0.2	centrifugation	23	3000	7.5	16	30
< 0.2	filtering	23	-	-	-	-



Example SEM images of the different grain size fractions in the different Sultz-sous-Forêts samples

K-Ar age values of the different grain sizes separated for the four selected Soultz-samples

sample (depth)	type	grain size (μm)	K ₂ O (%)	⁴⁰ Ar rad (10 ⁻⁶ cm ³ /g STP)	⁴⁰ Ar rad (%)	40K/36Ar	40Ar/36Ar	K-Ar age (Ma)
4798	vein	4-10	8.54	73.2	78.0	67390	1340	279.8 (3.4)
(2176.9 m)	vein	2-4	9.73	85.0	93.2	252355	4326	274.0 (3.1)
	vein	1-2	9.83	95.7	98.6	1117688	21442	274.3 (3.0)
	vein	0.4-1	9.81	93.7	97.4	646356	11461	279.3 (3.2)
	vein	0.2-0.4	9.59	91.5	97.4	642664	11384	252.3 (3.0)
	vein	< 0.2	9.09	88.7	97.6	682585	12345	247.9 (3.4)
4754	vein	4-10	9.10	65.7	88.1	166608	2480	256.4 (4.6)
(2167.7 m)	vein	2-4	9.86	78.2	99.3	2450736	40477	238.7 (3.5)
	vein	1-2	9.58	78.7	99.1	1972568	33007	248.0 (3.3)
	vein	0.4-1	8.51	73.0	95.4	392728	6378	238.3 (2.9)
	vein	0.2-0.4	7.98	65.7	94.4	338352	5325	230.5 (2.6)
	vein	< 0.2	6.64	59.0	89.6	158069	2830	211.0 (2.7)
4754	host	4-10	8.22	25.6	85.6	311390	2051	255.5 (6.5)
(2167.7 m)	host	2-4	8.96	32.9	91.4	470034	3442	236.4 (6.0)
	host	1-2	9.10	40.6	95.5	768444	6637	213.4 (5.2)
	host	0.4-1	8.48	38.5	94.7	650590	5632	201.4 (4.9)
	host	0.2-0.4	7.27	37.6	94.4	534256	5292	190.9 (4.6)
	host	< 0.2	6.74	35.4	94.0	484321	4875	193.6 (5.7)
2537	pervasive	4-10	4.32	28.4	32.7	12048	438	156.1 (2.8)
(1570.3 m)	pervasive	2-4	4.86	31.6	89.3	207279	2743	153.8 (2.5)
	pervasive	1-2	4.77	32.8	87.2	160659	2299	135.6 (1.8)
	pervasive	0.4-1	4.62	33.7	84.2	119853	1875	133.3 (1.7)
	pervasive	0.2-0.4	4.34	35.3	81.6	89431	1610	110.4 (1.6)
	pervasive	< 0.2	4.39	38.8	91.5	199770	3488	93.9 (1.4)

X-ray diffraction sample preparation

Random powders

Small rock-fragments were wetground using a disc mill (700r/min; 10-15sec) to form a powder-paste. After drying, the sample was loaded into a sample holder as a randomly oriented powder and covered with a rough glass slide, which reduces the degree of particle alignment. The sample holder was held vertically and carefully tapped on the table to maximize random orientation. The resulting X-ray diffraction patterns of randomly ordered powder samples give an idea of the proportion of clay and non-clay mineral components.

Texture slides

Well-washed samples were crushed into small pieces and disaggregated in an ultrasonic bath for at least half an hour. The $< 2\mu\text{m}$ clay fraction was separated by centrifugation and prepared by pipetting 45mg of clay suspended in 1.5ml of water onto a 3 cm x 3 cm glass slide. During sedimentation, the clay particles align parallel to the surface, which enhances (001) basis reflections. In contrast, the $hk0$ peaks are suppressed.

Thin films for CTD determinations

2.5mg of sample powder and 0.5ml of distilled water were disaggregated in an ultrasonic bath for some seconds. Afterwards, the solution was dropped onto a silicon single crystal glass slide (Schliephake 1970). For samples containing mixed-layered swelling clay, Na-saturated samples were prepared and mixed with 0.5ml distilled water and 5mg of polyvinylpyrrolidone (PVP), following the procedure of Eberl et al. (1996)

IMajor elemental results of the whole rock material and grain-sizes fractions of the Soultz-granite measured by ICP-MS

Fe %	Ca %	P %	Mg %	Ti %	Al %	Na %	K %	grain size (µm)
1.07	1.85	0.089	0.23	0.476	6.87	0.64	3.3	4754h > 63
1.22	2.66	0.103	0.28	0.381	7.92	0.9	3.12	4754h 10-63
1.29	1.93	0.061	0.32	0.352	8.49	1.18	3.08	4754h 4-10
1.49	0.94	0.046	0.42	0.285	9.61	1.043	3.31	4754h 2-4
1.59	0.37	0.03	0.41	0.207	8.78	0.678	3.77	4754h 1-2
1.93	0.11	0.029	0.43	0.189	>10	0.426	3.86	4754h 0.4-1
2.1	0.16	0.017	0.4	0.106	9.51	0.153	3.29	4754h 0.2-0.4
2.25	0.33	0.019	0.43	0.089	>10	0.211	4.98	4754h < 0.2
1.24	2.42	0.12	0.28	0.453	7.53	0.962	2.76	4754h whole rock
0.82	1.39	0.052	0.26	0.276	6.21	0.179	2.89	4754v > 63
1.15	1.55	0.051	0.33	0.367	7.75	0.196	3.01	4754v 10-63
1.37	0.86	0.04	0.39	0.391	8.87	0.21	3.69	4754v 4-10
1.54	0.38	0.035	0.45	0.35	>10	0.203	4.38	4754v 2-4
1.55	0.08	0.021	0.34	0.246	9.65	0.135	4.24	4754v 1-2
1.78	0.08	0.014	0.33	0.114	>10	0.072	4.44	4754v 0.4-1
1.84	0.09	0.011	0.32	0.078	>10	0.061	4.68	4754v 0.2-0.4
1.96	0.31	0.016	0.39	0.047	>10	0.183	5.19	4754v < 0.2
0.86	1.73	0.08	0.26	0.28	6.42	0.126	2.96	4754v whole rock
2.33	0.4	0.01	0.47	0.082	8.79	0.082	4.89	4798 10-63
2.56	0.24	0.011	0.59	0.099	>10	0.13	4.31	4798 4-10
2.67	0.23	0.009	0.61	0.088	>10	0.089	5	4798 2-4
2.71	0.13	0.01	0.5	0.097	>10	0.076	4.72	4798 1-2
2.58	0.05	0.008	0.44	0.075	>10	0.052	5.13	4798 0.4-1
2.63	0.18	0.011	0.54	0.072	>10	0.139	4.77	4798 0.2-0.4
2.24	1.55	0.018	0.68	0.045	7.8	0.081	2.89	vein whole rock
2.15	3.2	0.014	0.88	0.1	6.23	1.539	3	host whole rock
2.07	1.49	0.093	0.61	0.364	7.3	3.137	3.17	2537 >63 mü
2.61	1.81	0.145	1.14	0.513	6.67	2.503	3.3	2537 10-63 mü
2.42	1.8	0.116	0.91	0.486	7.33	2.893	3.62	2537 4-10 mü
2.68	1.17	0.11	1.06	0.465	7.26	2.953	3.54	2537 2-4 mü
3.59	1.05	0.124	1.44	0.527	8.1	2.867	3.7	2537 1-2 mü
3.35	0.85	0.08	1.33	0.415	7.91	2.759	3.68	2537 0.4-1 mü
3.76	0.87	0.063	1.56	0.341	8.27	2.37	3.87	2537 0.2-0.4 mü
3.65	0.78	0.078	1.65	0.31	7.52	1.863	3.3	2537 < 0.2 mü
2	1.3	0.072	0.7	0.315	7.39	3.057	3.32	2537 whole rock

TEM-preparation at EMAL, University of Michigan

Sample preparation

- Vacuum impregnation of rock chips with L.R. White resin to prevent collapse of smectite interlayers (Kim et al. 1995)
- Glueing on a glass slide with sticky-wax
- Cutting with an oil saw as thin as possible
- Thinning and grinding by hand as thin as possible
- Glue Cu-washers (ca. 3mm in average) on area of interest with special glue. Cleaning, then drying for 24 hours
- Removal of washers carefully with a knife, removal of the Cu-washers from the glass slide by melting the sticky wax glue.
- Carefully cleaning of the washers with acetone

Ion-mill thinning

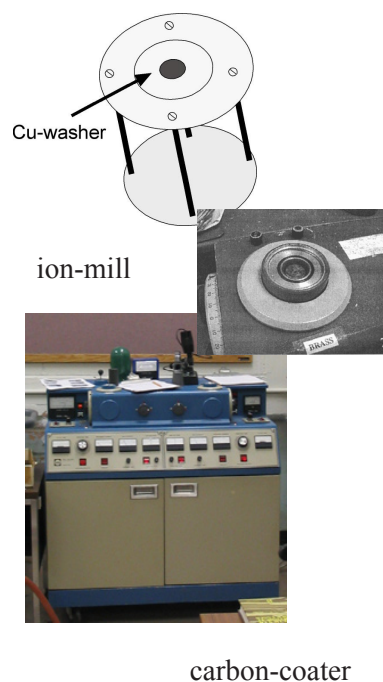
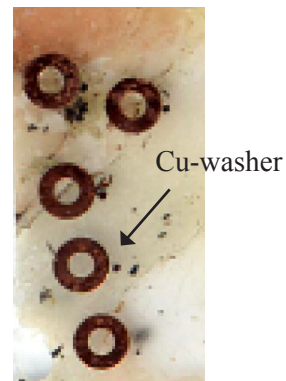
- The Cu-washer (with sample) is placed in a special sample holder
- Loading the ion-mill and evacuation of the chamber
- Turn on gun-voltage adjust current limit and high voltage to 0.5mA and 6kV
- activate specimen rotation
- gun current should be set at 1mA

Carbon-coating

- load sample in the carbon coater
- prepare carbon stick, mount carbon coater and start coating under ca. 8×10^{-2} torr vacuum



TEM



Microchemical data for illite in the Schauenburg Fault and the Soultz-sous-Forêts borehole, normalized to $O_{10}(OH)_2$, interlayer (Σ int) and octahedral charges (Σ oct)

SCHAUENBURG

rhyolite

Na	Mg	Al IV	Al VI	Si	K	Ca	Fe	Σ oct	Σ int
0.25	0.39	0.63	1.30	3.37	0.66	0.00	0.29	0.67	0.91
0.20	0.39	0.60	1.37	3.40	0.64	0.00	0.22	0.61	0.85
0.21	0.37	0.54	1.39	3.46	0.63	0.00	0.20	0.57	0.83
0.09	0.32	0.52	1.43	3.48	0.68	0.00	0.18	0.50	0.77
0.00	0.26	0.49	1.40	3.51	0.72	0.00	0.24	0.51	0.72
0.00	0.23	0.54	1.41	3.46	0.82	0.00	0.21	0.44	0.82
0.06	0.30	0.41	1.41	3.59	0.66	0.00	0.20	0.49	0.72
0.00	0.27	0.51	1.41	3.49	0.71	0.01	0.23	0.50	0.72
0.07	0.27	0.48	1.42	3.52	0.67	0.00	0.23	0.50	0.74
0.00	0.32	0.50	1.41	3.50	0.68	0.01	0.20	0.52	0.69
0.06	0.30	0.52	1.39	3.48	0.68	0.00	0.25	0.55	0.74
0.00	0.31	0.47	1.42	3.53	0.68	0.00	0.20	0.51	0.68
0.00	0.31	0.39	1.45	3.61	0.55	0.00	0.21	0.52	0.55
0.00	0.28	0.49	1.40	3.51	0.64	0.00	0.27	0.55	0.64
0.16	0.32	0.47	1.39	3.53	0.58	0.03	0.24	0.55	0.76
0.13	0.32	0.50	1.37	3.50	0.59	0.00	0.28	0.60	0.72
0.10	0.34	0.47	1.40	3.53	0.59	0.00	0.22	0.56	0.68
0.10	0.35	0.56	1.35	3.44	0.58	0.00	0.31	0.66	0.68
0.10	0.31	0.56	1.43	3.44	0.66	0.00	0.21	0.53	0.77
0.00	0.29	0.53	1.49	3.47	0.63	0.01	0.18	0.47	0.64
0.09	0.31	0.54	1.41	3.46	0.66	0.00	0.23	0.54	0.75
0.16	0.34	0.49	1.42	3.51	0.59	0.00	0.20	0.54	0.75
0.16	0.37	0.44	1.37	3.56	0.57	0.00	0.22	0.60	0.73
0.00	0.38	0.57	1.37	3.43	0.63	0.00	0.26	0.64	0.63

cataclasite

Na	Mg	Al IV	Al VI	Si	K	Ca	Fe	Σ oct	Σ int
0.00	0.02	0.78	2.06	3.22	0.22	0.00	0.09	0.11	0.22
0.00	0.00	0.75	2.02	3.25	0.19	0.00	0.15	0.15	0.19
0.00	0.00	0.73	2.14	3.27	0.13	0.00	0.06	0.06	0.13
0.00	0.00	0.74	1.98	3.26	0.22	0.00	0.18	0.18	0.22
0.00	0.00	0.73	2.18	3.27	0.06	0.00	0.05	0.05	0.06
0.00	0.11	0.67	1.78	3.33	0.55	0.01	0.10	0.21	0.56
0.05	0.04	0.87	2.23	3.13	0.06	0.00	0.01	0.04	0.11
0.00	0.10	0.79	2.07	3.21	0.22	0.00	0.03	0.13	0.22
0.04	0.13	0.78	2.02	3.22	0.24	0.00	0.03	0.16	0.29
0.05	0.05	0.89	2.23	3.11	0.06	0.00	0.01	0.06	0.11
0.07	0.06	0.83	2.15	3.17	0.13	0.00	0.02	0.08	0.21
0.08	0.03	0.84	2.21	3.16	0.07	0.00	0.01	0.04	0.15
0.06	0.03	0.86	2.24	3.14	0.03	0.01	0.01	0.03	0.10
0.06	0.05	0.87	2.24	3.13	0.02	0.00	0.01	0.05	0.08
0.00	0.05	0.82	1.97	3.18	0.41	0.01	0.08	0.13	0.42
0.00	0.08	0.78	1.90	3.22	0.47	0.01	0.08	0.16	0.48
0.00	0.12	0.70	1.87	3.30	0.45	0.02	0.06	0.18	0.47
0.00	0.02	0.86	2.09	3.14	0.28	0.00	0.06	0.08	0.28
0.00	0.07	0.78	1.91	3.22	0.46	0.00	0.10	0.17	0.46
0.06	0.16	0.66	1.74	3.34	0.55	0.02	0.08	0.24	0.63

0.05	0.12	0.72	1.92	3.28	0.34	0.01	0.06	0.19	0.40
0.00	0.09	0.79	2.04	3.21	0.25	0.01	0.04	0.13	0.26
0.00	0.07	0.72	1.98	3.28	0.35	0.01	0.04	0.11	0.36
0.05	0.07	0.79	2.11	3.21	0.16	0.00	0.03	0.10	0.21
0.00	0.00	0.91	2.28	3.09	0.04	0.00	0.01	0.01	0.04
0.00	0.04	0.78	2.14	3.22	0.16	0.00	0.03	0.07	0.16

granite

Na	Mg	Al IV	Al VI	Si	K	Ca	Fe	Σ oct	Σ int
0.48	0.30	0.97	1.93	3.03	0.04	0.01	0.09	0.39	0.53
0.10	0.24	0.13	1.37	3.87	0.88	0.00	0.02	0.26	0.98
0.10	0.22	0.20	1.32	3.80	0.85	0.04	0.04	0.25	0.99
0.35	0.49	0.69	1.42	3.31	0.53	0.00	0.15	0.64	0.89
0.36	0.49	0.75	1.55	3.25	0.50	0.00	0.06	0.55	0.85
0.39	0.41	0.64	1.54	3.36	0.52	0.00	0.07	0.48	0.91
0.27	0.20	0.11	1.39	3.89	0.64	0.00	0.00	0.20	0.92
0.33	0.17	0.00	1.47	3.94	0.66	0.00	0.00	0.17	0.99
0.29	0.17	0.11	1.43	3.89	0.65	0.00	0.00	0.17	0.94
0.35	0.42	0.77	1.61	3.23	0.41	0.02	0.09	0.51	0.78
0.25	0.18	0.17	1.43	3.83	0.64	0.00	0.00	0.18	0.89
0.17	0.18	0.27	1.53	3.73	0.78	0.00	0.00	0.18	0.95
0.27	0.23	0.99	1.98	3.01	0.05	0.02	0.11	0.35	0.34
0.11	0.14	0.04	1.42	3.96	0.88	0.00	0.00	0.14	1.00
0.17	0.13	0.03	1.43	3.97	0.68	0.00	0.00	0.13	0.86
0.21	0.18	0.86	1.99	3.14	0.03	0.01	0.13	0.31	0.26
0.25	0.24	0.67	1.74	3.33	0.40	0.03	0.08	0.31	0.68

SOULTZ-SOUS-FORETS**2059 vein (1431m)**

Na	Mg	Al IV	Al VI	Si	K	Ca	Fe	Σ oct	Σ int
0.00	0.16	0.75	1.64	3.25	0.72	0.00	0.18	0.33	0.72
0.00	0.20	1.02	1.58	2.99	0.77	0.00	0.23	0.43	0.77
0.00	0.19	0.54	1.51	3.47	0.77	0.00	0.19	0.37	0.77
0.00	0.00	0.74	1.71	3.27	0.79	0.00	0.18	0.18	0.79
0.00	0.13	0.81	1.56	3.20	0.89	0.00	0.22	0.35	0.89
0.00	0.15	0.80	1.55	3.20	0.90	0.00	0.20	0.35	0.90
0.00	0.00	0.69	1.52	3.31	0.93	0.00	0.26	0.26	0.93
0.00	0.20	0.71	1.51	3.30	0.74	0.00	0.24	0.44	0.74
0.00	0.25	0.67	1.49	3.34	0.76	0.00	0.21	0.46	0.76
0.00	0.17	0.69	1.50	3.32	0.82	0.00	0.23	0.40	0.82
0.00	0.16	0.80	1.55	3.21	0.85	0.00	0.22	0.38	0.85
0.00	0.23	0.68	1.46	3.33	0.77	0.00	0.25	0.48	0.77
0.00	0.13	0.75	1.65	3.25	0.75	0.00	0.17	0.30	0.75
0.00	0.19	0.78	1.48	3.22	0.90	0.00	0.24	0.43	0.90
0.00	0.14	0.71	1.57	3.30	0.76	0.00	0.20	0.34	0.76
0.00	0.14	0.72	1.51	3.28	0.86	0.00	0.22	0.36	0.86
0.00	0.19	0.76	1.51	3.24	0.82	0.00	0.24	0.43	0.82
0.00	0.15	0.75	1.61	3.25	0.75	0.00	0.20	0.35	0.75
0.00	0.16	0.80	1.49	3.21	0.90	0.04	0.23	0.39	0.90
0.00	0.15	0.53	1.45	3.47	0.75	0.02	0.27	0.42	0.75
0.00	0.00	0.44	1.45	3.56	0.85	0.05	0.29	0.29	0.85
0.00	0.00	0.83	1.70	3.17	0.82	0.03	0.15	0.15	0.82

0.00	0.00	0.71	1.62	3.29	0.79	0.04	0.24	0.24	0.79
0.00	0.09	0.73	1.58	3.27	0.81	0.05	0.21	0.30	0.81
0.00	0.21	0.66	1.55	3.35	0.70	0.00	0.21	0.42	0.70
0.00	0.00	0.70	1.74	3.31	0.71	0.00	0.18	0.18	0.71
0.00	0.19	0.81	1.58	3.19	0.76	0.03	0.19	0.38	0.76
0.00	0.20	0.90	1.44	3.10	0.86	0.03	0.27	0.47	0.86
0.00	0.00	0.78	1.74	3.22	0.75	0.00	0.14	0.14	0.75

2537 granite (1570m)

Na	Mg	Al IV	Al VI	Si	K	Ca	Fe	Σ oct	Σ int
0.36	0.46	0.61	1.42	3.39	0.60	0.00	0.10	0.56	0.96
0.22	0.25	0.89	1.68	3.12	0.68	0.00	0.09	0.33	0.89
0.21	0.25	0.81	1.67	3.19	0.72	0.00	0.06	0.31	0.92
0.18	0.24	0.84	1.67	3.17	0.76	0.00	0.06	0.29	0.94
0.27	0.20	0.82	1.72	3.19	0.71	0.00	0.04	0.24	0.98
0.35	0.14	0.92	1.78	3.09	0.69	0.00	0.04	0.18	1.04
0.19	0.15	0.83	1.81	3.18	0.65	0.00	0.03	0.18	0.84
0.21	0.23	0.91	1.72	3.10	0.71	0.00	0.05	0.28	0.91
0.12	0.32	0.76	1.63	3.25	0.70	0.00	0.05	0.37	0.82
0.21	0.11	0.91	1.85	3.09	0.60	0.00	0.05	0.16	0.81
0.20	0.10	0.92	1.84	3.09	0.70	0.00	0.04	0.14	0.89

4754 vein (2160m)

Na	Mg	Al IV	Al VI	Si	K	Ca	Fe	Σ oct	Σ int
0.00	0.30	0.79	1.64	3.21	0.64	0.00	0.12	0.41	0.64
0.15	0.24	0.83	1.67	3.18	0.69	0.00	0.10	0.33	0.84
0.00	0.19	0.31	1.63	3.69	0.54	0.00	0.08	0.27	0.54
0.12	0.22	0.13	1.62	3.87	0.41	0.00	0.06	0.28	0.53
0.00	0.20	0.46	1.68	3.55	0.55	0.00	0.08	0.27	0.55
0.13	0.21	0.12	1.58	3.88	0.45	0.00	0.08	0.29	0.58
0.00	0.20	0.38	1.63	3.63	0.58	0.00	0.08	0.28	0.58
0.00	0.20	0.70	1.67	3.31	0.69	0.00	0.11	0.31	0.69
0.00	0.14	0.72	1.67	3.29	0.75	0.00	0.13	0.27	0.75
0.00	0.22	0.69	1.64	3.32	0.68	0.00	0.11	0.32	0.68
0.00	0.19	0.72	1.70	3.29	0.64	0.00	0.11	0.30	0.64
0.16	0.37	0.71	1.51	3.29	0.69	0.00	0.12	0.48	0.85

4754 granite (2167m)

Na	Mg	Al IV	Al VI	Si	K	Ca	Fe	Σ oct	Σ int
0.00	0.11	0.67	1.39	3.34	0.83	0.00	0.19	0.29	0.83
0.00	0.08	0.64	1.43	3.37	0.95	0.06	0.21	0.29	0.95
0.00	0.06	0.62	1.38	3.39	0.98	0.08	0.24	0.29	0.98
0.00	0.09	0.61	1.43	3.39	0.92	0.06	0.21	0.30	0.92
0.00	0.12	0.59	1.46	3.42	0.85	0.06	0.19	0.31	0.85
0.00	0.09	0.67	1.51	3.34	0.92	0.09	0.13	0.21	0.92
0.00	0.09	0.68	1.54	3.32	0.89	0.08	0.12	0.20	0.89
0.00	0.07	0.73	1.57	3.27	0.92	0.06	0.12	0.19	0.92
0.00	0.06	0.64	1.38	3.36	1.02	0.07	0.23	0.29	1.02
0.00	0.09	0.63	1.38	3.36	1.02	0.07	0.23	0.32	1.02
0.00	0.12	0.67	1.56	3.33	0.85	0.06	0.12	0.24	0.85
0.00	0.10	0.65	1.52	3.35	0.89	0.07	0.12	0.22	0.89
0.00	0.06	0.72	1.53	3.29	0.95	0.08	0.13	0.18	0.95
0.00	0.05	0.76	1.59	3.24	0.94	0.06	0.12	0.17	0.94
0.00	0.07	0.62	1.41	3.39	0.95	0.08	0.21	0.27	0.95

0.00	0.12	0.59	1.46	3.41	0.85	0.06	0.19	0.30	0.85
0.00	0.04	0.81	1.59	3.20	0.96	0.07	0.11	0.15	0.96
0.00	0.10	0.65	1.45	3.35	0.92	0.06	0.19	0.29	0.92
0.00	0.06	0.62	1.46	3.38	0.96	0.07	0.18	0.23	0.96
0.00	0.06	0.62	1.52	3.38	0.89	0.06	0.17	0.23	0.89

4798 vein (2176m)

Na	Mg	Al IV	Al VI	Si	K	Ca	Fe	Σ oct	Σ int
0.16	0.28	0.93	1.61	3.08	0.76	0.00	0.13	0.41	0.92
0.19	0.24	0.88	1.67	3.12	0.64	0.00	0.13	0.37	0.83
0.16	0.25	0.88	1.65	3.13	0.71	0.00	0.12	0.36	0.87
0.00	0.26	0.83	1.63	3.18	0.72	0.00	0.13	0.39	0.72
0.13	0.25	0.89	1.63	3.12	0.75	0.00	0.12	0.37	0.88
0.18	0.25	0.87	1.61	3.14	0.76	0.00	0.11	0.36	0.94
0.18	0.24	0.85	1.64	3.15	0.72	0.00	0.11	0.35	0.90
0.00	0.14	0.92	1.63	3.09	0.72	0.00	0.19	0.33	0.72
0.00	0.12	0.95	1.58	3.06	0.75	0.00	0.22	0.34	0.75
0.00	0.25	0.91	1.65	3.10	0.70	0.00	0.13	0.38	0.70
0.00	0.26	0.90	1.71	3.10	0.65	0.00	0.11	0.37	0.65
0.00	0.24	0.80	1.61	3.20	0.74	0.00	0.15	0.39	0.74
0.00	0.29	0.82	1.59	3.18	0.75	0.00	0.13	0.42	0.75
0.00	0.25	0.88	1.67	3.12	0.69	0.00	0.13	0.38	0.69
0.13	0.27	0.78	1.61	3.22	0.70	0.00	0.12	0.39	0.83
0.12	0.22	0.82	1.62	3.18	0.74	0.00	0.14	0.35	0.86
0.00	0.22	0.92	1.65	3.09	0.75	0.00	0.14	0.36	0.75
0.00	0.22	0.83	1.64	3.17	0.73	0.00	0.14	0.36	0.73
0.00	0.20	0.95	1.61	3.05	0.85	0.00	0.17	0.37	0.85
0.00	0.20	0.92	1.63	3.08	0.80	0.00	0.16	0.36	0.80
0.00	0.14	0.78	1.70	3.22	0.77	0.00	0.12	0.25	0.77
0.00	0.21	0.77	1.63	3.24	0.72	0.00	0.14	0.35	0.72
0.00	0.21	0.80	1.66	3.21	0.71	0.00	0.13	0.34	0.71
0.00	0.21	0.82	1.69	3.19	0.68	0.00	0.13	0.34	0.68
0.13	0.19	0.82	1.66	3.19	0.70	0.00	0.14	0.33	0.83
0.00	0.16	0.80	1.66	3.20	0.77	0.00	0.13	0.29	0.77

THESIS RELATED ABSTRACTS

LOW TEMPERATURE MINERAL ALTERATION IN FELSIC ROCKS ALONG THE SCHAUBURG FAULT, EASTERN RHINE GRABEN SHOULDER, SW-GERMANY

Anja M. Schleicher¹, Laurence N. Warr¹ and Don R. Peacor²

¹Geological-Paleontological Institute, Ruprecht Karl University, INF 234, 69120 Heidelberg, Germany; ²Department of Geological Sciences, The University of Michigan, Ann Arbor, MI, 48109, U.S.A

The results of an XRD, SEM and HRTEM study of low temperature altered cataclasites are presented from along the eastern Rhine Graben shoulder in SW Germany. The E-W trending Schauburg Fault, situated close to Heidelberg, marks a vertical contact between Permian rhyolite and Variscan granite. Sampling occurs within 500 m of the main N-S trending Rhine Graben bounding fault. Geological mapping of the clay-rich fault zone reveals an oblique strike-slip displacement of ca.100 m, with a down-throw to the south. Alteration of the cataclasite is locally so extensive that the original igneous textures are no longer evident. Significant quantities of illite and kaolinite formed both as replacement reactions of feldspars (plagioclase and K-feldspar) and as neocrystallized pore-filling minerals. Kaolinite is particularly enriched within the fault zone, with several generations of pseudohexagonal stacks partially infilling pore-spaces within the fault rock. Based on the type and distribution of clay minerals along the Schauburg Fault, a series of fluid-rock interaction events can be recognized. The origin of these events is discussed in terms of both Mesozoic and Tertiary thermal activities of the Rhine Graben region.

39th Annual Meeting of The Clay Minerals Society, Boulder Colorado / USA (2002)

THE FORMATION OF CLAY MINERALS IN FAULTED GRANITE OF THE RHINE RIFT SYSTEM

Anja M. Schleicher¹, Laurence N. Warr¹ and Don R. Peacor², Ben A. van der Pluijm²

¹Geological-Paleontological Institute, Ruprecht Karl University, INF 234, 69120 Heidelberg, Germany; ²Department of Geological Sciences, The University of Michigan, Ann Arbor, MI, 48109, U.S.A

Although the Rhine Graben is one of the best studied rift systems in the world, there is still relatively little known about the fluid-rock history of the faulted basement rocks, other than in the Soultz-Sous-Forets (HDR borehole). Effective modelling of the regional flow of fluids within the rift sequence and its underlying basement is dependent on knowledge concerning changes in permeability and porosity of basement faults, which can be empirically assessed by studying the alteration history of cataclasite samples. In this contribution we present the results of a combined X-ray diffraction and electron microscopy (SEM and HRTEM) study of low temperature altered cataclasites in the basement granite from two contrasting localities. 1) The Soultz-sous-Forets borehole site (sampled below 1417 m), that is located in the western part of the rift basin, and 2) the E-W trending Schauburg Fault, positioned along the eastern Rhine Graben shoulder. This latter structure marks a vertical contact between Permian rhyolite and Variscan granite and is positioned immediately adjacent to the N-S trending basin boundary fault. The alteration mineralogy of the cataclasites sampled from these localities reveal notable differences, which are considered to reflect variations in the faults burial-uplift and fluid history. The Soultz samples contain mostly anhedral and fibrous illite-muscovite (predominantly 2M polytype) and less chlorite as the main alteration products, which occur both as pore-filling minerals and as replacement products of feldspar (both

plagioclase and K-feldspar) and biotite. In contrast, in the Schauenburg Fault 1M_d illite/smectite polytypes dominate, along with significant quantities of kaolinite. These minerals are also formed by replacement of feldspars and as neocrystallized pore-filling material. Kaolinite is particularly abundant in the center of the fault, where several generations of well-developed pseudohexagonal stacks can be recognized, partially infilling pore-spaces of the fault rock. The origin of these clay growth events is discussed in terms of both Mesozoic and Tertiary thermal history and meteoric input along the margins of the Upper Rhine Graben region.

EGS Nice / France (2003)

TEXTURAL DEVELOPMENT IN GRANITIC FAULT ROCKS OF THE RHINE GRABEN, CENTRAL EUROPE: A XTG AND HRTEM STUDY

A.M. Schleicher¹, L.N. Warr¹, B.A. van der Pluijm²

¹ Geologisch-Paläontologisches Institut, Ruprecht-Karls-Universität INF 234, 69120 Heidelberg, Germany, ² Department of Geological Sciences, The University of Michigan, Ann Arbor, MI 48109, U.S.A.

The Rhine Graben of central Europe provides an excellent area for studying the neotectonic and structural development of active, intracontinental rift systems. Despite numerous investigations of the areas history, there is relatively little known concerning the microstructural and textural evolution of alteration products in faulted granitic basement. In this study we examine two localities from different parts of the Rhine Graben: the Soultz-sous-Forets borehole site (sampled below 1417 m), located in the western part of the rift basin, and the E-W trending Schauenburg Fault, which crops out at the surface along the eastern graben shoulder. Fault rock samples (cataclasites and associated hydrothermal veins) were analyzed by X-ray diffraction, X-ray texture goniometry (XTG) and electron microscopy (SEM and HRTEM) in order to obtain textural, compositional and microstructural data. Significant differences are observed both in mineralogy and texture. The main alteration products of the Soultz samples are predominantly 2M polytypes of anhedral and fibrous muscovite with minor chlorite, which mainly occurs as replacement products of feldspar and biotite. The white mica fabric is slightly better developed in the host granite (maximum intensity in m.r.d. 3.1-3.7), but also shows reasonably good oblate fabrics in the hydrothermal veins (m.r.d. 2.7-3.0). In the Schauenburg Fault, 1M_d illite/smectite polytypes dominate, along with significant quantities of kaolinite. XTG results reveal complex fabrics across the fault zone. Textural patterns often have multiple maxima attributable to the presence of relatively large vermiform stacks of illite and kaolinite. The best fabrics are developed in cataclasites lying along the fault plane (m.r.d. >3.33). These results demonstrate that the formation of authigenic and hydrothermal phyllosilicates in these faulted granites play a critical role in influencing the permeability anisotropy, with enhanced fabric development along the shoulder of the Rhine Graben and poorer textures characterizing the younger, hydrothermally altered granite within the basin.

GSA Seattle / USA (2003)

PERMO-MESOZOIC HYDROTHERMAL ILLITES IN THE ALTERED SOULTZ-SOUS-FORETS GRANITE, FRANCE

A.M. Schleicher¹, L.N. Warr², B. Kober³, N. Clauer², E. Laverret³

¹Geologisch-Paläontologisches Institut der Universität Heidelberg, INF 234, 69 120 Heidelberg, Germany; ²Centre de Géochimie de la Surface (CGS/EOST) 1 rue Blessig, 67084, Strasbourg, France ; ³Institut für Umweltgeochemie INF 234, 69120 Heidelberg, Germany

This study presents petrographic, crystallographic and K-Ar results for hydrothermal illites of the altered Variscan granite of the EPS-1 drilling in Soultz-sous-Forêts, France. The drilling, situated in the Rhine Graben basin, is part of the “hot-dry-rock” project designed to explore geothermal heat as an energy resource. Based on XRD, SEM, HRTEM and K-Ar isotopic investigations of 8 different grain size fractions of four key samples collected from the lower parts of the borehole (below 1550 m levels), we demonstrate a Mesozoic age for illite formation. These well crystallized, pure illite phases are highly concentrated in phyllic hydrothermal veins, and are present in smaller quantities within the matrix of the pervasively altered granite. The predominant mineral within the veins is an euhedral, 2M1 illite polytype variety, formed by both neocrystallization in pore spaces and as direct replacement products of feldspars (both plagioclase and K-feldspar). K-Ar ages of the various grain sizes yield a mixture of ages ranging between 211 and 280 Ma for these illites. In contrast, the host rock granite samples contain an additional generation of fibrous illite crystallites, mainly grown as replacement of plagioclase and minor K-feldspar. Here, the finer fractions (0.2-2 micron) yield a larger age span, ranging between 95 and 195 Ma, whereas the coarser fractions yield ages as old as 255 Ma. A mixture of illite phases of varying ages is also indicated by the complex crystallite thickness distributions (CTDs) determined using the program “MudMaster”. The vein-illites reveal a size distribution close to log-normal for the most abundant 2-4 micron fractions. However, for the finer grain sizes, the distributions become progressively non-lognormal. In contrast, the illites of the host rock granite yield both asymptotic shapes (> 1 micron sizes) and non-lognormal shapes (< 1 micron sizes). Our results imply, that the late Eocene to the present-day development of the Rhine Graben rift system had no or little effect on the formation of hydrothermal illites at these depths in the Soultz-sous-Forêts granite.

40th Annual Meeting of The Clay Minerals Society, Richland, Washington St. / USA (2004)

MESOZOIC ILLITES IN THE HYDROTHERMALLY ALTERED GRANITE BASEMENT OF THE EPS-1 DRILLING (SOULTZ-SOUS-FORÊTS / FRANCE)

A.M. Schleicher¹, L.N. Warr², B. Kober³, N. Clauer², E. Laverret³

¹Geologisch-Paläontologisches Institut der Universität Heidelberg, INF 234, 69 120 Heidelberg, Germany; ²Centre de Géochimie de la Surface (CGS/EOST) 1 rue Blessig, 67084, Strasbourg, France ; ³Institut für Umweltgeochemie INF 234, 69120 Heidelberg, Germany

Although a large number of geoscientific studies have been conducted on the Variscan granite basement of the EPS-1 drilling in Soultz-sous-Forêts in France, within the context of exploiting thermal energy from this site, the actual age of hydrothermal mineral growth has remained unresolved. In this XRD, SEM, HRTEM and K-Ar isotopic study, we demonstrate that the abundant formation of illite is largely of Mesozoic age and of an episodic nature. Investigations were undertaken on whole rock samples and on various size fractions (8 fractions in total) of both pervasively altered granite and hydrothermal vein-alterations from the lower part of the borehole (samples taken below 1550 m). Euhedral, 2M polytype illite predominates in the vein samples and K-Ar results yields apparent (mixed) ages of between 211 and 280 Ma. This type of illite crystallized as pore-filling minerals and as replacement products of feldspar (both plagioclase and K-feldspar). Illite crystallite thickness distributions (CTDs determined using the program “MudMaster”) produce close to log-normal distribution for the most abundant 2-4 micron fraction, but size distributions become progressively non-lognormal toward finer grain sizes. In contrast, a generation of younger fibrous illite is recognized in the altered granite samples. The youngest apparent ages recorded on < 0.2 micron fractions range between 95 and 195 Ma, whereas the coarser fractions yield ages as old as 255 Ma. These mixtures are confirmed by the complex nature of CTDs, with asymptotic shapes for grain fractions > 1 micron, and non-lognormal shapes for < 1 micron fractions. Our study implies that the late Eocene development of the Rhine Graben had little or no influence on

illite formation in the altered matrix and veins of the Soultz-sous-Forêts granite at these depths.
32nd IGC Florence / Italy (2004)

THE NATURE OF MESOZOIC HYDROTHERMAL ILLITES IN THE SOULTZ-SOUS-FORÊTS GRANITE, UPPER RHINE GRABEN

A.M. Schleicher¹, L.N. Warr², B. Kober³, N. Clauer², E. Laverret³

1Geologisch-Paläontologisches Institut der Universität Heidelberg, INF 234, 69 120 Heidelberg, Germany; 2Centre de Géochimie de la Surface (CGS/EOST) 1 rue Blessig, 67084, Strasbourg, France ; 3Institut für Umweltgeochemie INF 234, 69120 Heidelberg, Germany

The Variscan granite of the EPS-1 drilling in Soultz-sous-Forêts contains abundant illite of hydrothermal origin. In this contribution, we present the results of X-ray diffraction (XRD, XTG), microscopy (SEM, HRTEM) and K-Ar isotopic investigations of 8 different grain size fractions of four key samples (veins, vein margins and pervasively altered granite) between 1570 – 2150 m depth. The phyllitic veins consist almost entirely of well crystallized pure illite phases of the 2M1 polytype, formed both by neocrystallization in pore spaces and direct replacement products of plagioclase and K-feldspars. In contrast, the illite is present in smaller quantities within the matrix of the vein margins and pervasively altered granite. These rocks contain larger amounts of fibrous illite crystallites of the 1M polytype, mainly grown as replacement of plagioclase. K-Ar data of the various grain sizes of the veins yield a mixture of ages ranging between 211 and 280 Ma for these illites. In the host rock samples, the finer more fibrous grain sizes (0.2-2 micron) yield a larger age span, ranging between 95 and 195 Ma, whereas the coarser fractions yield ages as old as 255 Ma. A mixture of illite phases of varying character is also indicated by the complex crystallite thickness distributions (CTDs) determined using the program “MudMaster”. Vein illites reveal a size distribution close to log-normal for the most abundant 2-4 micron fractions. However, for the finer grain sizes, the distributions becomes progressively non-lognormal. In contrast, the illites of the host rock granite yield both asymptotic shapes (> 1 micron sizes) and non-lognormal shapes (< 1 micron sizes). Our results imply, that the late Eocene to the present-day development of the Rhine Graben rift system had no or little effect on the formation of hydrothermal illites at these depths in the Soultz-sous-Forêts granite.

RST Strasbourg / Frankreich (2004)